Autophagy and its role in synapse function

Inaugural-Dissertation
to obtain the academic degree
Doctor rerum naturalium (Dr. rer. nat.)

submitted to the Department of Biology, Chemistry and Pharmacy
of Freie Universität Berlin

by

SHEILA SOOK-HI HOFFMANN
from Munich, Germany

2019

The work was conducted from April 2015 until December 2018 under the supervision of Prof. Dr. Craig C. Garner at the German Center for Neurodegenerative Diseases (DZNE) in the Helmholtz Association.

I hereby confirm that I have written the thesis independently using only the literature and aids mentioned and without illicit assistance from third parties.

1st Reviewer:

Prof. Dr. Craig C. Garner

2nd Reviewer:

Prof. Dr. Stephan J. Sigrist

Thesis defense on 11.04.2019

Table of Contents

1. Summary

The regulated turnover of synaptic vesicle (SV) proteins is thought to involve the ubiquitin-dependent tagging and degradation of SV proteins through endo-lysosomal and autophagy pathways. Yet, it remains unclear which of these pathways are used, when they become activated and whether SVs are cleared en-mass together with SV proteins or whether both are degraded selectively. Equally puzzling is how quickly these systems can be activated and whether they function in real-time to support synaptic health. To address these questions, I have developed an imaging based system that simultaneously labels presynaptic proteins while monitoring the appearance of autophagosomes and/or late endosomes within the presynaptic bouton.

Moreover, by tagging three synaptic proteins (Synaptophysin, Synaptotagmin, Synapsin) with a light-activated reactive oxygen species (ROS) generator, Supernova, it was possible to temporally control the damage of specific SV proteins and assess its consequence to autophagy mediated clearance mechanisms and synaptic function. My results show that, in mouse hippocampal neurons, presynaptic autophagy can be induced in as little as 5-10 minutes (after Synaptophysin-Supernova bleaching) and eliminates primarily the damaged protein rather than the SV en-mass. Additionally, I could show that induction of ROS-activated presynaptic autophagy requires the close association of Supernova with SVs.

Importantly, I also found that autophagy is essential for synaptic function, as ROS damage to e.g. Synaptophysin only compromises synaptic function when autophagy is simulaneously blocked, as measured in FM dye uptake and electrophysiology experiments. These data support the concept that presynaptic boutons have a robust, highly regulated clearance system to react in real-time to maintain not only synapse integrity, but also synapse function.

Additionally, I was able to further characterize neurons from Bassoon KO mice, which depict higher autophagy levels at boutons and along axons compared to neurons from WT mice. Therefore, they may be a useful tool to study presynaptic autophagy. In my study, imaging based experiments confirmed that the autophagy-related phenotype in Bassoon KO neurons does not show a neurodegenerative progression and that the increase in autophagy is dependent on poly-ubiquitination as well as the autophagy-related protein Atg5.

To summarize, I was able to provide new insights into the timing, the cargo and the function of presynaptic autophagy. Furthermore, my findings support the concept that functional autophagy is important for the clearance of damaged proteins, whereas excessively induced autophagy can be detrimental for synapse health. Thus, synaptic autophagy needs to be in balance.

2. Zusammenfassung

Es wird vermutet, dass der gerichtete Umsatz von Proteinen des synaptischen Vesikels (SV) die Markierung des abzubauenden Proteins mit Ubiquitin-Molekülen und den katalytischen Abbau durch Endolysosomen und Autophagosomen involviert. Dennoch ist bislang nicht bekannt, welche Stoffwechselwege genau benutzt werden, wann sie aktiviert werden und auch ob SV als Ganzes – mitsamt ihrer Proteine – oder ob diese beiden Einheiten separat abgebaut werden.

Ebenso ist bislang nicht bekannt, wie schnell diese Systeme aktiviert werden können und ob sie in Echtzeit fungieren, um die Erhaltung der gesunden Synapse zu unterstützen. Um diese Fragen zu beantworten habe ich eine bildgebende Methode entwickelt, die gleichzeitig präsynaptische Proteine markiert und das Auftreten von Autophagosomen und/oder später Endosomen im präsynaptischen Endknöpfchen anzeigt.

Des Weiteren war es mir möglich, eine zeitlich genau definierte Beschädigung spezifischer präsynaptischer Proteine durchzuführen und ihre Konsequenz in Bezug auf autophagische Mechanismen und die synaptische Funktion zu ermitteln. Dies gelang durch die Markierung dreier präsynaptischer Proteine (Synaptophysin, Synaptotagmin und Synapsin) mit einem lichtinduzierbaren Generator von schädlichen reaktiven Sauerstoffspezies (ROS) namens Supernova. Meine Ergebnisse aus Neuronen aus dem Maus-Hippocampus zeigen, dass präsynaptische Autophagie innerhalb von 5 bis 10 Minuten (nach der Bestrahlung von Synaptophysin-Supernova) induzierbar ist und dass sie bevorzugt das beschädigte Protein abbaut anstatt das synaptische Vesikel als Ganzes. Auβerdem konnte ich zeigen, dass die licht-abhängige Induzierung (mit Hilfe von Supernova) von präsynaptischer Autophagie die nahe Assoziation Supernovas mit den synaptischen Vesikeln benötigt.

Zudem konnte ich erste Hinweise darauf liefern, dass Autophagie essentiell für die einwandfreie Funktion der Synapse ist, da lichtinduzierter Schaden nur die synaptische Funktion – gemessen anhand von FM Farbaufnahme und Elektrophysiologie – beeinträchtigt, wenn Autophagie gleichzeitig inhibiert ist. Diese Daten befürworten das Konzept, dass präsynaptische Endknöpfchen ein robustes, stark reguliertes Proteinabbausystem besitzen, das in der Lage ist, sowohl die Integrität des präsynaptischen Endknöpfchens als auch die korrekte synaptische Funktion aufrechtzuerhalten.

Ferner war es mir möglich, Neurone aus Bassoon KO Mäusen, welche erhöhte Autophagie in synaptischen Endknöpfchen und entlang von Axonen im Vergleich zu Neuronen aus WT Mäusen aufweisen, zu analysieren. Aufgrund dieser Eigenschaft stellen sie ein nützliches Instrument dar, um präsynaptische Autophagie zu studieren. In einem Teil meiner Studie konnten bildgebende Experimente bestätigen, dass die erhöhte Autophagie in Bassoon KO Mäusen keinen zwingend

neurodegenerativen Verlauf zeigt und dass der Anstieg in Autophagie in Bassoon KO Mäusen sowohl von Poly-Ubiquitinierung als auch vom Autophagie-Gen Atg5 abhängig ist.

Zusammenfassend konnte ich neue Erkenntnisse über die zeitliche Abfolge, den Cargo und die Funktion von präsynaptischer Autophagie darlegen. Außerdem unterstützen meine Ergebnisse das Konzept, dass funktionale Autophagie unabdingbar für den Abbau von beschädigten Proteinen ist, während zu stark induzierte Autophagie nachteilig für den Allgemeinzustand der Synapse sein kann. Folglich sollten synaptische Autophagielevel stets in Balance sein.

3. Introduction

The integrity of vertebrate synapses requires robust cellular programs that monitor the activity states of thousands of proteins, eliminating those that are misfolded or damaged. Failure of these programs can lead to the accumulation of non-functional proteins that reduce the efficiency of synaptic transmission and/or promote synaptic and neuronal degeneration (Liang and Sigrist, 2018; Vijayan and Verstreken, 2017; Waites and Garner, 2011). As other cells, neurons are endowed with several surveillance and clearance systems that will be discussed in the following chapters.

3.1 Autophagy as one of the main degradational systems

To maintain cell growth and differentiation, eukaryotic cells depend on protein synthesis and degradation. Protein turnover occurs not only extensively within the cell but also specifically – meaning that some proteins get degraded in a faster rate than others (Ciechanover, 2005; Cohen et al., 2013; Sheehan et al., 2016). Two main systems are responsible for the degradation of intracellular components: the ubiquitin-proteasome-system (UPS) and the lysosomal system (Knecht et al., 2009).

The catalytic unit of the UPS is the proteasome. It is a large cylindrical protein complex that disassembles polyubiquitinated proteins to smaller peptides (Ciechanover, 2005; Hanna and Finley, 2007). It has been especially implicated in the turnover of misfolded soluble proteins, whereas the lysosomal system is also able to degrade whole organelles, protein aggregates and integral membrane proteins (Lamark and Johansen, 2010; Lilienbaum, 2013).

During lysosomal degradation, cargos targeted for destruction get delivered to the lysosome, a compartment containing acidic hydrolases, either through endosomes or through autophagy (Knecht et al., 2009). Three different types of autophagy are described. First, microautophagy is the direct sequestration of cytosolic components to the lysosome by membrane invagination. Second, chaperone-mediated autophagy (CMA) is the uptake of unfolded proteins across the lysosome membrane (Mizushima et al., 2008). Third, macroautophagy (hereafter referred to as autophagy) is a catabolic process that delivers cellular components varying from long-lived and aggregated proteins to whole organelles to the lysosomal compartment in a unique cytosolic vesicle called autophagosome (Lilienbaum, 2013; Rubinsztein et al., 2012).

Besides occurring at a basal rate in healthy cells (Musiwaro et al., 2013; Ravikumar et al., 2010; Rubinsztein et al., 2012), autophagy was initially described as a reaction to stress such as nutrient deprivation (Mizushima et al., 2004; Russell et al., 2014; Takeshige et al., 1992; Tsukada

and Ohsumi, 1993). More precisely, amino acid shortage leads to a bulk degradation of proteins for the purpose of rapid amino acid retrieval without time and energy consuming *de novo* synthesis (Kopitz et al., 1990; Takeshige et al., 1992). Under normal growth conditions the kinase mammalian target of rapamycin (mTOR) negatively regulates autophagy initiation whereas under nutrient depletion mTOR gets inactivated in order to induce autophagy (Ganley et al., 2011; Heras-Sandoval et al., 2014; Hosokawa et al., 2009; Kamada et al., 2000).

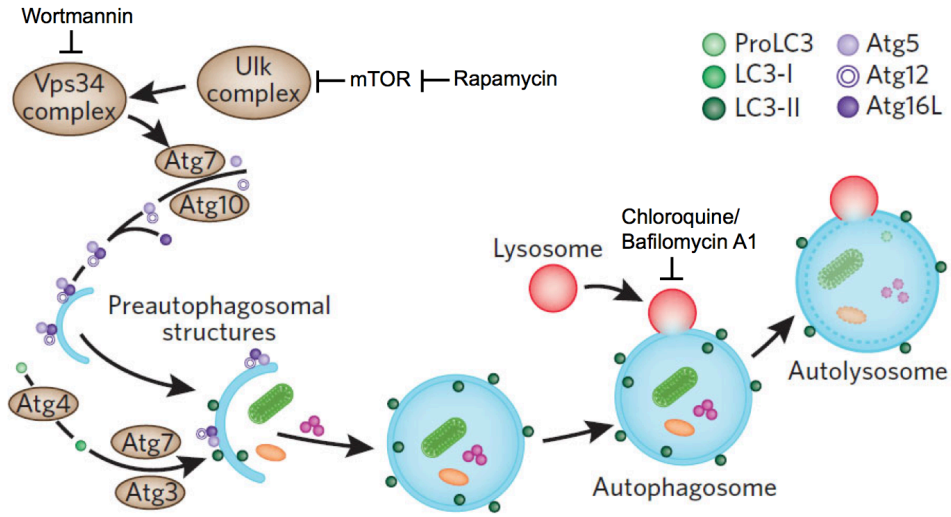

Figure 1: Schematic of autophagy. The formation of autophagosomes/autophagic vacuoles (AVs) is dependent on the Unc-51 like autophagy activating kinase (ULK) complex and Phosphatidylinositol 3-phosphate (PI3P) provision by the Phosphatidylinositol 3-kinase (Vps34) complex. A double-membrane, labeled by the Microtubule-associated protein light chain 3 (LC3-II) that is conjugated to phosphatidylethanolamine (PE), engulfs cytoplasmic content such as protein aggregates and mitochondria. Afterwards, the formed autophagosome matures and fuses with lysosomes (forming an autolysosome) for final degradation of its content. Adapted from Fleming et al. (Fleming et al., 2011).

There are various tools to manipulate autophagy (Figure 1). With starvation being mentioned, one common tool is the use of rapamycin, a potent inhibitor of mTOR. Its addition to the medium leads to the activation of autophagy in a variety of cells (Codogno et al., 2011; Galluzzi et al., 2016; Hernandez et al., 2012; Hosokawa et al., 2009; Kamada et al., 2000). In contrast, wortmannin robustly blocks the formation of autophagosomes by inhibiting the class III Phosphoinositide 3 kinase (PI3K) Vps34, which is essential for autophagy initiation (Klionsky et al., 2012; Ravikumar et al., 2010).

Interestingly, more recent studies show that autophagy is not only responsible for bulk degradation under nutrient starvation but also for the degradation of selective cargo such as TrkB (Topomyosin receptor kinase B) (Kononenko et al., 2017) and ROS damaged mitochondria (Ashrafi et al., 2014). Additionally, inhibition of the UPS strongly induces autophagy (Ding et al.,

2007). This indicates that both degradational systems are functionally co-regulated and connected with each other and that autophagy can compensate for the degradation of soluble proteins if the capacity of the proteasome is exceeded (Lamark and Johansen, 2010; Lilienbaum, 2013). Furthermore, autophagy and the endo-lysosomal system are interlinked, as autophagosomes cannot only fuse with mature lysosomes but also with endosomes to form amphisomes (Klionsky et al., 2014; Sanchez-Wandelmer and Reggiori, 2013). This not only demonstrates the interdepence of these different degradational systems and their high fluidity, but also the challenges to study them separately.

The major hallmark of autophagy is the formation of double-membraned autophagosomes (Baba et al., 1994; Ericsson, 1969; Klionsky et al., 2012; Lamb et al., 2013) (Figure 1). Autophagosomes are also characterized by the abundance of the ubiquitin-like protein Microtubule-associated protein light chain 3 (LC3). It becomes conjugated to phosphatidylethanolamine (PE) in the autophagosomal membrane through autophagy-related proteins (Atgs), which function similar to E3 ligases and are evolutionary highly conserved (Ichimura et al., 2000; Klionsky and Codogno, 2013; Mizushima et al., 2010). Upon lipidation, LC3 changes its distribution from microtubule-associated (evenly distributed) to autophagosome-associated (punctate). Besides LC3 and Atgs, p62 is a main marker for autophagy. It is an adaptor protein that recognizes and binds ubiquitin on proteins as well as lipid-conjugated LC3 and thereby loads the forming autophagosome with designated cargo proteins for degradation (Duran et al., 2011; Linares et al., 2013; Pankiv et al., 2007; Shvets et al., 2008). Once autophagosomes are formed, they are trafficked towards lysosomes (Maday and Holzbaur, 2014; Maday et al., 2012) while potentially undergoing maturation. Eventually, autophagosomes fuse with lysosomes to form autolysosomes and their content gets degraded via hydrolytic enzymes (Cheng et al., 2015; Klionsky et al., 2012).

The source of the forming autophagosome, the isolation membrane (phagophore), is strongly under debate. Ravikumar et al. (2010) could show that the plasma membrane directly contributes to the formation of Atg16L1 positive precursors and mature autophagosomes. However, many other membrane origins are postulated such as the endoplasmatic reticulum (ER), the Golgi complex or endosomes (Bento et al., 2016; Vijayan and Verstreken, 2017). Interestingly, one synapse-specific candidate for the membrane source might be the synaptic vesicle (SV) pool as VAMP2, an abundant SV protein, becomes enriched within autophagosomal membrane structures (Okerlund et al., 2017). These findings suggest that SVs or endosomal membranes are at least one source for early autophagic membranes in the presynaptic compartment.

Considering the high flux of autophagosomes under normal condition (Chu, 2006), it might be advantageous for experimental reasons to manipulate autophagic turnover with reagents like

chloroquine or bafilomycin A1. They operate by blocking the fusion of autophagosomes with lysosomes and lysosomal acidification itself, which is necessary for the functionality of lysosomal hydrolases, thus inhibiting the turnover of autophagosomes. This in turn leads to an accumulation/built-up of autophagosomes and the net increase in autophagy induction can be quantified (Galluzzi et al., 2016; Klionsky et al., 2012).

3.2 Autophagy in neurodegeneration

As post-mitotic cells with long processes, neurons have to be maintained for an entire lifetime (Bishop et al., 2010; Tammineni et al., 2017; Vijayan and Verstreken, 2017). As a result, it is not surprising that neurons are strongly dependent on functional and stable proteostasis, making them especially susceptible to protein damage during aging and disease (Rubinsztein et al., 2011).

In Alzheimer's disease (AD) brains, there is a clear up-regulation of autophagy manifesting in increased numbers of autophagosomes within dystrophic neurites (Boland et al., 2008; Lee et al., 2010; Nixon et al., 2005) implying a response to the disease state. On the other hand, a higher abundance of autophagosomes can also indicate a weakened autophagic flux or lysosomal dysfunction (Chu, 2006; Nixon, 2013; Tammineni et al., 2017). For instance, depletion of the ubiquitous transmembrane protein Presenilin 1 (PS1) that is mutated in many familial AD patients prevents substrate proteolysis due to an impairment of autolysosome acidification (Lee et al., 2010). Hence, the phenotype of higher autophagy levels in AD could reflect at least two things: 1) increased autophagy induction as a reaction to higher cellular demands or because of an intrinsic disbalance of autophagy or 2) impaired autophagy turnover leading to a built-up and aggregation of proteins that are ultimately detrimental to neurons. Enhanced autophagy induction could thus be a promising therapeutic target in the first case, whereas in the second case, it would lead to an additional built-up of autophagic intermediates and thus a worsening of the disease state (Vijayan and Verstreken, 2017).

However, in other diseases characterized by aggregate-prone proteins such as Parkinson's disease (PD) and Huntington's disease (HD), autophagy is not necessarily elevated (Martinez-Vicente et al., 2010; Nixon, 2013; Rubinsztein et al., 2012; Spencer et al., 2009). In detail, HD models not only exhibit a defect in recognition of cytosolic cargo and empty autophagosomes (Martinez-Vicente et al., 2010) but also a protective effect against neurodegeneration when autophagy is extrinsically induced by e.g. mTOR inhibitors. This supports the hypothesis that autophagy is one of the key clearance mechanisms for mutant Huntingtin (Ravikumar et al., 2004) making HD neurons particularly vulnerable for autophagy failure.

Another particular dysfunction of autophagy was observed in Parkinson's disease. More precisely, two genes that are mutated in autosomal recessive PD, PINK1 and Parkin, were shown to be involved in the selective autophagic degradation of mitochondria (referred to as mitophagy). Thus, defective clearance of damaged mitochondria and reduced ATP production are thought to contribute to the neurodegenerative phenotype in PD patients (Corti et al., 2011; Nixon, 2013; Pickrell and Youle, 2015).

The observation that autophagy is not engaged in some neurodegenerative diseases, suggests that this failure might contribute to the accumulation of protein aggregates and subsequent reduced neuronal survival (Ebrahimi-Fakhari et al., 2013; Kegel et al., 2000; Nixon, 2013; Yue et al., 2009). This latter concept is supported by the analysis of knockout mice of Atg5 or Atg7, two essential autophagy-related proteins, which exhibit robust hallmarks of neurodegeneration (Hara et al., 2006; Komatsu et al., 2006). Additionally, impaired retrograde transport of autophagosomes alone leads to a neurodegenerative phenotype suggesting that not only the initiation of autophagy, but also the maturation and subsequent degradation of autophagic vacuoles (AVs) is indispensible for the brain's integrity (Cai et al., 2010; Kononenko et al., 2017; Lee et al., 2011).

In a similar field of research, autophagy and its role in the aging brain are being intensively studied. For example, the naturally occurring polyamine Spermidine is able to extend the lifespan of various animal models and even of human immune cells (Eisenberg et al., 2009). These findings led to various studies investigating the mechanism of action of Spermidine and intriguingly, Spermidine administration leads to an improvement of age-related memory impairment through up-regulation of autophagy in *Drosophila*. More precisely, feeding flies with Spermidine prevented the age-related increase of the active zone and its proteins by enhanced autophagic clearance thus counteracting age-induced active zone (AZ) changes and impaired plasticity (Gupta et al., 2016; Vijayan and Verstreken, 2017).

Taken together, a balanced autophagy system is crucial for neuronal maintenance and health.

3.3 The Presynapse

The communication between neurons (=synaptic transmission) occurs through highly specialized contact sites called synapses. Synapses consist of a presynapse (also called bouton) and a postsynapse (Rizzoli and Betz, 2005; Waites and Garner, 2011). Synaptic transmission is not only dependent on the release of neurotransmitter from the presynaptic site into the synaptic cleft, but also on the ability of receptor molecules on the postsynaptic site to bind these neurotransmitters in order to pass the stimulus along (Rizzoli, 2014).

A closer look at the central presynapse of mammals shows an extremely organized compartment with large numbers of synaptic vesicles (SVs), which are filled with neurotransmitter, and a protein dense region at the presynaptic membrane, the active zone (AZ). The AZ is the site where SVs dock, fuse and release their content into the synaptic cleft via exocytosis (Ackermann et al., 2015). This process is followed by membrane and SV protein retrieval through endocytosis within the peri-active zone (Sudhof, 2012) and the subsequent renewal of fusion-competent SVs. This so-called SV cycle has been the focus of an enormous number of studies ever since its discovery (Haucke et al., 2011; Rizzoli, 2014; Sudhof, 2004).

Synapses are typically far away from the cell body and the delivery of synaptic proteins to the distal tips of axons poses a major challenge. After synthesis in the endoplasmatic reticulum (ER), synaptic proteins are sorted within the Golgi apparatus. They leave the Golgi apparatus as distinct precursor SVs (SV proteins vs. AZ proteins) as nicely shown by Maas et al. (Maas et al., 2012). However, for peripherally associated SV proteins anterograde co-transport along the axon with SVs (Hirokawa et al., 2010) is very likely due to their dynamic association with SVs and relative binding affinities (Rizzoli, 2014). Additionally, it was shown that small fractions of soluble proteins, such as Synapsin, temporarily move as fast as the SV protein Synaptophysin (Roy et al., 2007) leading to the proposed scheme: following translation, soluble SV proteins diffuse in the cytosol and reversibly bind to precursor SVs to be co-transported towards synapses (Rizzoli, 2014).

Once a precursor SV reaches the presynapse, it is posited to fuse with the plasma membrane leading to a SV precursor patch within the presynaptic membrane. These membrane patches facilitate the sorting and enrichment of SV proteins (Rizzoli, 2014) – eventually leading to the endocytosis and formation of mature SVs with the correct stoichiometry of all its important integral membrane proteins: 1) the SNARE protein Synaptobrevin2/Vamp2 – necessary for fusion; 2) Synaptotagmin as a calcium sensor; 3) a neurotransmitter transporter to load the SV; 4) the protein SV2 and 5) the very abundant protein Synaptophysin (Rizzoli, 2014; Takamori et al., 2006). However, endosomal sorting is also a possibility to enrich SVs with designated proteins but the mechanism behind it is poorly understood so far.

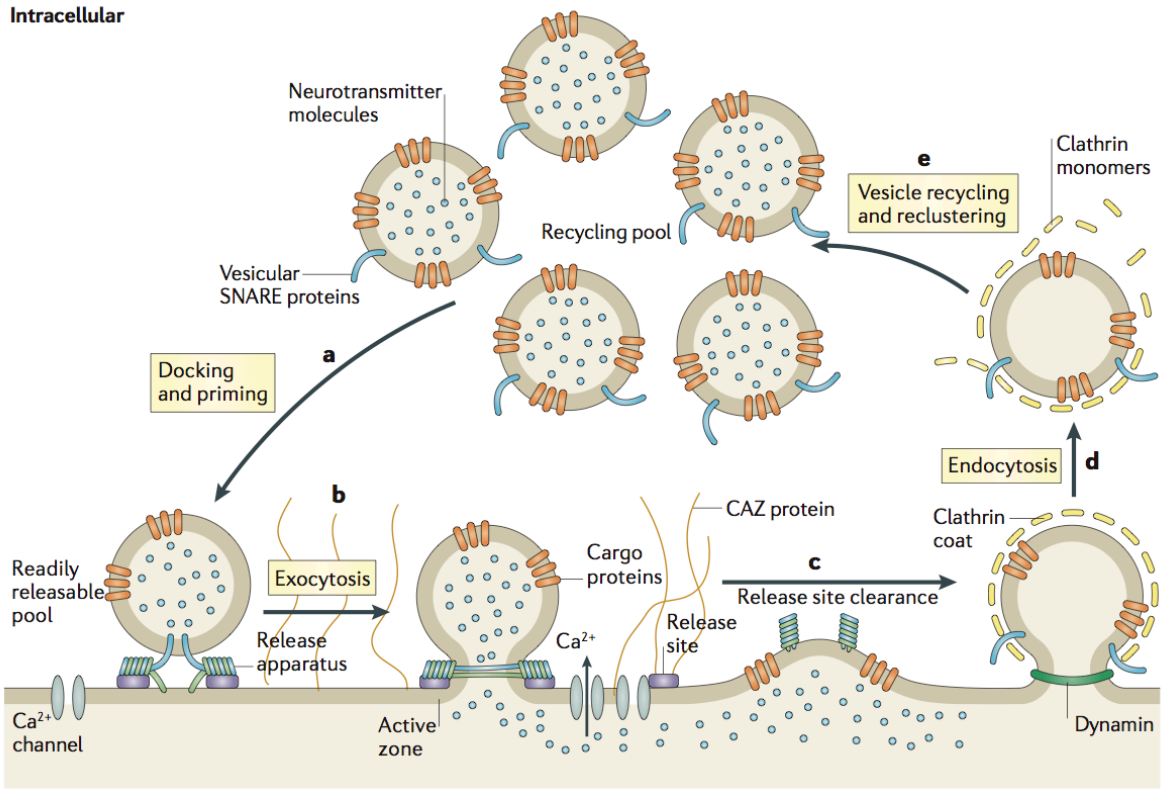

Figure 2: Schematic of the synaptic vesicle cluster. SVs remain within the recycling pool until they get docked and primed (a) in order to release their content via exocytosis (b) towards the synaptic cleft. Retrieval of SV membrane and proteins occurs predominantly through clathrin-mediated endocytosis (d) subsequent to release site clearance (c). Afterwards, SVs become reacidified and reclustered (e) into the SV pool. Adapted from Haucke et al. (Haucke et al., 2011).

Subsequent to endocytosis, the newly formed SV becomes acidified and loaded with neurotransmitter (Figure 2), before being recruited into the vesicle cluster, where it is stabilized by the actin-binding protein Synapsin (Haucke et al., 2011). If the synapse receives a stimulus, Synapsin becomes phosphorylated releasing SVs from the cluster allowing them to transit to the plasma membrane (Chi et al., 2001; Leal-Ortiz et al., 2008) where they can release their content. Interestingly, the SV cluster consists of more than one population of SVs. In the rat central synapse ~ 5% of the vesicles are part of the readily releasable pool (RRP) that is already docked and primed at the AZ (Rosenmund and Stevens, 1996; Schikorski and Stevens, 2001). The RRP can be released within milliseconds. The second pool is the recycling pool that comprises ~ 10% of all vesicles and that can show fast mixing with the RRP. Lastly, the reserve pool accounts for ~ 85% of the vesicle cluster. These latter pools are largely immobile (crosslinking, possibly by Synapsin) and only released under intense or prolonged stimulation (Rizzoli and Betz, 2005).

The site of the neurotransmitter release is the active zone (AZ). Proteins associated with this membrane specialization represent a third group of presynaptic proteins (besides SV proteins and SV cluster proteins). AZ proteins are, among others, comprised of the high molecular weight

scaffold proteins Piccolo and Bassoon (Waites et al., 2013), and proteins essential for docking, priming and fusion of SVs with the plasma membrane called RIM, Munc13 and RIM-binding protein (Ackermann et al., 2015).

Taken together, the bouton is a highly specialized compartment with dozens of proteins, without which communication between neurons would fail.

3.4 Presynaptic autophagy

Presynapses are not only far away from the neuronal soma, the primary site of protein synthesis, but also packed with ~ 300,000 proteins (Wilhelm et al., 2014). Their functioning is essential for the central nervous system (CNS) as many neurological disorders show accumulation of neuronal protein aggregates followed by synaptic defects and subsequent cell death (Wang et al., 2017). High numbers of proteins and a fast turnover rate of SV proteins within the synaptic vesicle cycle – especially when neurons are very active (Heuser and Reese, 1973; Rizzoli, 2014; Rizzoli and Betz, 2005) – pose a unique challenge to protein quality control mechanisms and degradational systems (Labbadia and Morimoto, 2015; Vijayan and Verstreken, 2017) within presynaptic boutons.

Regarding this challenge, three questions arise: First, do neurons have a local autophagy machinery at the synapse that is independent of the soma and how fast can it be switched on? Second, is synaptic autophagy a maintenance mechanism under basal conditions or a clearing/coping mechanism that is only active after an insult? Third, if autophagy is an insult-dependent clearance mechanism, what exactly is the cargo of synaptic autophagy and does the synapse have a specific cargo-recognition mechanism?

Considering the first question, Hernandez et al. (Hernandez et al., 2012) could show in a nice electron microscopy (EM) study that autophagosomes appear within the presynaptic terminal upon mTOR inhibition with rapamycin for 7 hours. They also measured decreased evoked dopamine release following rapamycin treatment (Hernandez et al., 2012). Additionally, it has been shown that autophagosomes appear in presynaptic boutons of hippocampal neurons in response to increased levels of Sonic hedgehog for 48 hours, a neuronal development signaling protein (Petralia et al., 2013). However, both studies involve long-term treatments with an autophagy inducer and analyses hours after the initial induction, thus it is not possible to conclude that autophagosomes form locally at presynaptic sites.

Autophagosomes are also present in axonal growth cones of dorsal root ganglia (DRG) neurons under basal conditions and move retrogradely towards the soma (Maday and Holzbaur, 2014; Maday et al., 2012), in a Dynein-dependent manner (Cheng et al., 2015), where they fuse with lysosomes (Cheng et al., 2015; Maday, 2016; Maday and Holzbaur, 2016; Wang et al., 2015).

During this transport, autophagosomes undergo maturation, potentially by fusion with acidified endosomes (=amphisomes) (Maday and Holzbaur, 2016).

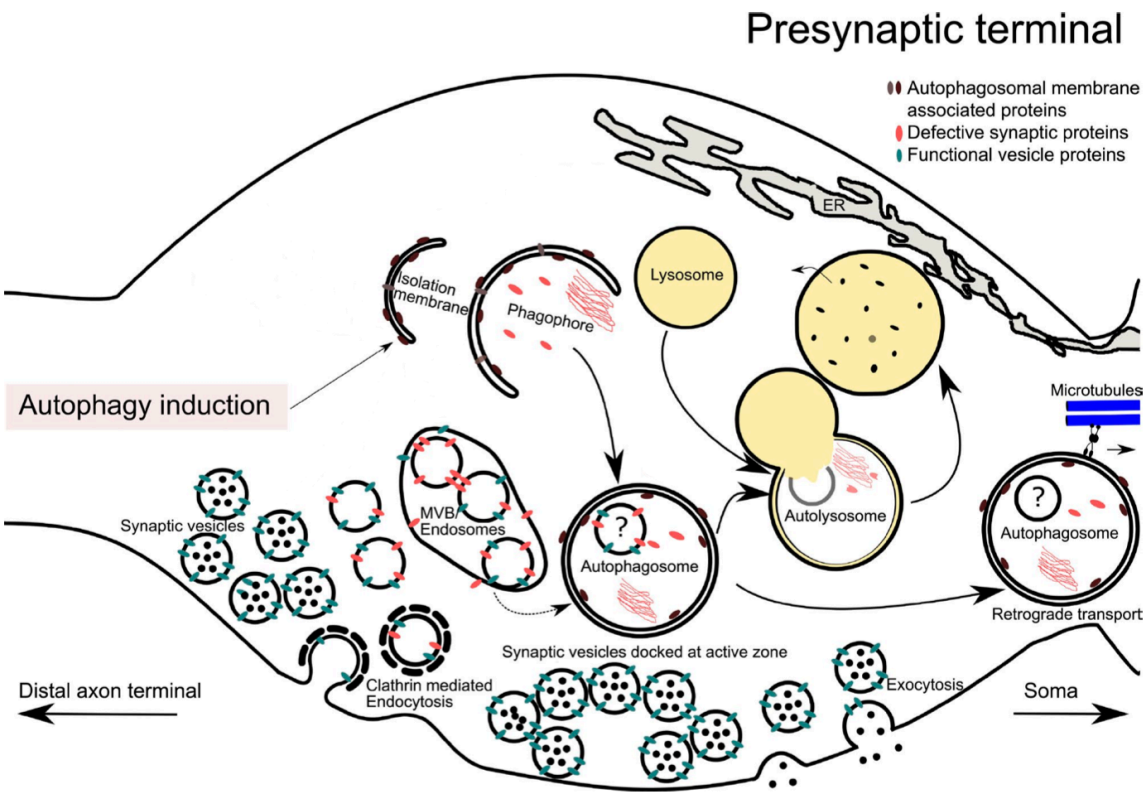

Figure 3: Schematic of hypothetical autophagy at the presynaptic terminal. While autophagosomes have been found at presynaptic boutons, the cargo of these autophagosomes is still poorly understood. For instance, it is not known whether synaptic autophagosomes engulf protein aggregates or whole synaptic vesicles. Note, it is still strongly debated whether mature lysosomes are present at the presynaptic bouton. Adapted from Vijayan & Verstreken (Vijayan and Verstreken, 2017).

Intriguingly, extensive SV recycling upon high neuronal activity can increase the number of autophagosomes in axonal bundles (Wang et al., 2015) approximately 3-4 hours after the stimulus, implying a relationship between synaptic function, protein damage and perhaps the aging of synaptic proteins (Figure 3). Consistently, other studies could show that high synaptic activity leads to an increase in presynaptic autophagy at the fly neuromuscular junctions (NMJ) 20-30 minutes after stimulation (Soukup et al., 2016; Vanhauwaert et al., 2017). Importantly, autophagy is not limited to axons and presynaptic boutons but also appears at postsynaptic sites in an activity-dependent manner (Shehata et al., 2012). Together these data suggest that synapses may locally control the clearance of aging/damaged proteins, but how?

Several recent studies have demonstrated that the presynaptic AZ protein Bassoon is a key regulator of presynaptic autophagy through its direct interaction with the LC3 ligase Atg5. Here the authors could show that in boutons lacking Bassoon, presynaptic autophagy was elevated

and associated with a reduction of the normally very abundant SV protein Synaptophysin. This process was Atg5-dependent indicating that Bassoon and Atg5 may locally regulate the degradation of SVs (Okerlund et al., 2017). Furthermore, Binotti et al. (Binotti et al., 2015) found that Rab26, a small GTPase enriched on SVs, is able to direct SVs into preautophagosomal structures through its effector protein Atg16L. Finally studies at the *Drosophila* NMJ revealed that two proteins involved in SV endocytosis, Endophilin A and Synaptojanin1, are essential for synaptic autophagy (Soukup et al., 2016; Vanhauwaert et al., 2017).

Together these data support the hypothesis that autophagosomes are formed locally within presynaptic boutons and transport their cargos to the soma for further degradation following their fusion with lysosomes. However, at present, insult-dependent autophagy function and the (specificity of the) cargo of presynaptic autophagy are not well understood. It is also not entirely clear if autophagosomes form locally at boutons or if they move into them after being formed in the axon or in the soma.

3.4.1 Bassoon and its role in presynaptic autophagy

The active zone (AZ) proteins, RIM and Munc13, are very well studied and have been shown to be required for SV exocytosis (Ackermann et al., 2015). Two of the largest AZ proteins, Piccolo and Bassoon, are more enigmatic, as they appear non-essential for synaptic transmission (Fejtova and Gundelfinger, 2006; Jin and Garner, 2008) though tightly coupled to the formation of nascent synapses (Ziv and Garner, 2004). Intriguingly, shRNA mediated loss of both Piccolo and Bassoon leads to a decrease of numerous synaptic proteins and severe synapse degeneration. These phenotypes appear partly mediated by the loss of interaction of Piccolo and Bassoon with the E3 ligase Siah1 (Waites et al., 2013). Specifically under double knock down (DKD) conditions, Siah1 is released from the two AZ proteins and becoming active, thus resulting in higher amounts of ubiquitinated substrates. This then leads to the subsequent proteasomal and endo-lysosomal degradation of ubiquitinated synaptic proteins and a degenerative phenotype (Waites et al., 2013).

Bassoon is a ~ 420kDa protein with two zinc finger domains (ZnF) and three coiled-coil domains (CC). Its ZnFs interact with and thereby negatively regulate Siah1 (Waites et al., 2013) whereas ist second CC interacts with the autophagy-related protein Atg5 (Okerlund et al., 2017). The latter interaction was shown to locally inhibit Atg5 function within the autophagy pathway as autophagy is robustly increased in synapses from Bassoon KO mice. Atg5 is an E3 ligase that is crucial for the conjugation of LC3 to phagophore membranes during early autophagic steps. However, elevated autophagy in DKD neurons, though dependent on polyubiquitination, does

not require Siah1 indicating that Piccolo's and Bassoon's contribution to autophagic degradation (Okerlund et al., 2017) might be different from their role in Siah1-dependent synapse integrity (Waites et al., 2013).

In general, mechanisms regulating quality control and turnover of synaptic proteins are not well understood. This is why additional studies are necessary to further unravel Bassoon's direct function in presynaptic autophagy.

3.5 Other synaptic protein clearance mechanisms

Due to its special architecture, the synapse requires spatially regulated protein quality control mechanisms (Vijayan and Verstreken, 2017). These include not only autophagy but also the UPS and the endo-lysosomal system. The UPS targets polyubiquitinated proteins towards degradation. It comprises several proteins including the proteasome, ubiquitin-activating enzymes (E1), ubiquitin-conjugating enzymes (E2), ubiquitin ligases (E3) and deubiquitinases (DUB), to enable precise regulation of protein turnover (Alvarez-Castelao and Schuman, 2015).

Speese et al. (Speese et al., 2003) could show that components of the UPS, E1 and the 20S proteasome subunit, are present in presynaptic boutons of *Drosophila* NMJs. Additionally, they found that the SV priming protein DUNC-13 is degraded through the proteasome. Intriguingly, other synaptic proteins such as Syntaxin and Synaptotagmin were not degraded within the analyzed 1-hour time frame (Speese et al., 2003). In a different study, Syntaxin1 was shown to be targeted to the proteasome by the E3 ligase Staring (Chin et al., 2002) while Synaptophysin became degraded after ubiquitination by the E3 ligase Siah (Wheeler et al., 2002). One caveat is that both studies were performed in non-neuronal cell lines and not in differentiated neurons suggesting that the mechanisms in synapses might be different.

Another candidate for the sorting of synaptic proteins destined for degradation is the ESCRT (endosomal sorting complex required for transport) machinery. It catalizes the formation of multivesicular bodies (MVBs), which are indeed found in presynaptic boutons (Ceccarelli et al., 1973). In detail, the ESCRT machinery controls endosome to lysosome traffic of ubiquitinated proteins destined for degradation (Raiborg and Stenmark, 2009). Interestingly, at least two studies in *Drosophila* NMJs described that endosomal trafficking facilitates the replacement of dysfunctional SV components leading to a rejuvenation of SV protein pools (Fernandes et al., 2014; Uytterhoeven et al., 2011).

Another great study in rat hippocampal neurons showed that two SV proteins, SV2 and VAMP2, get degraded in an activity-dependent manner whereas the degradation of other SV proteins such as Synaptotagmin1 is not activity-dependent. Additionally, they found that ESCRT

components accumulate at synapses under stimulation and that the observed activity-dependent SV2 and VAMP2 clearance is not only ESCRT- but also Rab35-dependent (Sheehan et al., 2016). This study not only demonstrates the importance of ESCRT-dependent SV protein turnover, but also illuminates other findings in which SV proteins were shown to have very different half-lives (Cohen et al., 2013), providing evidence that instead of the degradation of entire SVs, regulated degradation of specific SV proteins may occur.

3.6 Chromophore-assisted light inactivation (CALI)

Chromophore-assisted light inactivation (CALI) was first described in studies showing that short pulses of high-intensity laser light could heat-inactivate proteins, to which a chromophore/ photosensitizer was targeted for example by antibody conjugation. Interestingly, the heat only denatured proteins in immediate proximity leaving other cell components unaffected (Jay, 1988).

One decade later, Surrey et al. (Surrey et al., 1998) were able to spatiotemporally inactivate proteins that harbor a genetically inserted epitope tag or the chromophore itself. Afterwards, it was confirmed that the inactivation is not caused by increased temperature but by photogenerated free radicals (=reactive oxygen species, ROS) (Liao et al., 1994) (Figure 4).

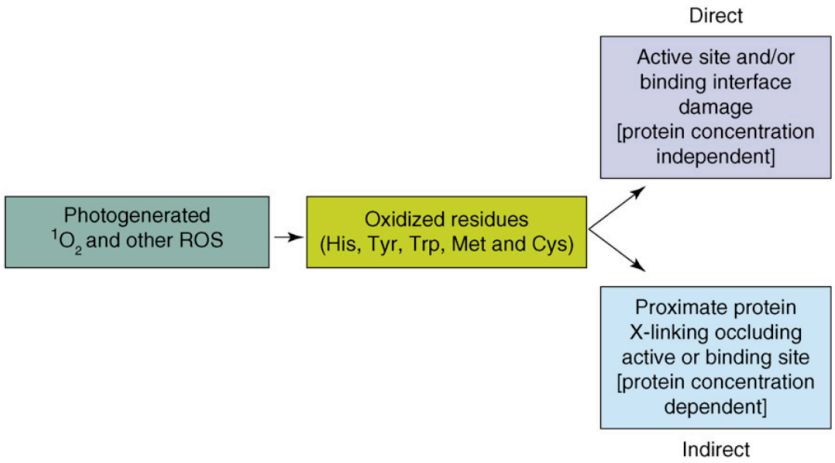

Figure 4: Schematic of potential photodamage pathways in CALI. Note that oxidized residues may lead to a direct or indirect damage of protein active sites. Adapted from Jacobson et al. (Jacobson et al., 2008).

Photosensitizers come in various forms but one important break-trough was the creation of a fully genetically encoded photosensitizer called Killerred that can be used in living cells. It is a dimeric red fluorescent protein that is derived from the hydrozoan chromoprotein anm2CP, a

homolog of GFP, and that generates ROS resulting in protein inactivation upon illumination with green light (Bulina et al., 2006; Jarvela and Linstedt, 2014).

In order to reduce problems linked to the dimerization tendency of Killerred, a monomeric version of Killerred, called Supernova, was generated (Takemoto et al., 2013). When genetically fused to a target protein, Supernova exhibits proper localization while still maintaining potent photosensitizer capabilities. In addition, cells were more viable when Supernova was expressed compared to cells expressing Killerred. The half-radius of the photodamage is as small as 3-4nm, thus within the distance of a protein-protein interaction (Takemoto et al., 2013).

Utilization of mitochondrial targeted Killerred (mt-KR) in HeLa cells leads to increased ROS levels, the loss of mitochondrial membrane potential and finally to a Parkin-dependent degradation of tagged mitochondria by autophagy (mitophagy) (Wang et al., 2012; Yang and Yang, 2011). Similarly, Ashrafi et al. (Ashrafi et al., 2014) showed that bleaching of mt-KR in axons of rat hippocampal neurons leads to the fragmentation and subsequent loss of affected mitochondria. In parallel, the autophagic marker GFP-LC3 accumulated at a subpopulation of the damaged mitochondria approximately 20 minutes after bleaching (Ashrafi et al., 2014). These findings indicate that Killerred and other CALI approaches are useful tools to spatiotemporally activate mitophagy.

Thus, it seems reasonable to predict that recombinant photosensitizers could be used to selectively damage synaptic proteins. Consistent with this concept, tethering the photosensitizing flavin-binding protein miniSOG to the SV protein Synaptophysin was shown to inhibit synaptic transmission in cultured hippocampal neurons in a light-dependent manner, presumably by locally damaging Synaptophysin or adjacent SNARE proteins (Lin et al., 2013), though the mechanism was not examined.

4. Aim of the study

Defining the role of degradative systems within the synapse during health and disease requires a better understanding of when and where each is turned on and which subsets of proteins are eliminated. For example, those critical for the real-time maintenance of synaptic function should be locally regulated and operating on a second to minute time scale, while those responding to chronic damage may act on longer time scales like hours. Yet, the fundamental mechanisms regulating these systems remain enigmatic.

To address these essential questions, the goal of my study was to develop a strategy to preferentially monitor autophagy within presynaptic boutons, e.g. after chemical induction of autophagy. Additionaly, I wanted to create a tool to selectively damage synaptic proteins within presynaptic boutons and assess how synaptic clearance systems respond to this damage and how neuronal function may be affected by it.

5. Material and Methods

5.1 Construction of Vectors

Monitoring autophagy within presynaptic boutons was achieved by creating a set of lentiviral expression vectors that express different XFP-tagged synaptic proteins (Figure 5). All vectors are based on the commercially available vector FUGW (plasmid #14883, Addgene). In order to co-express mCherry-tagged Synaptophysin (Syp) and eGFP-LC3, Synaptophysin-mCherry (Synaptophysin, NM_012664.3) was synthesized with a downstream glycine linker that was fused to a self-cleaving 2A peptide (Kim et al., 2011). This element was then exchanged with GFP in the FUGW vector (Addgene) by ligation. Subsequently, the eGFP-LC3 (LC3, U05784.1) segment from FU-ptf-LC3 (Okerlund et al., 2017) was subcloned in frame after the P2A sequence resulting in the vector FU-Syp-mCherry-P2A-eGFP-LC3. This vector served as a template for tagging Synaptophysin with Supernova. This was achieved by synthesizing Supernova (Supernova, AB522905) (Takemoto et al., 2013) with flanking restriction sites that allowed the direct exchange of mCherry with Supernova by ligation to form FU-Syp-Supernova-P2A-eGFP-LC3. For the simultaneous expression of a short hairpin RNA to knock down Atg5 transcripts, a U6 promoter driven shRNA cassette was cloned upstream of the ubiquitin promoter. The shRNA (5'-CCA TCT GAG CTA CCC AGA TAA TTC AAG AGA TTA TCT GGG TAG CTC AGA TTT TTT TGG AA-3') was cloned into the vector to form F-U6-shAtg5-U-Syp-Supernova-P2A-eGFP-LC3. A scrambled shRNA against rat Clathrin served as negative control (F-U6-scRNA(SC)-U-Syp-Supernova-P2A-eGFP-LC3). In order to express Supernova within the lumen of SVs, Supernova cDNA sequences were inserted at residue 184 in Synaptophysin (Syp-lumSN) together with a GSG linker, by Gibson assembly (Gibson et al., 2009) followed by subcloning to create FU-Syp-lumSN-P2A-eGFP-LC3). Ligation of a PCR amplified Supernova transcript at the C-terminus of Synaptophysin and after the downstream sequence of eGFP-LC3 generated the eGFP-LC3 empty vector FU-Syp-Supernova. To allow monitoring of Rab7, LC3 was replaced from this vector by Rab7 cDNA (XM_005632015.2). The Rab7 was PCR amplified from plasmid DNA and exchanged with LC3 in FU-Syp-Supernova-P2A-eGFP-LC3 by Gibson assembly (Gibson et al., 2009) to form FU-Syp-Supernova-P2A-eGFP-Rab7. In order to express Supernova at further synaptic sites and to reveal eGFP-LC3 expression, Syp was exchanged with Synapsin (Syn) or Synaptotagmin1 (Syt) in FU-Syp-Supernova-P2A-eGFP-LC3. Therefore, Synapsin (NM_019133) or Synaptotagmin1 (NM_001252341) were PCR amplified from plasmid DNA (Chang et al., 2018; Waites et al., 2013), agarose gel purified and subjected to a Gibson assembly reaction with the purified Syp-deleted FU-Syp-Supernova-P2A-eGFP-LC3 vector to form FU-Syn-Supernova-P2A-eGFP-LC3 and FU-Syt-Supernova-P2A-eGFP-LC3.

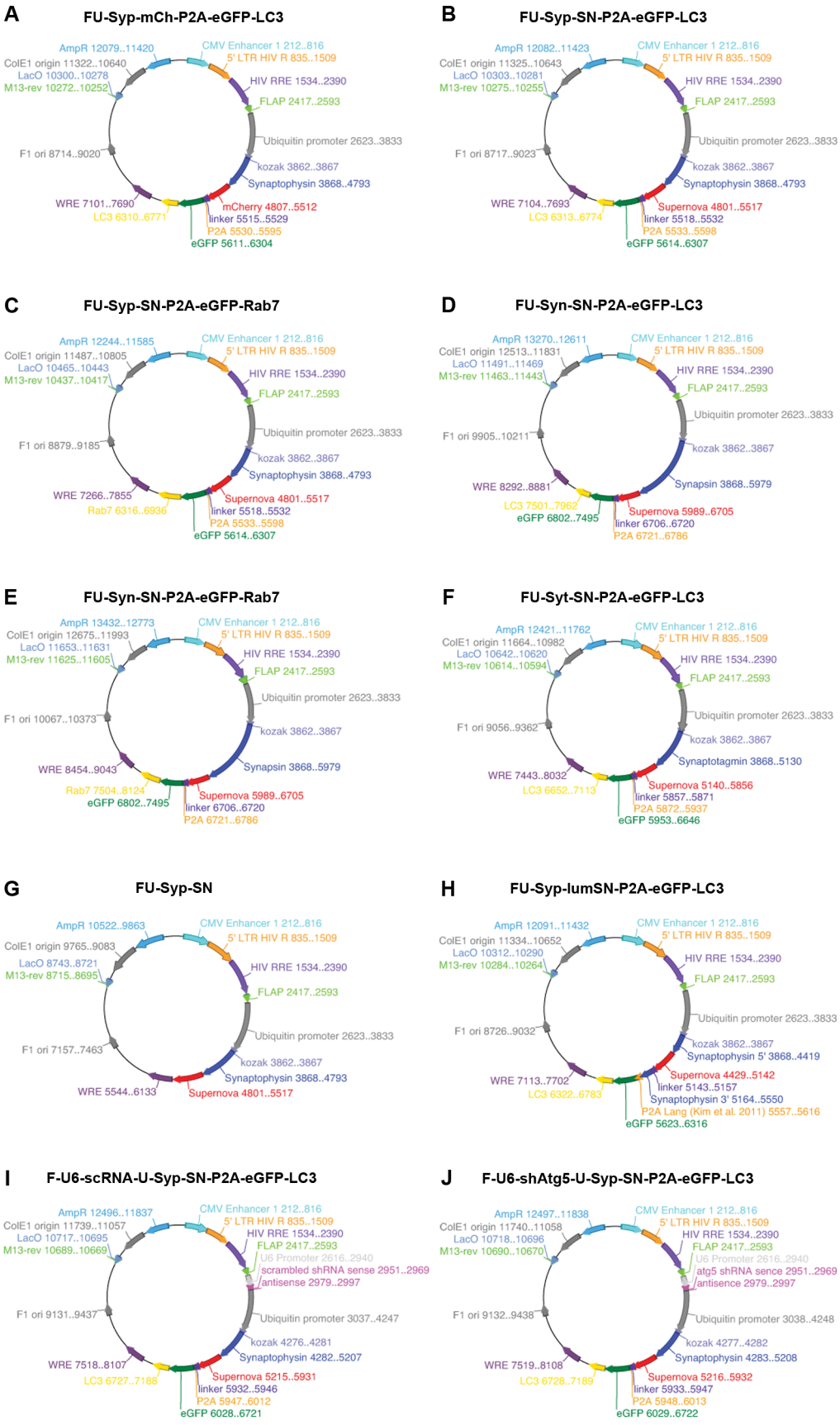

Figure 5 (legend on next page)

Figure 5: Lentiviral vectors. All vectors are based on the lentiviral shuttle vector FUGW by Lois et al. (Lois et al., 2002). (A) FU-Syp-mCherry-P2A-eGFP-LC3. (B) FU-Syp-Supernova-P2A-eGFP-LC3. (C) FU-Syp-Supernova-P2A-eGFP-Rab7. (D) FU-Syn-Supernova-P2A-eGFP-LC3. (E) FU-Syn-Supernova-P2A-eGFP-Rab7. (F) FU-Syt-Supernova-P2A-eGFP-LC3. (G) FU-Syp-Supernova. (H) FU-Syp-lumSupernova-P2A-eGFP-LC3. (I) F-U6-scRNA-U-Syp-Supernova-P2A-eGFP-LC3. (J) F-U6-shAtg5-U-Syp-Supernova-P2A-eGFP-LC3.

Again, to allow monitoring of Rab7 after Syn-Supernova bleaching, LC3 was replaced in FU-Syn-Supernova-P2A-eGFP-LC3 by Rab7 to form FU-Syn-Supernova-P2A-eGFP-Rab7. The vectors FU-eGFP-LC3 and FU-RFP-LC3 were created by exchanging GFP in the FUGW vector with the eGFP-LC3/RFP-LC3 (LC3, U05784.1) segment from FU-ptf-LC3 (Okerlund et al., 2017). The vector FU-eGFP-shAtg5 and FU-eGFP-UbK_0 was generated as described previously (Okerlund et al., 2017). All final constructs were verified by both restriction digest and sequencing.

5.2 Cell culture

HeLa/HEK293 cells and primary mouse hippocampal neurons were cultured under sterile conditions on laminar flow clean benches (Safe 2020, Thermo Fisher Scientific, Waltham, USA) and incubated in a humidified 5% CO_2 and 95% air atmosphere at 37°C (HERAcell 150i CO_2 incubator, Thermo Fisher Scientific, Waltham, USA).

5.2.1 HeLa/HEK293 cell culture and infection

HeLa or HEK293 cells were maintained in DMEM complete medium (DMEM, 10%FCS, 1%P/S) (Thermo Fisher Scientific, Waltham, USA). Medium was changed every 2 to 4 days. HeLa cells were routinely passaged at 80% confluence. Cells were washed with PBS and subsequently treated with 0.05% Trypsin-EDTA (Thermo Fisher Scientific, Waltham, USA) for 1 min at 37°C. Trypsin was inhibited using DMEM complete medium, afterwards cells were detached from the flask by pipetting, counted and re-plated at a density of 30k per 1cm^2 onto glass coverslips. 24 hours after plating, HeLa cells were infected with lentivirus adding 100µl per 6-well. 3 days after infection, DMEM was exchanged to EBSS medium (Thermo Fisher Scientific, Waltham, USA) supplemented with 100µM chloroquine (Sigma-Aldrich, St. Louis, USA) in order to induce autophagy and incubated for 2 hours at 37°C. Control cells were left untreated.

5.2.2 Preparation of cultured cortical/hippocampal neurons

All procedures for experiments involving animals were approved by the animal welfare committee of Charité Medical University and the Berlin state government. For live cell imaging and immunocytochemistry, mouse cortical or hippocampal neuron cultures from mouse WT animals (C57BL/6J) of either sex were prepared on glass coverslips using the Banker protocol (Banker and Goslin, 1988; Meberg and Miller, 2003) or on µ-Slide 8 Well culture dishes (ibidi GmbH, Martinsried, Germany). For Banker cultures, astrocytes were prepared from mouse WT cortices P0-2 and seeded on 6-well or 12-well plates at a density of 10k per 1cm^2 5-7 d before the addition of neurons (see below). Neuronal cultures were prepared from cortices or hippocampi dissected from WT mice P0-2 brains in cold Hanks' Salt Solution (Millipore, Darmstadt, Germany), followed by a 30 min incubation in enzyme solution (DMEM (Gibco, Thermo Fisher Scientific, Waltham, USA), 3.3mM Cystein, 2mM $CaCl_2$, 1mM EDTA, 20U/ml Papain (Worthington, Lakewood, USA)) at 37°C. Papain reaction was inhibited by the incubation of cortices or hippocampi in inhibitor solution DMEM, 10% fetal calf serum (FCS) (Thermo Fisher Scientific, Waltham, USA), 38mM BSA (Sigma-Aldrich, St. Louis, USA) and 95mM Trypsin Inhibitor (Sigma-Aldrich, St. Louis, USA) for 5 min. Afterwards, cells were triturated in NBA (Neurobasal-A Medium, 2% B27, 1% Glutamax, 0.2%P/S) (Thermo Fisher Scientific, Waltham, USA) by gentle pipetting up and down. Isolated neuronal cells were plated onto nitric acid washed and poly-l-lysine coated glass coverslips with paraffin dots at a density of 10k per 1cm^2. After 1.5h the coverslips were placed upside down onto the prepared astrocytes and co-cultured in NBA at 37°C and 5%, for 13-15 d (days in vitro, DIV) before starting experiments. For cultures on multi-well culture dishes, dissociated hippocampal neurons were plated directly onto µ-Slide 8 Well Grid-500 ibiTreat culture dishes (ibidi GmbH, Martinsried, Germany) at a density of 25k per 1cm^2 and maintained in NBA at 37°C, 5% CO_2, for 13-15 d before starting experiments.

5.3 Lentivirus production

All lentiviral particles were provided by the Viral Core Facility of the Charité – Universitätsmedizin Berlin and were prepared as described previously (Lois et al., 2002). Briefly, HEK293T cells were cotransfected with 10µg of shuttle vector, 5µg of helper plasmids pCMVdR8.9, and 5µg of pVSV.G with X-tremeGENE 9 DNA transfection reagent (Roche Diagnostic). Virus containing cell culture supernatant was collected after 72h and filtered for purification. Aliquots were flash-frozen in liquid nitrogen and stored at −80°C. Primary hippocampal neurons or HeLa/HEK293 cells were infected with 5µl per 1cm^2 (sparse infection for imaging) or with 20µl per 1cm^2 (high infection for electron microscopy and Western Blot) of the viral solution (0.5-1x10^6 IU/ml) 2-3 d post-plating.

5.4 Immunocytochemistry

5.4.1 Immunocytochemistry of HeLa/HEK293 cells

Cells were fixed with 4% PFA in PBS for 4 min at RT and washed with PBS twice. All following steps were performed at RT. Permeabilization of the cells was obtained by three washing steps with PBS + 0.2% Tween-20 (PBS-T) for a total of 30 min followed by incubation with PBS-T with 5% normal goat serum (NGS) (=blocking solution) for another 30 min. The primary antibody was diluted in blocking solution and cells were incubated in this solution for 45 min. The following antibodies were used: primary antibodies against LC3 (1:500; rabbit; MBL International, Woburn, USA; Cat# PM036Y), p62 (1:200; mouse; BD, Heidelberg, Germany; Cat# 610833). Afterwards cells were washed three times in PBS-T for 10 minutes each. The secondary antibody, diluted in PBS-T 1:1000 (Thermo Fisher Scientific, Waltham, USA), was put onto the cells for 60 min and washed away twice with PBS-T and once with PBS for 10 minutes each. Finally, coverslips were mounted using ProLong Diamond Antifade Mountant (Thermo Fisher Scientific, Waltham, USA).

5.4.2 Immunocytochemistry of hippocampal neurons

Primary mouse hippocampal neurons (expressing FU-Syp-mCherry/Supernova-P2A-eGFP-LC3 or uninfected), DIV 13-15, were treated with either 1µM or 2µM rapamycin (Sigma-Aldrich, St. Louis, USA) for either 10 min or 2 hours, or with 1µM wortmannin (InvivoGen, San Diego, USA) in addition to rapamycin. Untreated cells were used as a control. Additionally, untreated cells, expressing FU-Syp-mCherry/Supernova-P2A-eGFP-LC3, were used to examine the colocalization of Syp-Supernova/mCherry and Homer1. After treatment, cells were fixed with 4% PFA in PBS for 4 minutes and washed twice with PBS (10 min each). Afterwards, cells were permeabilized with PBS + 0.2% Tween-20 (PBS-T) three times for 10 minutes each. Following a 30 minutes incubation with 5% normal goat serum (NGS) in PBS-T (=blocking solution), neurons were incubated with primary antibodies, diluted in blocking solution, for 45 minutes at RT. The following antibodies were used: primary antibody against LC3 (1:500; rabbit; Sigma-Aldrich, St. Louis, USA; Cat# L7543), Homer1 (1:1000; guinea pig; Synaptic Systems, Göttingen, Germany; Cat# 160004), Synaptophysin1 (1:1000; mouse; Synaptic Systems, Göttingen, Germany; Cat# 101011), MAP2 (1:2000; chicken; Millipore, Darmstadt, Germany; Cat# AB5543), p62 (1:500; rabbit; MBL International, Woburn, USA; Cat# PM045), Killerred (recognizes Supernova) (1:1000; rabbit; evrogen, Moscow, Russia; Cat# AB961), GFP (1:1000; chicken; Thermo Fisher Scientific, Waltham, USA; Cat# A10262), mCherry (1:1000; rabbit; Abcam, Cambridge, UK; Cat#

ab167453), Bassoon (1:500; guinea pig; Synaptic Systems, Göttingen, Germany; Cat# 141004), Synaptotagmin1 (1:1000; mouse; Synaptic Systems, Göttingen, Germany; Cat# 105011), Synapsin1 (1:1000; rabbit, Abcam, Cambridge, UK; Cat# ab64581), Chmp2b (1:200; rabbit; Abcam, Cambridge, UK; Cat# ab33174). Afterwards cells were washed three times in PBS-T for 10 minutes each, incubated with the secondary antibody, diluted in PBS-T 1:1000 (Thermo Fisher Scientific, Waltham, USA), for 60 minutes and washed twice with PBS-T and once with PBS for 10 minutes each. Finally, coverslips were dipped in H_2O and mounted in ProLong Diamond Antifade Mountant (Thermo Fisher Scientific, Waltham, USA).

5.4.3 Immunocytochemistry of Bassoon KO neurons

Primary mouse hippocampal neurons from Bassoon knockout mice and wildtype littermates were prepared in Magdeburg as described previously (Davydova et al., 2014). Neurons (expressing FU-ptf-LC3/FU-RFP-LC3/FU-eGFP-shAtg5), DIV 13-15, were either treated with 1µM wortmannin for 16 hours or left untreated and fixed and quenched with 25mM glycine in PBS. Afterwards, cells were permeabilized and blocked with PBS + 2% BSA + 5% NGS + 0.2% Tween-20 for 1 hour. Subsequently, neurons were incubated with primary antibodies, diluted in PBS + 2% BSA + 5% NGS (=blocking solution), for 1 hour at RT. The following antibodies were used: primary antibody Synaptophysin1 (1:1000; mouse; Synaptic Systems, Göttingen, Germany; Cat# 101011). Afterwards cells were washed three times in blocking solution for 10 minutes each, incubated with the secondary antibody (Thermo Fisher Scientific, Waltham, USA), diluted in blocking solution, for 60 minutes and washed once with blocking solution and twice with PBS for 10 minutes each. Finally, coverslips were dipped in H_2O and mounted in ProLong Diamond Antifade Mountant (Thermo Fisher Scientific, Waltham, USA).

5.5 Western Blot analyses

Cultured hippocampal neurons, either infected with lentivirus at DIV 2-3 (TD) or uninfected (UT), were grown on 6-well-plates (6 Well Advanced TC™ Plate, greiner bio-one, Kremsmünster, Austria) at a density of 20k per $1cm^2$ until DIV 13-17. For rapamycin experiments, cells were treated with 1µM rapamycin and 100nM bafilomycin A1 (Sigma-Aldrich, St. Louis, USA) or with bafilomycin A1 alone (control) for 2 hours before lysis. All following steps were performed at 4°C. Neurons were kept on ice and washed twice with cold PBS. Subsequently, cells were detached by mechanical force. For total lysates, isolated cells were centrifuged at 4000rpm for 10 min and resuspended in 100µl lysis buffer (50mM Tris pH 7.9, 150mM NaCl, 5mM EDTA, 1%

Triton X-100, 1% NP-40, 0.5% Deoxycholate, protease inhibitor cOmplete Tablets 1x) and incubated for 5 minutes on ice. Afterwards, cell suspension was centrifuged at 13000rpm for 10 min after which the supernatant was transferred into a new tube. For synaptosome suspension (and cytosol fraction) preparation, cortical or hippocampal neurons were treated with 2µM rapamycin for either 10 minutes or 2 hours. Next, cells were lysed in Syn-PER Synaptic Protein Extraction Reagent (Thermo Fisher Scientific, Waltham, USA) according to the manufacturers instructions. Briefly, cells were washed with cold PBS, detached by mechanical force in 100-200µl Syn-PER Reagent and centrifuged at 1200g for 15 min. The supernatant was centrifuged at 15000g for 20 min and the cytosol fraction was collected. Last, the synaptosome pellet was resuspended in Syn-PER Reagent. Subsequently, the protein concentration was determined using the Pierce BCA Protein Assay Kit (Thermo Fisher Scientific, Waltham, USA). The same amount of total protein (6.5-10µg) was then separated by SDS-PAGE and transferred onto a PVDF membrane. Afterwards, the membrane was blocked in 5% milk in TBS-T (20mM Tris, 150mM NaCl, 0.1% Tween-20) for 1 hour followed by primary antibody incubation (1:1000 in 3% milk in TBS-T) over night or for 72 hours at 4°C. The following antibodies were used: primary antibody against mCherry (1:1000; rabbit; Abcam, Cambridge, UK; Cat# ab167453), LC3 (1:1000; rabbit; Sigma-Aldrich, St. Louis, USA; Cat# L7543), beta-Tubulin III (1:2000; mouse; Sigma-Aldrich, St. Louis, USA; Cat# T8660), Actin (1:1000; rabbit; Sigma-Aldrich, St. Louis, USA; Cat# A2066), Killerred (recognizes Supernova) (1:1000; rabbit; evrogen, Moscow, Russia; Cat# AB961) and Synaptophysin1 (1:1000; mouse; Synaptic Systems, Göttingen, Germany; Cat# 101011). Afterwards, the membrane was washed three times with TBS-T for 10 minutes each and incubated with HRP-conjugated secondary antibody (1:2500 in 3% milk in TBS-T) (Sigma-Aldrich, St. Louis, USA). for 1 hour at RT. Afterwards, the membrane was washed three times with TBS-T and bands were visualized using the imaging system Fusion FX7 (Vilber, Collégien, France) using 20x LumiGLO Reagent and 20x Peroxidase (Cell Signaling, Danvers, USA).

5.6 Dihydroethidium assay

HEK293 cells were seeded on a µ-Slide 8 Well (ibidi GmbH, Martinsried, Germany) culture dish with a density of 30k per 1cm^2 and transfected one day later using X-tremeGENE 9 DNA Transfection Reagent (Roche Diagnostics, Mannheim, Germany) according to the manufacturers instructions. 24-48 hours after transfection, DMEM medium was changed and dihydroethidium (DHE) was added to a final concentration of 10µM (Thermo Fisher Scientific, Waltham, USA) in DMEM complete medium. DHE incubation for 20 min at 37°C was followed by two washing steps

with 37°C warm PBS. Afterwards, PBS was exchanged with tyrodes buffer and live cells were imaged before bleaching, immediately after bleaching and 15 minutes after bleaching.

5.7 Bleaching of Supernova

5.7.1 Bleaching of HEK293 cells expressing Supernova-constructs

HEK293 cells were seeded on glass coverslips and transfected with FU-Syp-Supernova-P2A-eGFP-LC3 using X-tremeGENE 9 DNA Transfection Reagent according to the manufacturers instructions. At DIV 2 post transfection, live cell experiments were performed using a custom-built chamber designed for liquid perfusion at 37°C. Cells were imaged in tyrodes buffer pH 7.4 (119mM NaCl, 2.5mM KCl, 25mM HEPES, 2mM $CaCl_2$, 2mM $MgCl_2$, 30mM glucose). The Supernova signal was bleached for three times 30 s, respectively, using 563nm wavelength light from a mercury lamp (100% HXP 120 V, 43 HE filter set 563/581). Images were acquired before and after each bleaching step. Additionally, images were acquired 5 and 15 minutes after bleaching.

5.7.2 Bleaching of primary hippocampal neurons expressing Supernova/mCherry-constructs

Primary hippocampal neurons grown in µ-Slide 8 Well Grid-500 ibiTreat (ibidi GmbH, Martinsried, Germany) culture dishes expressing FU-Syp/Syn/Syt-Supernova/mCherry/lumSupernova-P2A-eGFP-LC3/Rab7 were imaged at DIV 13-15 in Neurobasal Medium without phenol red (Thermo Fisher Scientific, Waltham, USA) at 37°C. Afterwards, a smaller diaphragm restricted area within the field of view was bleached for 60 seconds using 563nm wavelength light from a mercury lamp (100% HXP 120 V, 43 HE filter set 563/581). Immediately after bleaching, a second image was taken, confirming the radius of the bleached area. Neurons were fixed at different time points (2-10 min, 56-64 min, 116-124 min) after bleaching Supernova/mCherry and immunostained with antibodies against Supernova (using a Killerred antibody), mCherry, GFP, Bassoon, Chmp2b, Synaptotagmin1, Synaptophysin1 and/or LC3 (for procedure see immunocytochemistry of hippocampal neurons) (Figure 6). To scavenge ROS, 60µM N-acetyl-L-cysteine (NAC) (in DMEM, Sigma-Aldrich, St. Louis, USA) was added right before the bleaching and kept on the cells until fixation. For autophagy inhibition, 1µM wortmannin was added right before the bleaching and kept on the cells till they were fixed. For

Synapsin dispersion experiments, fields of views were imaged, the medium was changed to tyrodes 60mM KCl, followed by immediate bleaching for 60 seconds. Subsequent bleaching, tyrodes 60mM KCl was exchanged to Neurobasal medium without phenol red and images were taken. Afterwards, neurons were fixed after 1 hour. After immunostaining, the same fields of view including the bleached areas were imaged utilizing the grid on the µ-Slide 8 Well Grid-500 culture dishes.

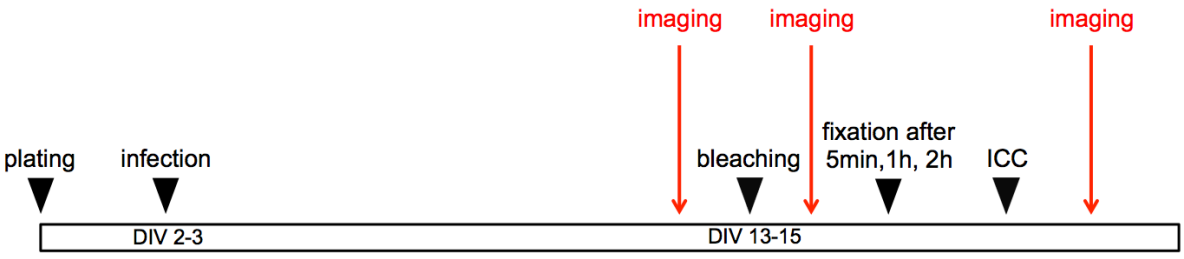

Figure 6: Schematic of bleaching of primary hippocampal neurons expressing Supernova-construct. Neurons were infected at 2-3 DIV and bleaching assay started at 13-15 DIV. After Bleaching and fixation, neurons were immunostained (ICC) against various proteins and reimaged using the alphabetical grid on the µ-Slide 8 Well Grid-500 plates.

5.8 Basal autophagy in primary hippocampal neurons

Primary hippocampal neurons in µ-Slide 8 Well Grid-500 ibiTreat (ibidi GmbH, Martinsried, Germany) culture dishes expressing FU-eGFP-LC3 were left untreated and fixed at DIV 13-15. Afterwards, neurons were immunostained with antibodies against GFP, Bassoon and Synaptophysin1, Synapsin1 or Synaptotagmin1 (for procedure see immunocytochemistry of hippocampal neurons).

5.9 FM dye uptake

Primary hippocampal neurons were used for live cell experiments. They were performed using a custom-built chamber designed for liquid perfusion at 37°C. For rapamycin experiments, neurons were treated with either 1µM rapamycin alone or with 1µM rapamycin and 1µM wortmannin for 2 hours prior to the experiment. Neurons were imaged in tyrodes buffer pH 7.4 (119mM NaCl, 2.5mM KCl, 25mM HEPES, 2mM $CaCl_2$, 2mM $MgCl_2$, 30mM glucose) and stimulated for 90 seconds in 90mM KCl buffer (31.5mM NaCl, 90mM KCl, 25mM HEPES, 2mM

$CaCl_2$, 2mM $MgCl_2$, 30mM glucose) containing FM 4-64 dye (Thermo Fisher Scientific, Waltham, USA) at a final concentration of 1µg per ml. After stimulation, cells were washed with 20ml tyrodes buffer and subsequently imaged. Untreated cells were used as a control. For Supernova experiments, primary hippocampal neurons, expressing FU-Syp-Supernova-P2A-eGFP-LC3 or FU-Syn-Supernova-P2A-eGFP-LC3, were used for live cell experiments. Neurons were stimulated for 90 seconds in 90mM KCl buffer containing FM 1-43 dye (Thermo Fisher Scientific, Waltham, USA) at a final concentration of 1µg per ml. After stimulation, cells were washed with 20ml tyrodes buffer and subsequently imaged. In order to inhibit autophagy during Supernova experiments, 1µM wortmannin was added to neurons 1 min before light activation of Supernova and ~ 5 min before stimulation. Note that wortmannin was present in all solutions (90mM KCl FM 1-43 dye, tyrodes washing).

5.10 Electron microscopy

Cultured hippocampal neurons were plated on astrocytes on carbon coated 6mm sapphire disks at a density of 20k per 1cm² and infected with FU-Syp-Supernova-P2A-eGFP-LC3 at DIV 2-3. To better correlate regions of interest at the fluorescence and electron microscopy level, carbon was coated in the shape of an alphabetical grid on sapphire disks with the help of a metal mask (finder grid, Plano GmbH, Wetzlar, Germany). After a total of 13-15 days in culture, the sapphire disks were transferred into uncoated µ-Slide 8 Well to perform the bleaching experiment (for procedure see bleaching of primary hippocampal neurons expressing Supernova-constructs). Cryo-fixation using a high pressure freezing machine (EM-ICE, Leica, Wetzlar, Germany) was conducted at different time points after bleaching (10 min, 40 min) in Neurobasal medium without phenol red with the addition of a drop of 10% Ficoll solution (Sigma-Aldrich, St. Louis, USA) to prevent ice crystal damage. After freezing, samples were cryo-substituted in anhydrous acetone containing 1% glutaraldehyde, 1% osmium tetroxide and 1% milliQ water in an automated freeze-substiution device (AFS2, Leica). The temperature was kept for 4h at -90°C, brought to -20°C (5°C/h), kept for 12h at -20°C and then brought from -20°C to +20°C (5°C/h). Once at room temperature, samples were *en-bloc* stained in 0.1% uranyl acetate in acetone, infiltrated in increasing concentration of Epoxy resin (Epon 812, EMS Adhesives, Delaware, USA) in acetone and finally embedded in pure Epon for 48h at 65°C. Sapphire disks were removed from the cured resin block by thermal shock. At this point the alphabetical grid was visible on the resin block and was used to find back the bleached regions. The corresponding areas were excised from the blocks for ultrathin sectioning. For each sapphire, as a control, an additional resin blocks was excised from the quadrant opposite to the bleached area. 50nm thick sections were obtained using an Ultracut ultramicrotome (UCT, Leica)

equipped with a Ultra 45 diamond knife (Ultra 45, DiATOME, Hatfield, USA) and collected on formvar-coated 200-mesh copper grids (EMS). Sections were counterstained with uranyl acetate and lead citrate and imaged in a FEI Tecnai G20 Transmission Electron Microscope (FEI, Hillsboro, USA) operated at 80-200 keV and equipped with a Veleta 2K x 2K CCD camera (Olympus, Hamburg, Germany). Around 200 electron micrographs were collected (pixel size = 0.7nm) for each sample. Data were analyzed blindly using the ImageJ software. Double-membraned structures per presynaptic terminal were counted.

5.11 Electrophysiology

Whole cell patch-clamp recordings were performed on autaptic hippocampal neurons at DIV 13–18. All recordings were obtained at ~ 25°C from neurons clamped at −70 mV with a Multiclamp 700B amplifier (Molecular Devices, Sunnyvale, USA) under the control of Clampex 10.4 software (Molecular Devices). Data were sampled at 10kHz and low-pass Bessel filtered at 3kHz. Series resistance was compensated at 70% and cells whose series resistance changed more than 25% throughout the recording session were excluded from the analysis. Neurons were immersed in standard extracellular solution consisting of 140mM NaCl, 2.4mM KCl, 10mM HEPES, 10mM glucose, 2mM $CaCl_2$ and 4mM $MgCl_2$. The borosilicate glass electrodes (3-8 MΩ) were filled with the internal solution containing 136mM KCl, 17.8mM HEPES, 1mM EGTA, 0.6mM $MgCl_2$, 4mM ATP-Mg, 0.3mM GTP-Na, 12mM phosphocreatine, and 50U/ml phosphocreatine kinase. All solutions were adjusted to pH 7.4 and osmolarity of ~ 300mOsm. Coverslips with cultured neurons were placed on Olympus IX73 microscope (Olympus, Hamburg, Germany) with 20x phase contrast objective. For Supernova bleaching, illumination from a Mercury Vapor Short Arc lamp (X-Cite 120PC Q, Excelitas Technologies, Waltham, USA) was filtered through a 560/20nm filter cube (Olympus U-FF mCherry) and controlled with a mechanical shutter. Lamp iris settings (100%) resulted in 71% bleaching of Supernova intensity (as compared to 22% of mCherry bleaching), after 60s of illumination. From each neuron, 6 sweeps of EPSCs were evoked with a 2ms voltage step from -70mV to 0mV at 0.2Hz. Sixty seconds illumination started immediately after end of 6^{th} sweep, and after 5 minutes of waiting second EPSC was recorded. Control condition without illumination included 6 min waiting period. During recordings with wortmannin, 1μM wortmannin solution was applied onto the cell using a fast-flow system with a rapid solution exchange time constant (20–30ms) from the beginning of first EPSC until end of recording session. Electrophysiological data were analyzed offline using Axograph X (Axograph Scientific, Berkeley, USA), Excel (Microsoft, Redmond, USA) and GraphPad Prism (GraphPad, La Jolla, USA).

5.12 Image acquisition and quantification

All images were acquired on a spinning disc confocal microscope (Zeiss Axio Observer.Z1 with Andor spinning disc and cobolt, omricron, i-beam laser) (Zeiss, Oberkochen, Germany) using either a 40x or 63x 1.4 NA Plan-Apochromat oil objective and an iXon ultra (Andor, Belfast, UK) camera controlled by iQ software (Andor, Belfast, UK). Images were processed using ImageJ and OpenView software (written by Dr. Noam Ziv, Technion Institute, Haifa, Israel). In brief with the OpenView software, multi-channel intensities were measured using a box routine associated with individual boutons. Boxes varied between 7x7 and 9x9 pixel in size, whereas settings were kept the same (e.g. thresholds). The average intensity (synaptic proteins, eGFP-LC3, FM 1-43/4-64 dye et cetera) was calculated from all picked puncta and normalized to the control (untreated or unbleached). For the LC3 intensity in the soma, for the bleaching efficacy of Supernova and for the DHE blue decrease analyses, neuronal somas or HEK293 cells were marked in ImageJ using the Polygon selection tool and mean intensities of the identified areas were measured. Intensities of numerous samples were averaged and plotted. Band intensities of Western Blots were analyzed with the help of ImageJ and the Analyze>Gels tool. For quantification of # of puncta separated axons or MAP2 positive dendrites were randomly picked and the number of puncta per unit length was counted manually. To quantify the number of excitatory synapses, Synaptophysin1/Homer1 double positive puncta along dendrites were counted manually. For Supernova experiments, axons were selected from live images showing no or little eGFP-LC3 staining before bleaching. All Supernova evaluations were normalized to the unbleached control. To determine the fraction of extrasynaptic eGFP-LC3 puncta positive for Syp-SN/Syn-SN/Syt-SN/Syp-lumSN/Synaptophysin1/Synaptotagmin1, multi-channel images were manually scanned for eGFP-LC3 puncta within the bleached area that were not colocalizing with Bassoon. Out of these extrasynaptic eGFP-LC3 puncta, the fraction of eGFP-LC3 puncta positive for a specific synaptic protein was quantified. The fraction of extrasynaptic Syp-SN/Syn-SN/Syt-SN/Syp-lumSN puncta positive for eGFP-LC3 was determined accordingly. For FM dye uptake intensities after rapamycin treatment, FM 1-43 positive puncta were analyzed using OpenView. For FM dye uptake intensities after Supernova bleaching, images of the Syp/Syn-Supernova signal taken before the bleaching were used as a mask to define Syp/Syn-Supernova positive puncta. Afterwards, FM 1-43 intensity in Syp/Syn-Supernova positive puncta was quantified using OpenView.

5.13 Experimental design and statistical analyses

Statistical design for all experiments can be found in the figure legends. Independent experiments equal independent cultures. All data representations and statististical analyses were done with GraphPad Prism.

6. Results

6.1 Rapamycin predominantly induces synaptic autophagy

To determine whether autophagy can be induced in hippocampal neurons, I first utilized the mTOR inhibitor rapamycin in Western Blot analyses. The soluble form of LC3 is defined as LC3-I and LC3 that is conjugated to the autophagosome is defined as LC3-II. Thus, LC3-II is an excellent marker to monitor autophagy (Fleming et al., 2011; Mizushima et al., 2010; Satoo et al., 2009). rapamycin is a widely used autophagy activator (Hernandez et al., 2012; Klionsky et al., 2012). For autophagy induction, hippocampal neurons were treated with 1µM rapamycin and 100nM bafilomycin A1 for 2 hours.

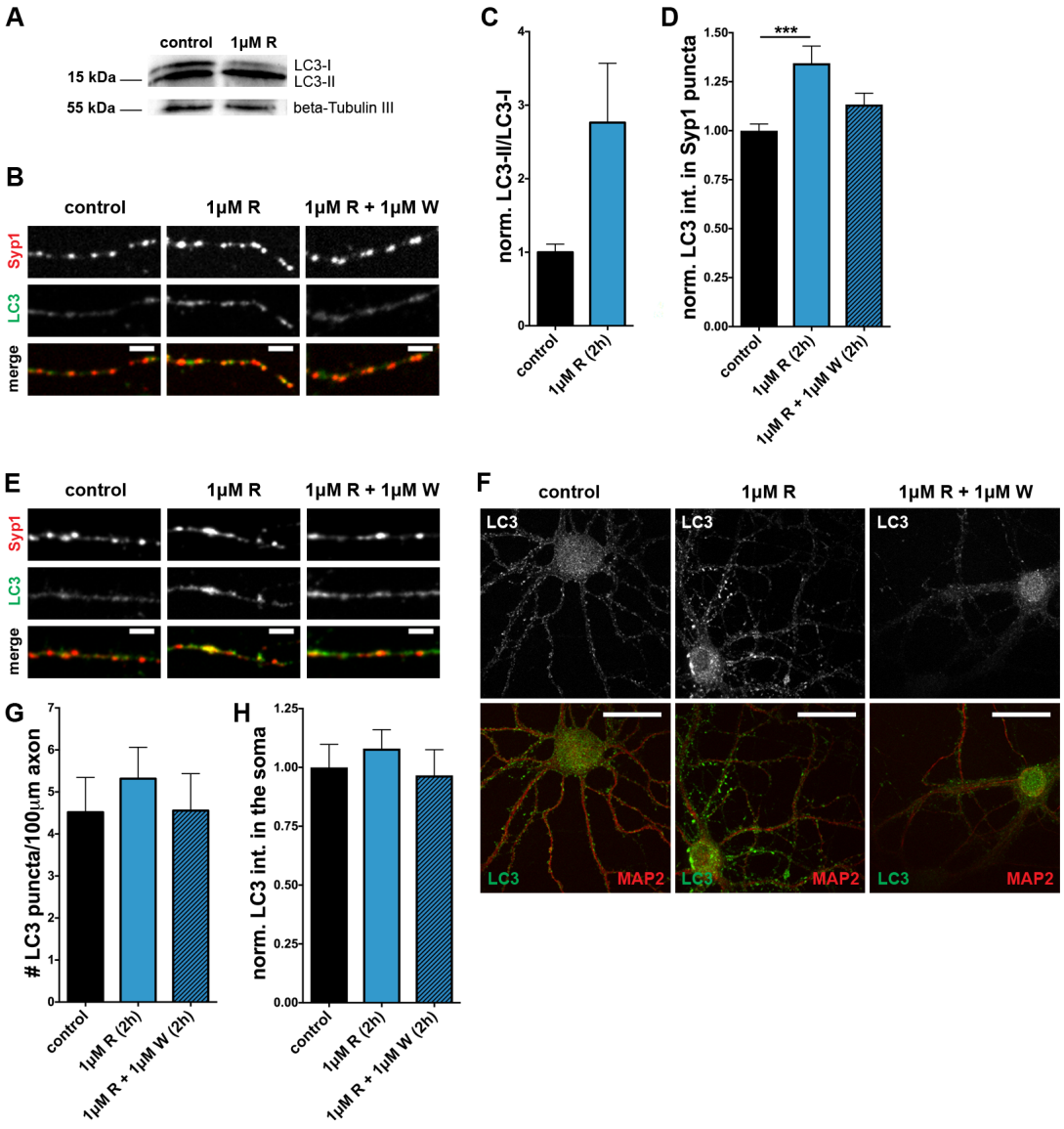

Figure 7: Rapamycin induces autophagy at synapses in hippocampal neurons. (A) Western Blot of lysates from hippocampal neurons treated with 100nM bafilomycin A1 alone (control) or 1µM

rapamycin and 100nM bafilomycin A1 (1μM R) for 2 hours and stained with antibodies against LC3 and beta-Tubulin-III. (B) Images of hippocampal neurons treated with either 1μM rapamycin (1μM R) or 1μM rapamycin and 1μM wortmannin (1μM R + 1μM W) for 2 hours before fixation and stained with antibodies against Synaptophysin1 (Syp1) and LC3. Control neurons were left untreated. (C) Quantification of the normalized LC3-II/LC3-I ratio from (A). Note that rapamycin causes a high but insignificant change in the ratio (control = 1 ± 0.111, 3 independent experiments; 1μM R = 2.76 ± 0.807, 3 independent experiments). (D) Quantification of the normalized LC3 intensity in Synaptophysin1 positive puncta from (B). Note that the LC3 intensity at rapamycin treated boutons is increased and that this effect is rescued by the addition of wortmannin (control = 1 ± 0.034, n = 643 synapses, 4 independent experiments; 1μM R = 1.35 ± 0.088, n = 607 synapses, 4 independent experiments; 1μM R + 1μM W = 1.13 ± 0.057, n = 532 synapses, 4 independent experiments). (E and F) Images of hippocampal neurons treated with either 1μM rapamycin (1μM R) or 1μM rapamycin and 1μM wortmannin (1μM R + 1μM W) for 2 hours before fixation and stained with antibodies against LC3 and Synaptophysin1 (E) or LC3 and the somatodendritic marker MAP2 (F). Control neurons were left untreated. (G) Quantification of the number of LC3 puncta per 100μm axon of (E). No differences in the number of LC3 puncta was observed between all conditions tested (control = 4.52 ± 0.828, n = 33 axons, 4 independent experiments; 1μM R = 5.32 ± 0.746, n = 33 axons, 4 independent experiments; 1μM R + 1μM W = 4.56 ± 0.880, n = 34 axons, 4 independent experiments). (H) Quantification of the normalized LC3 intensity in the soma from (F). Note that there is no change in the somatic LC3 (control = 1 ± 0.098, n = 22 somas, 4 independent experiments; 1μM R = 1.08 ± 0.080, n = 18 somas, 4 independent experiments; 1μM R + 1μM W = 0.97 ± 0.109, n = 18 somas, 4 independent experiments). Scale bars: 5μm (A and E), 40μm (F). Error bars represent SEM. ANOVA Tukey's multiple comparisons test (C, G and H) and unpaired T-test (D) were used to evaluate statistical significance. ****p<0.0001, ***p<0.001, **p<0.01, *p<0.05.

Indeed, an increased ratio between the lipidated LC3-II (Mizushima et al., 2010; Satoo et al., 2009) and the cytosolic form of LC3 (LC3-I) were observed, indicating that mTOR inhibition can induce autophagy in primary hippocampal neurons (Figure 7A and C).

Rapamycin was also shown to induce the formation of autophagosomes in the presynapse (Hernandez et al., 2012). In order to examine whether rapamycin is a potent drug to induce autophagy at synapses in my hands, hippocampal neurons were treated with 1μM rapamycin for 2 hours and subsequently fixed and stained for endogenous LC3 and Synaptophysin1 levels. Subsequently, synaptic LC3 intensities were measured in Synaptophysin1 positive synapses. Interestingly, rapamycin treatment leads to a significant increase in endogenous LC3 levels indicating that the cytoplasmically abundant protein LC3 accumulates at synaptic sites upon autophagy induction (Figure 7B and D). The observed increase in endogenous LC3 at synapses is dependent on autophagy induction as blocking the pathway with the PI3K inhibitor wortmannin (Blommaart, 1997; McNamara and Degterev, 2011) blocks the accumulation of LC3 upon rapamycin treatment resulting in endogenous LC3 levels that are not significantly different to control conditions without autophagy induction (Figure 7D).

As rapamycin treatment leads to an increase in endogenous LC3 at synapses, I further wanted to know whether this change also led to an accumulation of autophagic vacuoles leaving the synapse. Therefore endogenous LC3 positive puncta per axon unit length were counted. Surprisingly, within the 2 hours of autophagy induction, the number of LC3 puncta per 100μm

axon did not change. No differences between treated neurons and untreated control neurons could be observed (Figure 7E and G). In line with this, endogenous levels of LC3 are not altered in neuron somas after rapamycin treatment (Figure 7F and H). To summarize, these data indicate that rapamycin predominantly induces synaptic autophagy as monitored by antibody staining against endogenous LC3.

6.2 Rapamycin treatment leads to impaired FM dye uptake and loss of synapses

After being able to induce autophagy at synapses, I also examined whether increased autophagy rates have an impact on synapse integrity and/or function. Here, an FM dye uptake experiment, as a readout for synaptic function was chosen, as this reflects active endocytosis processes induced by preceding exocytosis events (Gaffield and Betz, 2006). FM dye uptake efficiencies were then compared between rapamycin treated and untreated hippocampal neurons. Dye uptake was induced using a high potassium stimulation followed by a thorough wash. Subsequently, live cells were imaged and FM dye intensities were quantified. Neurons treated with 1μM rapamycin for 2 hours showed a significant decrease in FM dye uptake compared to untreated control cells (Figure 8A and C). Interestingly, the amount of FM dye uptake was still reduced when the PI3K inhibitor wortmannin was present during the rapamycin treatment (Figure 8A and C).

An interesting question is whether the reduced synaptic function was also associated with affected synapse integrity following the induction of autophagy. This was tested by counting the number of puncta double positive for the presynaptic marker Synaptophysin1 (Syp1) and for the postsynaptic marker Homer1 per unit length of dendrite after treating neurons with rapamycin. Interestingly, autophagy induction by rapamycin leads to a significant decrease in the number of synapses along dendrites compared to untreated control cells (Figure 8B and D). Again the loss of synapses could not or only partially be rescued in the presence of wortmannin. Quantification of single positive puncta per dendrite unit length indicates a more severe effect of increased autophagy on the presynaptically localized synaptic vesicle protein Synaptophysin1 (Figure 8E) compared to the postsynaptically localized protein Homer1 (Figure 8F).

Together, these data imply that elevated autophagy through strong chemical induction leads to a reduced recycling efficiency at synapses, which may also reflect the decrease of the total recycling pool of vesicles, and ultimately to a loss of synapses.

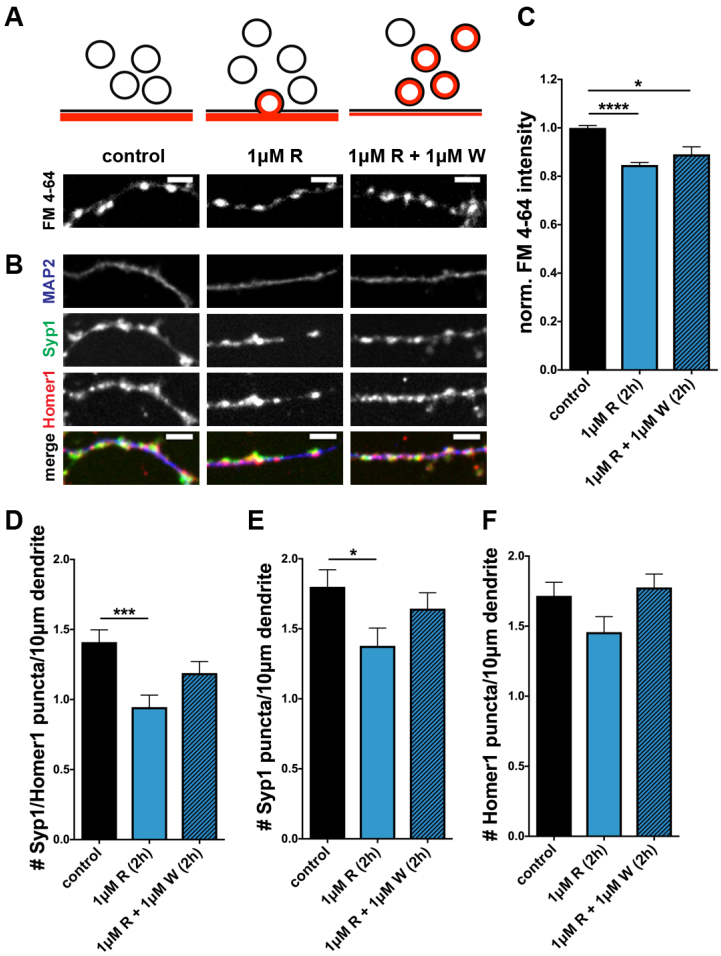

Figure 8: Rapamycin treatment leads to decreased FM dye uptake and a loss of Synaptophysin1/Homer1 positive synapses. (A) Schematic of FM dye uptake during a stimulus. Images of hippocampal neurons treated with either 1µM rapamycin (1µM R) or 1µM rapamycin and 1µM wortmannin (1µM R + 1µM W) for 2 hours before FM 4-64 dye uptake experiments. Control neurons were left untreated. (B) Images of hippocampal neurons treated with either 1µM rapamycin (1µM R) or 1µM rapamycin and 1µM wortmannin (1µM R + 1µM W) for 2 hours before fixation and stained with antibodies against Synaptophysin1 (Syp1), the postsynaptic marker Homer1 and MAP2. Control neurons were left untreated. (C) Quantification of the normalized FM 4-64 intensity from (A). Note that rapamycin treated boutons show less FM dye intensity (control = 1 ± 0.010, n = 1912 synapses, 4 independent experiments; 1µM R = 0.85 ± 0.010, n = 1493 synapses, 4 independent experiments; 1µM R + 1µM W = 0.89 ± 0.031, n = 133 synapses, 2 independent experiments). (D) Quantification of the number of synapses per 10µm dendrite from (B). Not that the number of synapses is significantly reduced in the rapamycin treated neurons and that this effect is partly rescued by addition of wortmannin (control = 1.41 ± 0.088, n = 48 dendrites, 4 independent experiments; 1µM R = 0.95 ± 0.085, n = 43 dendrites, 4 independent experiments; 1µM R + 1µM W = 1.19 ± 0.083, n = 46 dendrites, 4 independent experiments). (E) Quantification of the number of Synaptophysin1 positive puncta per 10µm dendrite from (B) (control = 1.80 ± 0.122, n = 45 dendrites, 4 independent experiments; 1µM R = 1.38 ± 0.127, n = 41 dendrites, 4 independent experiments; 1µM R + 1µM W = 1.64 ± 0.113, n = 41 dendrites, 4 independent experiments). (F) Quantification of the number of Homer1 positive puncta per 10µm dendrite from (B) (control = 1.72 ± 0.097, n = 45 dendrites, 4 independent experiments; 1µM R = 1.46 ± 0.110, n = 41 dendrites, 4 independent experiments; 1µM R + 1µM W = 1.78 ± 0.095, n = 41 dendrites, 4 independent experiments). Scale bars: 5µm. Error bars represent SEM. ANOVA Tukey's multiple

comparisons test was used to evaluate statistical significance. ****p<0.0001, ***p<0.001, **p<0.01, *p<0.05.

6.3 Establishing a vector system to specifically monitor presynaptic autophagy

The autophagy marker LC3 is an abundant protein present in both the axonal and the somatodendritic arbor, making it very difficult to distinguish between pre- and postsynaptic LC3 levels. Therefore I established a reporter construct (FU-Syp-mCherry-P2A-eGFP-LC3) that enables me to mainly monitor presynaptic and axonal autophagy. FU-Syp-mCherry-P2A-eGFP-LC3 is a lentiviral vector expressing the synaptic vesicle protein Synaptophysin tagged with mCherry and the autophagy marker LC3 fused to eGFP under the control of an ubiquitin promotor (Figure 10A). To allow the independent expression of Synaptophysin-mCherry and eGFP-LC3, the sequence of the self-cleaving peptide P2A was placed between the two coding sequences (Figure 10A). Through a sparse infection this vector system allows one to follow eGFP-LC3 level at Synaptophysin-mCherry positive synapses formed on top of uninfected neurons (Figure 9).

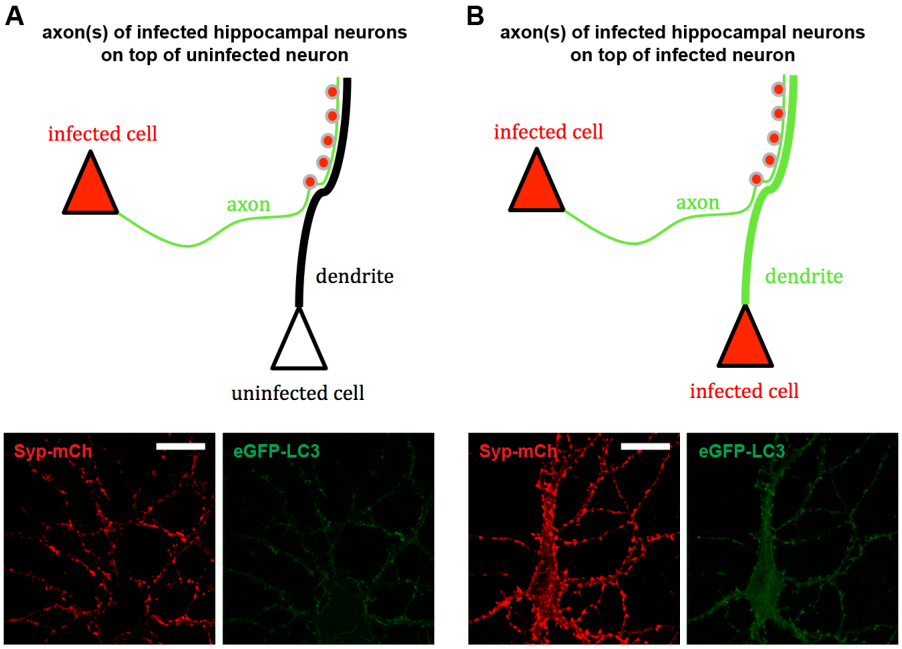

Figure 9: Monitoring presynaptic autophagy with FU-Syp-mCherry-P2A-eGFP-LC3. Schematic of sparse infection (A) versus high infection (B). Sparse infection (A) enables the reviewer to follow axons from infected neurons growing on top of uninfected neurons. The measurable eGFP-LC3 level only comes from the presynaptic/axonal compartment, as dendrites from uninfected neurons do not express eGFP-LC3. In contrast, high infection (B) leads to a high somatodendritic eGFP-LC3 background, making it impossible to discriminate between pre- and postsynaptic eGFP-LC3 signals. Scale bars: 30µm.

Initially, I analyzed whether the newly designed vector system was able to detect autophagy induction in transfected HeLa cells. Under basal conditions, Synaptophysin-mCherry and eGFP-LC3 both exhibited a largely diffuse cytoplasmic pattern. However, following autophagy induction with amino acid starvation (EBSS) and inhibition of autophagy turnover through chloroquine (Galluzzi et al., 2016; Klionsky et al., 2012) eGFP-LC3 altered its distribution from primarily diffuse/cytoplasmic to punctate (Figure 10B). Moreover, the newly formed LC3 positive vesicles colocalize with the autophagy receptor p62 (Figure 10B). Importantly, Synaptophysin-mCherry retained its diffuse cytosolic pattern and was not recruited into autophagic vacuoles (AVs) following autophagy induction.

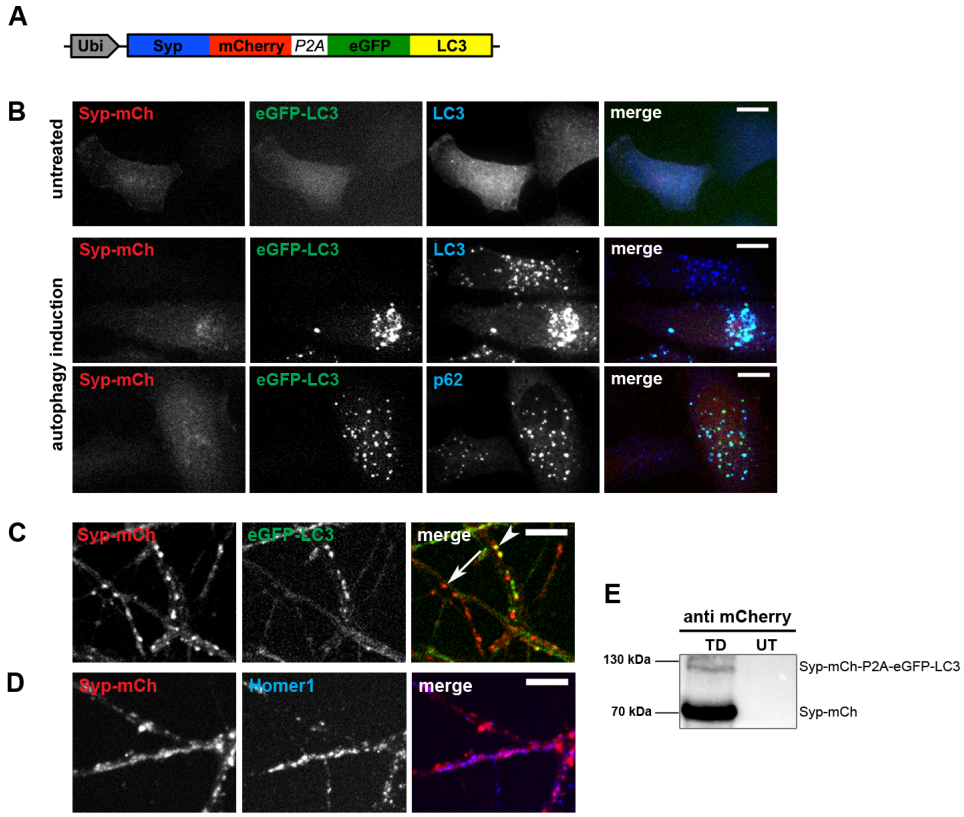

Figure 10: Validation of FU-Syp-mCherry-P2A-eGFP-LC3. (A) Schematic of lentiviral vector FU-Syp-mCherry-P2A-eGFP-LC3 expressing Synaptophysin(Syp)-mCherry and eGFP-LC3 under an ubiquitin promotor. P2A cleavage peptide separates the two proteins. (B) Autophagy induction (EBSS + 100µM chloroquine for 2 hours) of FU-Syp-mCherry-P2A-eGFP-LC3 expressing HeLa cells, demonstrating that following autophagy induction eGFP-LC3 puncta colocalize with both endogenous LC3 and p62, but not Syp-mCherry. (C) Live cell imaging of cultured hippocampal neurons expressing FU-Syp-mCherry-P2A-eGFP-LC3. Syp-mCherry and eGFP-LC3 exhibit different patterns indicating P2A mediated cleavage (arrow indicates Syp-mCherry puncta, arrowhead indicates colocalization of Syp-mCherry and eGFP-LC3). (D) Representative images of hippocampal neurons expressing FU-Syp-mCherry-P2A-eGFP-LC3 immunostained with antibodies against the postsynaptic protein Homer1. Colocalization of Syp-mCherry and Homer1 indicate presynaptic targeting of Syp-mCherry. (E) Western Blot of lysates from hippocampal neurons infected (TD) or uninfected (UT) with FU-Syp-mCherry-P2A-eGFP-LC3 and stained with mCherry antibodies. Upper band: uncleaved FU-Syp-mCherry-eGFP-LC3 fusion protein. Lower band: cleaved Syp-mCherry. High

ratio of Syp-mCherry/Syp-mCherry-P2A-eGFP-LC3 band indicates efficient cleavage. Scale bars: 10µm. Adapted from Hoffmann et al. (Hoffmann et al., forthcoming).

To analyze whether Synaptophysin-mCherry and eGFP-LC3 exhibited the appropriate subcellular localization in differentiated neuron cells, I performed live cell experiments with infected hippocampal neurons at 14 DIV. As shown in figure 10C, Synaptophysin-mCherry and eGFP-LC3 exhibit distinct distribution after protein synthesis (green and red spots), consistent with the efficient cleavage of the P2A peptide. Furthermore, Synaptophysin-mCherry was correctly recruited into the presynaptic compartment, as it specifically colocalizes with the postsynaptic density (PSD) protein Homer1 (Figure 10D) along uninfected dendrites.

As Synaptophysin-mCherry and eGFP-LC3 are expressed as a fusion protein and become cleaved after protein synthesis, I further checked protein cleavage efficiency through the P2A sequence (Kim et al., 2011). Western Blot analysis was performed with lysate from infected primary hippocampal cultures. Protein detection via mCherry antibody enabled the relative quantification of Synaptophysin-mCherry level compared to the fusion protein Syp-mCherry-P2A-eGFP-LC3. The Synaptophysin-mCherry protein band was expected to run at approx. 66.8kDa, while the fusion protein band was expected at approx. 115.5kDa. Indeed, the fusion protein level was only a minor fraction (<10% of total protein) of the cleaved Synaptophysin-mCherry level. The lysate of uninfected cells (UT) did not show any mCherry signal (Figure 10E).

These data indicate that FU-Syp-mCherry-P2A-eGFP-LC3 can be used to specifically monitor presynaptic autophagy.

6.4 FU-Syp-mCherry-P2A-eGFP-LC3 is a useful tool to monitor presynaptic autophagy

In the next set of experiments, I examined how the induction of autophagy with 2µM rapamycin (Boland et al., 2008; Hernandez et al., 2012; Spilman et al., 2010) affected the distribution of eGFP-LC3 relative to Synaptophysin-mCherry in neurons. Initially, rapamycin was added to sparsely FU-Syp-mCherry-P2A-eGFP-LC3 infected hippocampal cultures for 2 hours, as most previous studies had shown that a several-hour rapamycin incubation was sufficient to induce autophagy in neurons (Hernandez et al., 2012) (Figure 7). To identify 'synaptic' changes in eGFP-LC3 levels, I analyzed the average intensities of eGFP-LC3 puncta that colocalize with Synaptophysin-mCherry in fixed neurons. This revealed a modest (36%) but significant increase in eGFP-LC3 intensities within presynaptic boutons compared to untreated control neurons (Figure 11A and D). Monitoring the number of eGFP-LC3 puncta per unit length of axon revealed that 2 hours of rapamycin treatment significantly increased the number of eGFP-LC3 puncta present in axons compared to untreated control neurons (Figure 11A and E).

These data are consistent with the concept that rapamycin can induce the formation of AVs in hippocampal axons. However, given that vesicular transport is quite rapid, it is unclear whether during the 2-hour period the newly formed AVs arose at the synapses and dispersed into the axons and/or were generated within axons and then accumulated within presynaptic boutons. To distinguish between these possibilities, I examined whether AVs would appear in as little as 10 minutes following the addition of rapamycin. Surprisingly, I found that not only eGFP-LC3 puncta did appear in axons during this short period of induction (Figure 11B and G), but eGFP-LC3 intensity was dramatically increased within presynaptic boutons marked with Synaptophysin-mCherry (Figure 11B and F). Importantly, I also found that the eGFP-LC3 positive puncta were also positive for the autophagy cargo receptor p62 (Figure 11C and H), suggesting that autophagosomes are indeed forming locally within presynaptic boutons.

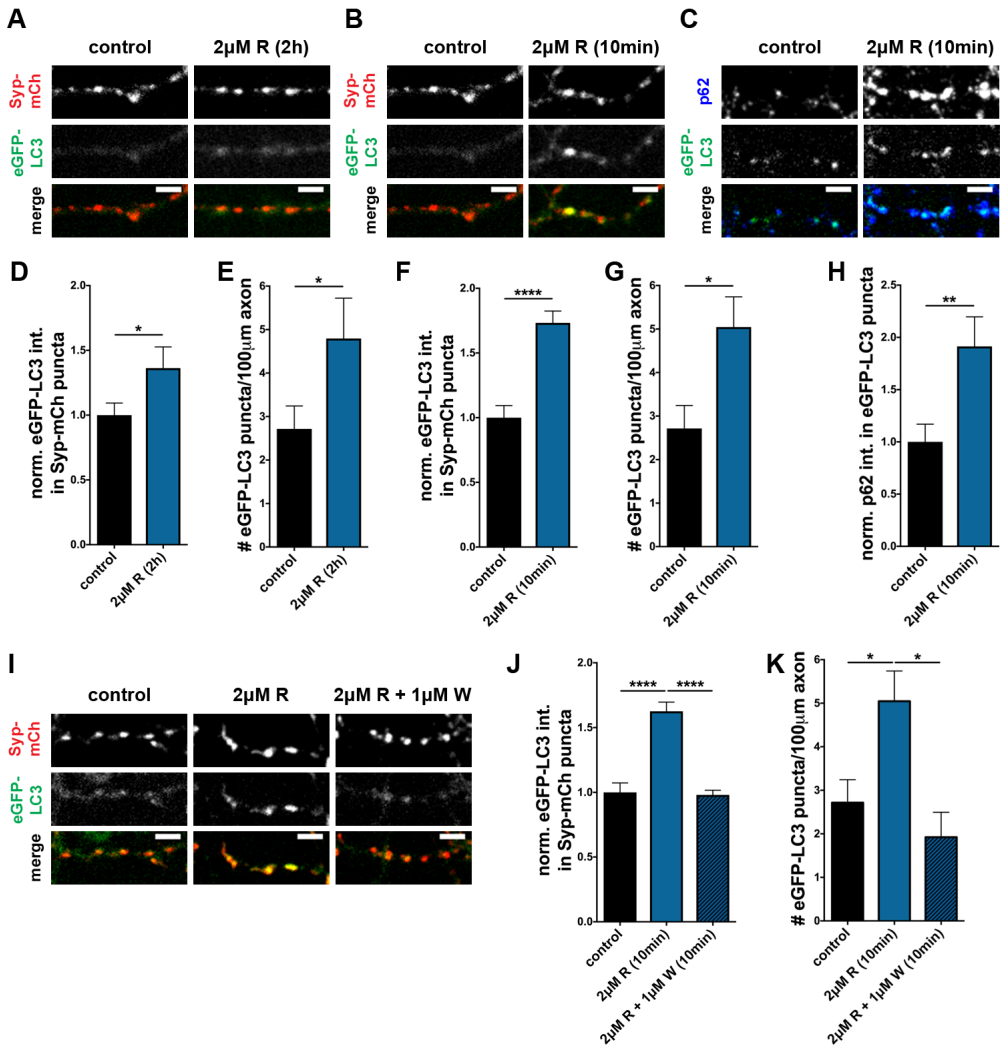

Figure 11: Rapamycin induces rapid autophagy at synapses in hippocampal neurons. (A-C) Images of hippocampal neurons expressing FU-Syp-mCherry-P2A-eGFP-LC3, treated with 2µM rapamycin (R) for 2 hours (A) or 10 minutes (B and C) before fixation (A-C) and staining with antibodies against

p62 (C). (D-H) Quantification of the normalized intensity of eGFP-LC3 levels at Syp-mCherry puncta (D and F) as well as the number of puncta/100µm of axon (E and G) after 2 hours (D and E) or 10 minutes (F and G) of 2µM rapamycin treatment. (D: control = 1 ± 0.094, n = 412 synapses, 3 independent experiments; 2µM R (2h) = 1.36 ± 0.164, n = 301 synapses, 3 independent experiments). (E: control = 2.72 ± 0.529, n = 40 axons, 4 independent experiments; 2µM R (2h) = 4.80 ± 0.928, n = 20 axons, 2 independent experiments). (F: control = 1 ± 0.094, n = 412 synapses, 3 independent experiments; 2µM R (10min) = 1.73 ± 0.092, n = 343 synapses, 3 independent experiments). (G: control = 2.72 ± 0.529, n = 40 axons, 4 independent experiments; 2µM R (10min) = 5.05 ± 0.695, n = 47 axons, 4 independent experiments). Quantification of the normalized p62 levels at eGFP-LC3 puncta (H) (H: control = 1 ± 0.170, n = 50 puncta, 3 independent experiments; 2µM R (10min) = 1.91 ± 0.283, n = 52 puncta, 3 independent experiments) confirming that eGFP-LC3 puncta depict autophagic organelles. (I) Images of hippocampal neurons infected with FU-Syp-mCherry-P2A-eGFP-LC3 and treated with 1µM wortmannin (W) prior and during a 10 minute incubation with 2µM rapamycin. (J and K) Quantification of (I) showing that wortmannin suppresses the induction of autophagy at Syp-mCherry puncta (J) and along axons (K) following the addition of rapamycin (J: control = 1 ± 0.073, n = 540 synapses, 4 independent experiments; 2µM R (10min) = 1.63 ± 0.071, n = 469 synapses, 4 independent experiments; 2µM R + 1µM W (10min) = 0.98 ± 0.036, n = 152 synapses, 2 independent experiments). (K: control = 2.72 ± 0.529, n = 40 axons, 4 independent experiments; 2µM R (10min) = 5.05 ± 0.695, n = 47 axons, 4 independent experiments; 2µM R + 1µM W (10min) = 1.92 ± 0.573, n = 20 axons, 2 independent experiments). Scale bars: 5µm. Error bars represent SEM. Unpaired T-test (D, E, F, G and H) and ANOVA Tukey's multiple comparisons test (J and K) was used to evaluate statistical significance. ****p<0.0001, ***p<0.001, **p<0.01, *p<0.05. Adapted from Hoffmann et al. (Hoffmann et al., forthcoming).

To further explore whether the observed rapamycin-induced AV formation at synapses is induced via the canonical autophagy pathway, which requires the PI3K Vps34, I included 1µM wortmannin together with rapamycin during the 10-minute incubation period. This manipulation abolished the accumulation of eGFP-LC3 puncta in both presynaptic boutons (Figure 11I and J) and along axons (Figure 11I and K). Taken together, these data indicate that the machinery necessary for the rapid generation of AVs in axons is located within or very near to presynaptic boutons and can be triggered by a PI3K-dependent pathway.

To corroborate the finding that rapamycin induces synaptic autophagy within 10 minutes (Figure 11F), cortical and hippocampal neurons were treated with 2µM rapamycin for either 10 minutes or 2 hours and subsequently lysed and prepared for Western Blot analyses. In order to quantify predominantly synaptic autophagy, synaptosomes (synaptosome suspension) were enriched leading to a strong Synaptophysin signal compared to the cytosol fraction (Figure 12A). Both LC3-I and LC3-II bands were increased after 10 minutes of rapamycin treatment in cortical (Figure 12A and C) and hippocampal neurons (Figure 12B and E) compared to untreated control cells. However, the increase in LC3-II is higher in hippocampal neurons than in cortical neurons indicating that hippocampal neurons are more sensitive to rapamycin-dependent autophagy induction. After a 2-hour treatment of rapamycin, LC3-I and LC3-II levels are still elevated in both cortical (Figure 12A and D) as well as hippocampal neurons (data not shown). Together,

these observations support the conclusion that synaptic autophagy can be induced by rapamycin treatment within a short minute time frame.

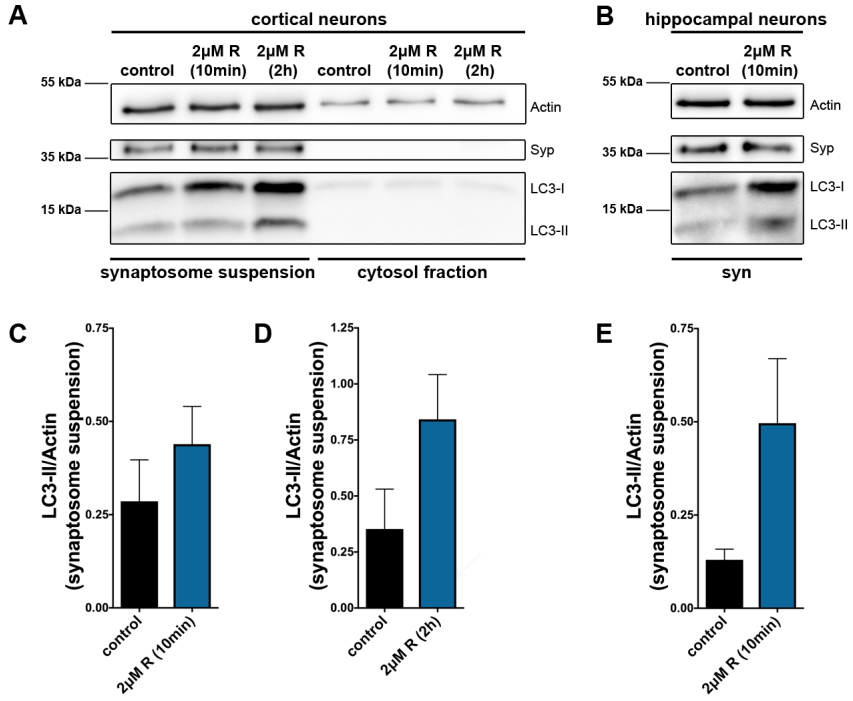

Figure 12: Rapid increase in endogenous LC3 by rapamycin treatment. (A and B) Western Blot of lysates from cultured cortical (A) and hippocampal (B) neurons treated with 2µM rapamycin (R) for 10 min (A and B) or 2 hours (A) and stained with antibodies against Actin, Synaptophysin (Syp) and LC3. Note the strong enrichment of LC3-I and LC3-II within the synaptosome suspension (syn) (left) compared to the cytosol fraction (right). Data indicate that synaptic autophagy can be rapidly induced by rapamycin treatment. (C-E) Quantification of LC3-II/Actin from the synaptosome suspensions from A (C and D) and B (E). (C: control = 0.29 ± 0.111, 5 independent experiments; 2µM R (10min) = 0.44 ± 0.101, 5 independent experiments). (D: control = 0.35 ± 0.178, 3 independent experiments; 2µM R (2h) = 0.84 ± 0.200, 3 independent experiments). (E: control = 0.13 ± 0.029, 3 independent experiments; 2µM R (10min) = 0.50 ± 0.173, 3 independent experiments). Error bars represent SEM. Unpaired T-test was used to evaluate statistical significance. Adapted from Hoffmann et al. (Hoffmann et al., forthcoming).

6.5 Establishing a vector system to spatiotemporally induce presynaptic autophagy

The ability of rapamycin to induce presynaptic autophagy within 10 minutes strongly suggests that presynaptic boutons contain clearance mechanisms, such as autophagy, that could in principle deal with locally damaged proteins in real-time. As a direct test of this hypothesis, I explored whether the real-time damage of SV proteins via the production of reactive oxygen species (ROS) could also trigger the rapid clearance of these molecules via e.g. autophagy. To accomplish this goal I made use of a molecular variant of GFP called Supernova (Takemoto et al.,

2013), a monomeric version of Killerred (Bulina et al., 2006), previously shown to generate ROS following its excitation with intense 543nm laser light. As with other photosensitizers, short-lived ROS generated by Supernova are expected to damage proteins within 1-4nm of the source (Linden et al., 1992; Takemoto et al., 2013). Thus to restrict the actions of the ROS to SVs, I initially fused Supernova to the cytoplasmic tail of the SV protein Synaptophysin (creating Synaptophysin-Supernova; Syp-SN). This was then subcloned and co-expressed with eGFP-LC3 via my lentiviral vector (FU-Syp-Supernova-P2A-eGFP-LC3) (Figure 14A).

Regarding ROS-induced damage, my working hypothesis was that the light-activated production of ROS by Supernova tethered to Synaptophysin would locally damage SV proteins within presynaptic boutons and thus trigger clearance mechanisms such as autophagy (Figure 13A). In contrast, unbleached synapses within the same network would not generate any ROS and serve as control synapses. If autophagy is indeed responsible for the clearance of damaged SV proteins, eGFP-LC3 organelles would appear at these bleached synapses (Figure 13C).

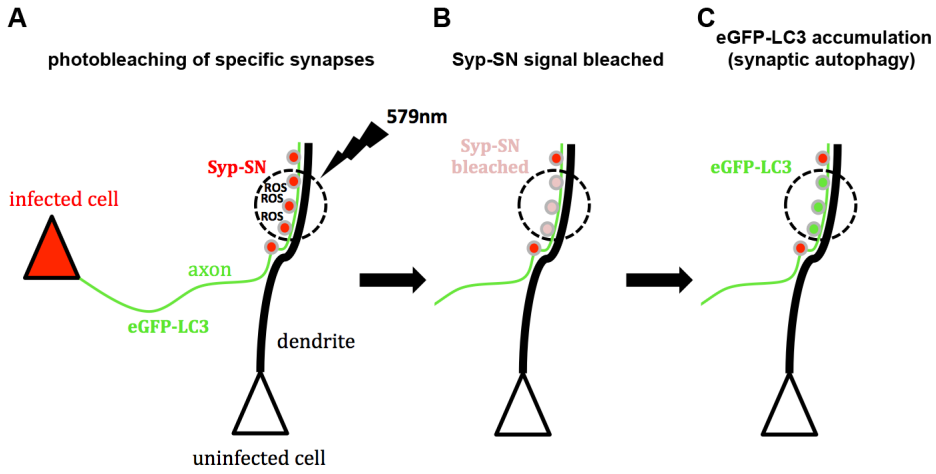

Figure 13: Inducing and monitoring presynaptic autophagy with FU-Syp-mCherry-P2A-eGFP-LC3. Schematic of working hypothesis. (A) Supernova-tagged Synaptophysin (Syp-SN) locates to synapses and bleaching thereof creates reactive oxygen species (ROS) with a half-radius of 3-4nm. (B) During bleaching, Supernova fluorescence decreases. (C) Damage of Syp-SN leads to activation of the autophagy clearance mechanism. Hence, eGFP-LC3 accumulates at bleached synapses.

As with the FU-Syp-mCherry-P2A-eGFP-LC3 vector, I verified that both the Synaptohysin-Supernova and eGFP-LC3 portions of the vector were expressed and processed. Specifically, I examined whether the eGFP-LC3 segment was correctly recruited to p62 positive AVs in HeLa cells starved with EBSS (amino acid starvation) and treated with chloroquine (=autophagy induction) (Figure 14B) and Synaptophysin-Supernova properly localized juxtaposed with Homer1 positive synapses (Figure 14E). Moreover, I confirmed in live cell experiments with HeLa cells expressing FU-Syp-Supernova-P2A-eGFP-LC3 that 80% of the Supernova fluorescence

was photobleached during a 60 seconds exposure of 563nm wavelength light from a mercury lamp (Figure 14C and D). Lastly, Western analyses were used to confirm the correct cleavage of the P2A peptide (Figure 14F).

Although bleaching is described to coincide with ROS generation (Jarvela and Linstedt, 2014), I additionally made use of the superoxide indicator dihydroethidium (DHE) to monitor for ROS production in my system. DHE exhibits blue light in the cytoplasm. In the presence of superoxides, DHE intercalates with the DNA and emits red light from the nucleus. This redistribution causes the blue fluorescence in the cytoplasm to drop upon ROS production, which is used as a measure of superoxide generation. Bleaching of FU-Syp-Supernova-P2A-eGFP-LC3 transfected HEK293 cells shows a significantly higher decrease in DHE_{blue} intensity compared to FU-Syp-mCherry-P2A-eGFP-LC3 transfected and untransfected (UT) control cells (Figure 15) confirming superoxide generation after Supernova bleaching, as previously shown (Takemoto et al., 2013). Note that DHE_{blue} intensity also decreases in the presence of FU-Syp-mCherry-P2A-eGFP-LC3 compared to UT control cells indicating that already bleaching mCherry leads to the production of ROS, however not as efficient as Supernova (Figure 15B).

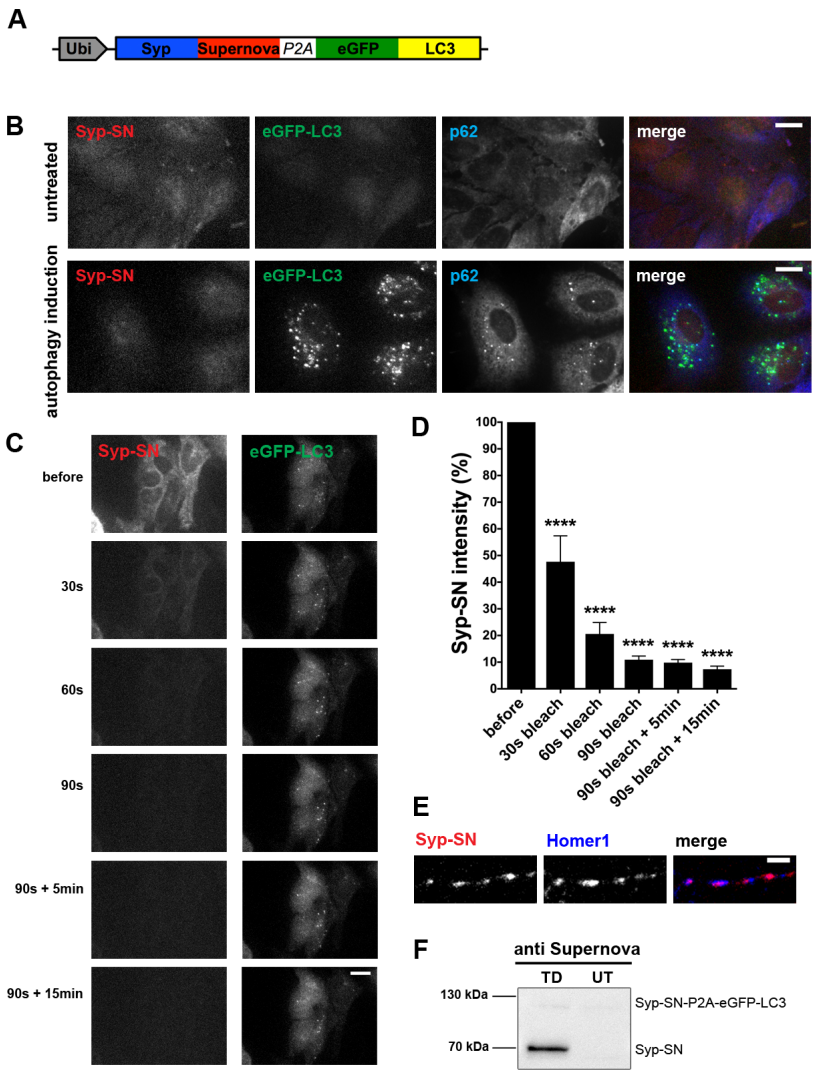

Figure 14: Validation of FU-Syp-Supernova-P2A-eGFP-LC3. (A) Schematic of lentiviral vector FU-Syp-Supernova-P2A-eGFP-LC3 expressing Synaptophysin-Supernova (Syp-SN) and eGFP-LC3 under an ubiquitin promotor. P2A cleavage peptide separates the two proteins. (B) Autophagy induction (EBSS + 100µM chloroquine for 2 hours) of FU-Syp-Supernova-P2A-eGFP-LC3 expressing HeLa cells, demonstrating that following autophagy induction eGFP-LC3 puncta colocalize with p62, but not Syp-Supernova. (C) Live cell imaging of HeLa cells expressing FU-Syp-Supernova-P2A-eGFP-LC3 before bleaching, after 30s, 60s and 90s bleaching and after an additional waiting period of 5 minutes and 15 minutes. (D) Quantification of (C) (before = 100 ± 0; 30s bleach = 47.69 ± 9.702; 60s bleach = 20.60 ± 4.264; 90s bleach = 10.91 ± 1.397; 90s bleach + 5min = 9.82 ± 1.179; 90s bleach + 15min = 7.35 ± 1.161; n = 6 cells, 1 experiment; statistical significance indicated by * compared to before). (E) Representative images of hippocampal neurons expressing FU-Syp-Supernova-P2A-eGFP-LC3 immunostained with antibodies against the postsynaptic protein Homer1. Colocalization of Syp-Supernova and Homer1 indicate presynaptic targeting of Syp-Supernova. (F) Western analysis of lysates from hippocampal neurons infected (TD) or uninfected (UT) with FU-Syp-Supernova-P2A-eGFP-LC3 and stained with Supernova (Killerred) antibodies. Upper band: uncleaved FU-Syp-Supernova-eGFP-LC3 fusion protein. Lower band: cleaved Syp-Supernova. High ratio of Syp-Supernova/Syp-Supernova-P2A-eGFP-LC3 band indicates efficient cleavage. Scale bars: 20µm (B and C) and 5µm (E). Error bars represent SEM. ANOVA Tukey's multiple comparisons test was used to evaluate statistical significance. ****p<0.0001, ***p<0.001, **p<0.01, *p<0.05.

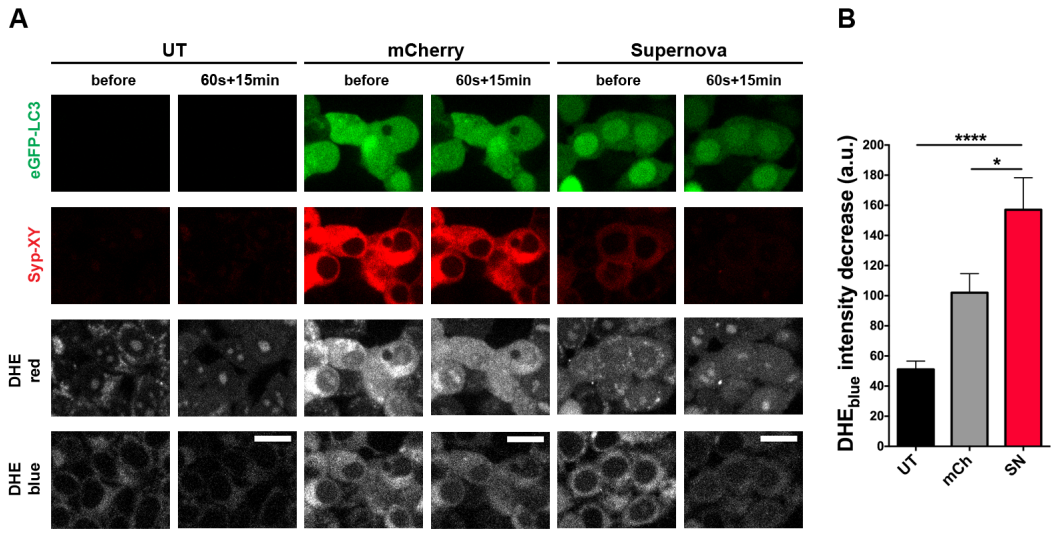

Figure 15: DHE assay confirms superoxide generation after Supernova bleaching. (A) Representative images of HEK293 cells expressing either no vector (UT), FU-Syp-mCherry-P2A-eGFP-LC3 (mCherry) or FU-Syp-Supernova-P2A-eGFP-LC3 (Supernova) before and 15 minutes after 60 seconds of bleaching, respectively. (B) Quantification of (A). Note that there is a significantly higher decrease in DHE_{blue} in FU-Syp-Supernova-P2A-eGFP-LC3 transfected cells compared to both controls (UT = 51.08 ± 5.566, n = 26 cells, 3 independent experiments; mCh = 102 ± 12.680, n = 36 cells, 4 independent experiments; SN = 157 ± 21.310, n = 31 cells, 4 independent experiments). Scale bars: 20µm. Error bars represent SEM. ANOVA Tukey's multiple comparisons test was used to evaluate statistical significance. ****p<0.0001, ***p<0.001, **p<0.01, *p<0.05. Adapted from Hoffmann et al. (Hoffmann et al., forthcoming).

6.6 Light-activated ROS generation triggers presynaptic autophagy

To explore whether a local increase in ROS production near SVs can induce presynaptic autophagy, primary hippocampal neurons grown on µ-Slide 8 Well culture dishes were sparsely infected with FU-Syp-Supernova-P2A-eGFP-LC3 at 2-3 DIV. Around 14 DIV, they were transferred to a spinning disc confocal microscope equipped with a temperature controlled live cell imaging chamber. Prior to bleaching, selected fields of view, axons from infected neurons growing on top of uninfected neurons, were selected and imaged during excitation with a 491nm laser (for the eGFP-LC3 signal) and a 561nm laser (for the Syp-Supernova signal) (Figure 6).

Subsequently, a subregion, selected with a field diaphragm, was bleached by exposing cells to 563nm light from a mercury lamp for 60 seconds (Figure 16A), a condition found to bleach approx. 80% of the initial fluorescence (Figure 14D). Cultures were fixed approx. 5, 60 or 120 minutes post bleaching and immuno-stained with antibodies against GFP and Supernova, allowing the post-hoc identification of synapses within and outside of the bleached area and the levels and redistribution of eGFP-LC3.

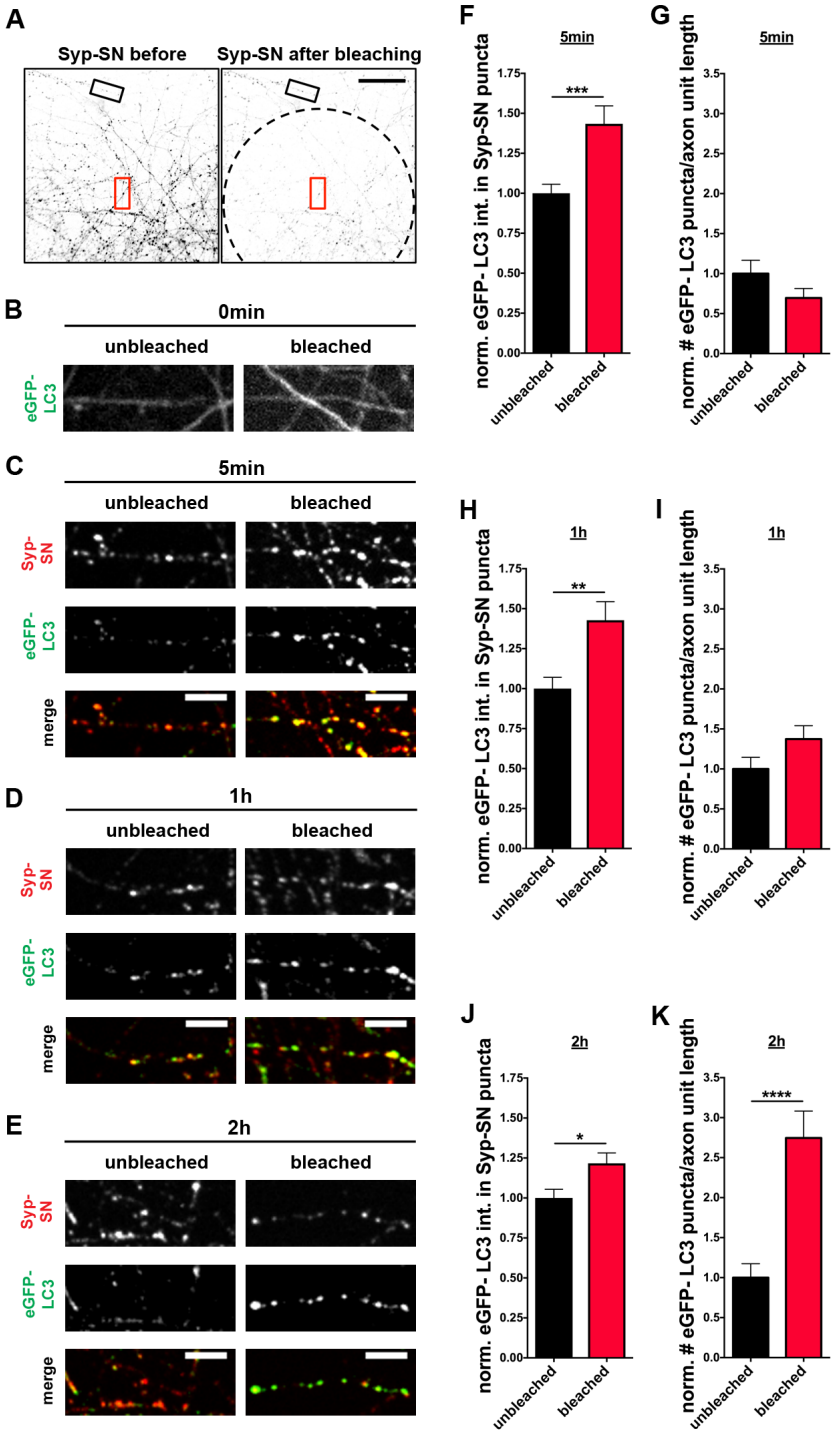

Figure 16: Rapid induction of autophagy by ROS-mediated damage by Synaptophysin-Supernova. (A) Low-magnification images of hippocampal neurons expressing FU-Syp-Supernova-P2A-eGFP-LC3 grown on top of uninfected neurons before and after photobleaching a region of interest (dashed line). Boxes represent areas within (red) and outside (black) bleached area used for analysis. (B) eGFP-LC3 distribution in axons from (C) before bleaching and antibody staining (live cell image). (C-E) Images of axon segments (5 minutes, 1 hour and 2 hours after bleaching) that were subsequently fixed and stained with antibodies against GFP to detect eGFP-LC3 and Supernova to detect Syp-SN. Data indicate that autophagy at synapses can be rapidly induced through Syp-SN photobleaching. (F) Quantification of normalized eGFP-LC3 intensities within Syp-SN puncta 5 minutes (C) after bleaching (unbleached = 1 ± 0.057, n = 119 synapses, 3 independent experiments; bleached = 1.43 ± 0.113, n = 132 synapses, 3 independent experiments). (G)

Quantification of the normalized number of eGFP-LC3 puncta per unit axon length, in axons 5 minutes after photobleaching (C) (unbleached = 1 ± 0.166, n = 17 axons, 3 independent experiments; bleached = 0.70 ± 0.119, n = 18 axons, 3 independent experiments). (H) Quantification of normalized eGFP-LC3 intensities within Syp-SN puncta 1 hour (D) after bleaching (unbleached = 1 ± 0.071, n = 132 synapses, 3 independent experiments; bleached = 1.43 ± 0.117, n = 167 synapses, 3 independent experiments). (I) Quantification of the normalized number of eGFP-LC3 puncta per unit axon length, in axons 1 hour after photobleaching (D) (unbleached = 1 ± 0.146, n = 24 axons, 3 independent experiments; bleached = 1.37 ± 0.166, n = 24 axons, 3 independent experiments). (J) Quantification of normalized eGFP-LC3 intensities within Syp-SN puncta 2 hours (E) after bleaching (unbleached = 1 ± 0.054, n = 136 synapses, 3 independent experiments; bleached = 1.22 ± 0.065, n = 141 synapses, 3 independent experiments). (K) Quantification of the normalized number of eGFP-LC3 puncta per unit axon length, in axons 2 hours after photobleaching (E) (unbleached = 1 ± 0.173, n = 23 axons, 3 independent experiments; bleached = 2.75 ± 0.336, n = 22 axons, 3 independent experiments). Scale bars: 50µm (B), 10µm (C, D and E). Error bars represent SEM. Unpaired T-test was used to evaluate statistical significance. ****p<0.0001, ***p<0.001, **p<0.01, *p<0.05. Adapted from Hoffmann et al. (Hoffmann et al., forthcoming).

Comparing the intensity of eGFP-LC3 at Syp-SN positive puncta within and outside the bleached area revealed a significant increase in synaptic eGFP-LC3 intensity in the bleached area within 5 minutes of initial bleaching (Figure 16C and F). However, at that time point, the number of eGFP-LC3 puncta per axon unit length is not changed compared to the unbleached control (Figure 16C and G). Similarly, 1 hour after bleaching, eGFP-LC3 levels are still elevated in Syp-SN positive synapses inside the bleached area compared to outside, with only a modest increase in the number of eGFP-LC3 puncta per unit length of axon (Figure 16D, H and I). Intriguingly, 2 hours after triggering ROS production, eGFP-LC3 levels remain somewhat elevated at Syp-SN positive synapses, and dramatically accumulate as small puncta along axons inside the bleached area (Figure 16E, J and K) compared to those outside. These latter data imply that the synaptic increase in ROS rapidly induces presynaptic autophagy and that subsequent flux carries the autophagosomal membranes into axons.

As bleaching mCherry also induces ROS, I next investigated the capability of mCherry bleaching mediated ROS production to induce synaptic autophagy. Intriguingly, Syp-mCh puncta show increased eGFP-LC3 levels compared to unbleached control boutons 1 hour after bleaching (Figure 17A). However, eGFP-LC3 levels after Syp-SN bleaching are significantly higher than after Syp-mCh bleaching (Figure 17A, B and D). Furthermore, 60µM of the ROS scavenger N-acetyl-L-cysteine (NAC), added to FU-Syp-Supernova-P2A-eGFP-LC3 infected cells before bleaching, diminishes the earlier observed increase in eGFP-LC3 intensities at synapses (Figure 17B, C and D). These data indicate that Supernova is a potent ROS generator and that the rapid induction of synaptic autophagy is caused by a light-activated local increase of ROS near SVs.

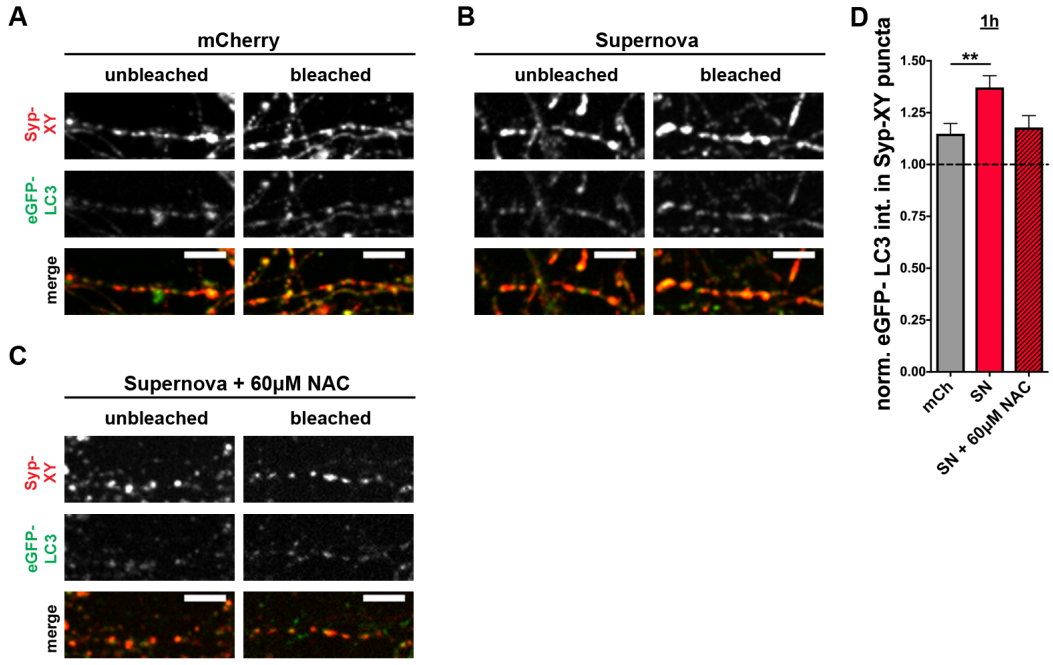

Figure 17: Bleaching-induced increase in eGFP-LC3 levels at presynaptic boutons is ROS-dependent. (A, B and C) Images of hippocampal neurons expressing FU-Syp-mCherry-P2A-eGFP-LC3 (A), FU-Syp-Supernova-P2A-eGFP-LC3 (B and C) that were fixed and stained with antibodies against GFP and Supernova/mCherry (XY) 1 hour after photobleaching, either in the absence (A and B) or presence of 60µM N-acetyl-L-cysteine (NAC) (C). (D) Quantification of normalized eGFP-LC3 intensities within Syp-XY puncta (mCh = 1.15 ± 0.049, n = 489 synapses, 4 independent experiments; SN = 1.37 ± 0.056, n = 450 synapses, 4 independent experiments; SN + NAC = 1.18 ± 0.057, n = 198 synapses, 3 independent experiments). Scale bars: 10µm. Error bars represent SEM. ANOVA Tukey's multiple comparisons test was used to evaluate statistical significance. ****p<0.0001, ***p<0.001, **p<0.01, *p<0.05. Adapted from Hoffmann et al. (Hoffmann et al., forthcoming).

To rule out that increased eGFP-LC3 levels after Syp-SN bleaching are simply caused by the slight overexpression of LC3 (eGFP-LC3), I also measured endogenous LC3 levels after bleaching neurons only expressing FU-Syp-Supernova (Figure 18A). In accordance with my previous findings (Figure 16), Syp-SN bleaching leads to a rapid increase in endogenous LC3 intensities at presynaptic boutons within minutes (Figure 18B and E) and LC3 levels remain elevated for additional 2 hours (Figure 18C, D, F, G). Both data with endogenous LC3 as well as eGFP-LC3 confirm that local light-activated ROS production can induce synaptic autophagy within a short time period as quick as 5 minutes.

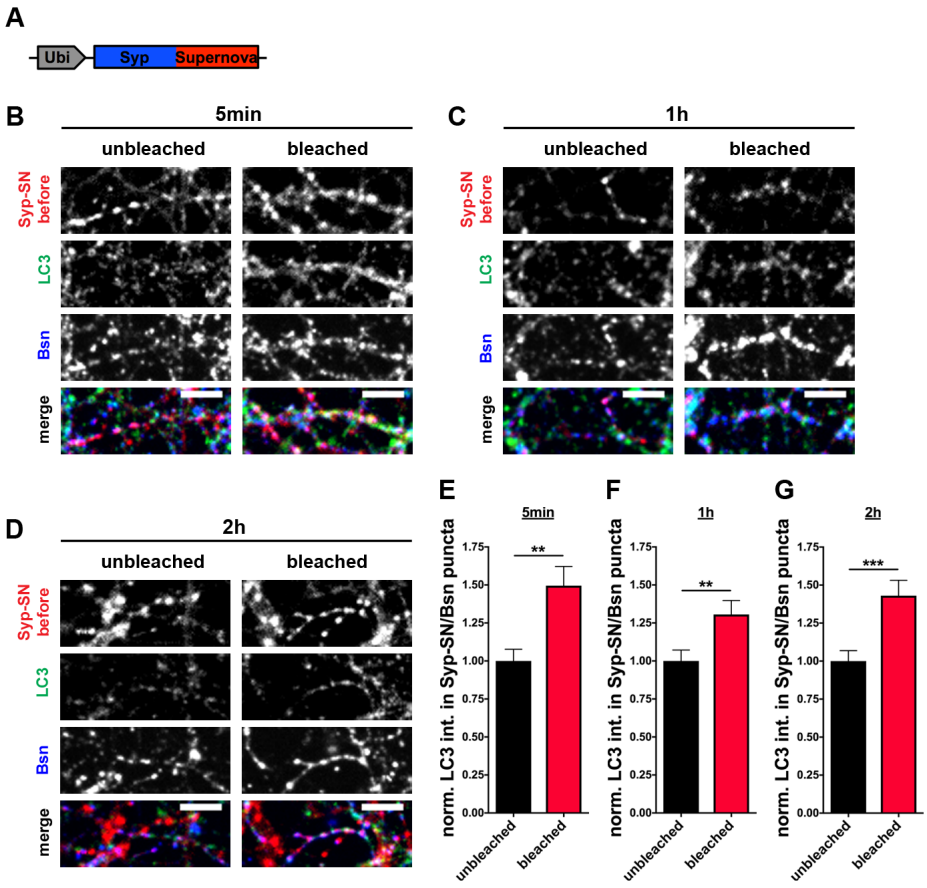

Figure 18: Rapid increase in endogenous LC3 by bleaching of Syp-Supernova. (A) Schematic of FU-Syp-Supernova expression vector. (B-D) Images of hippocampal neurons expressing FU-Syp-Supernova that were fixed and stained with antibodies against LC3 and Bassoon 5 min, 1 hour and 2 hours after bleaching. Data indicate that autophagy at synapses can be rapidly induced through Syp-SN photobleaching. (E) Quantification of normalized LC3 intensities within Syp-SN/Bsn puncta 5 min (B) after bleaching (unbleached = 1 ± 0.077, n = 74 synapses, 3 independent experiments; bleached = 1.50 ± 0.126, n = 75 synapses, 3 independent experiments). (F) Quantification of normalized LC3 intensities within Syp-SN/Bsn puncta 1 hour (C) after bleaching (unbleached = 1 ± 0.072, n = 59 synapses, 3 independent experiments; bleached = 1.31 ± 0.092, n = 49 synapses, 3 independent experiments). (G) Quantification of normalized LC3 intensities within Syp-SN/Bsn puncta 2 hours (D) after bleaching (unbleached = 1 ± 0.069, n = 60 synapses, 3 independent experiments; bleached = 1.43 ± 0.101, n = 60 synapses, 3 independent experiments). Scale bars: 10µm. Error bars represent SEM. Unpaired T-test was used to evaluate statistical significance. ****p<0.0001, ***p<0.001, **p<0.01, *p<0.05. Adapted from Hoffmann et al. (Hoffmann et al., forthcoming).

6.7 ROS-induced synaptic autophagy is PI3K- and Atg5-dependent

To investigate whether the observed ROS-induced increase in eGFP-LC3 puncta is dependent on the canonical PI3K/Vps34 autophagy pathway, 1µM wortmannin was added to neurons right before bleaching Syp-SN and maintained in the culture for the following 2 hours, after which neurons were fixed and analyzed. In cells that were not treated with wortmannin, eGFP-LC3

intensity within presynaptic boutons as well as the number of eGFP-LC3 puncta per unit length of axon remained elevated (Figure 19A, C and D) compared to the unbleached control. In contrast, the inclusion of wortmannin was found to inhibit the light-activated increase in eGFP-LC3 intensity within presynaptic boutons (Figure 19B and E), but had no effect on the number of eGFP-LC3 puncta per unit length of axon (Figure 19B and F). These data indicate that the ROS-induced increase in presynaptic autophagy may be dependent on the PI3K signaling pathway, while autophagy within axons is not. Note that while most of the Syp-SN is synaptic, extrasynaptic pools are likely present, presumably engaged in the active transport within mobile pools of SVs (Cohen et al., 2013; Maas et al., 2012; Tsuriel et al., 2006). Photobleached damage of this pool could thus contribute to a PI3K-independent form of axonal autophagy in axons, as already described for other cell types (Chu et al., 2007; Lemasters, 2014; Zhu et al., 2007).

Additionally, given the caveat that wortmannin is not a selective inhibitor of Vps34 (Bain et al., 2007), I made use of a knock down approach using an shRNA against the autophagy-related protein Atg5 (shAtg5) to inhibit autophagy (Okerlund et al., 2017). To ensure co-expression of Syp-SN, eGFP-LC3 and the shRNA, an U6 promoter and the small hairpin RNA were integrated upstream into the vector FU-Syp-Supernova-P2A-eGFP-LC3 (F-U6-shAtg5-U-Syp-Supernova-P2A-eGFP-LC3). A scrambled shRNA (scRNA/SC) served as a control (F-U6-scRNA(SC)-U-Syp-Supernova-P2A-eGFP-LC3). Strikingly, neurons expressing the scRNA depict increased eGFP-LC3 levels at Syp-SN puncta as well as an increased number of eGFP-LC3 puncta along axon segments 2 hours after bleaching (Figure 19G, I and J), thus resembling earlier results (Figure 19A, C and D). However, when shAtg5 is additionally expressed in neurons, its presence inhibits the light-activated increase of synaptic eGFP-LC3 and the number of eGFP-LC3 puncta (Figure 19H, K and L). These data confirm that ROS-induced eGFP-LC3 accumulation is dependent on the initiation of the canonical autophagy pathway.

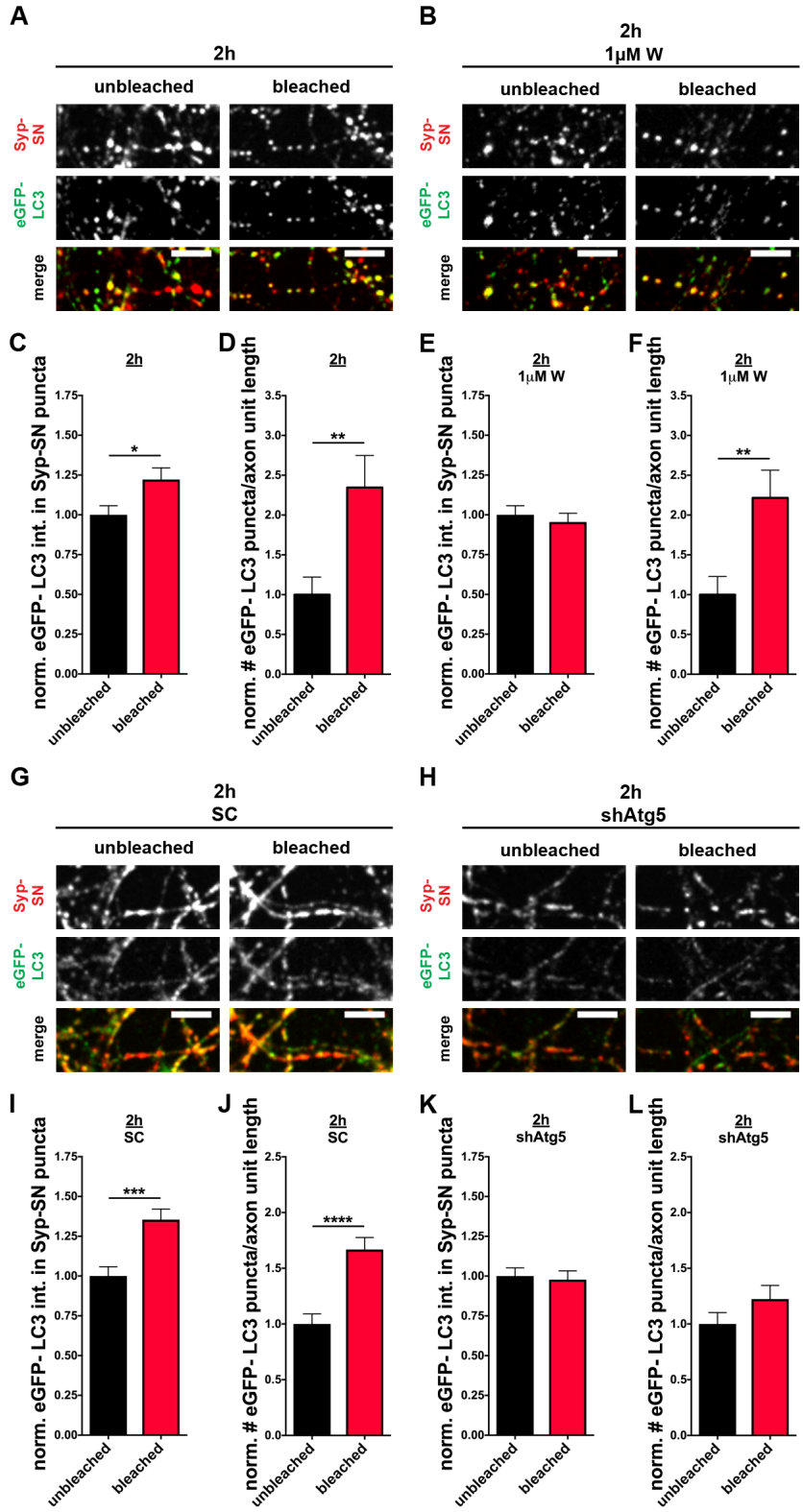

Figure 19: ROS-induced increase in eGFP-LC3 levels at presynaptic boutons is PI3K- and Atg5-dependent. (A and B) Images of hippocampal neurons expressing FU-Syp-Supernova-P2A-eGFP-LC3 that were fixed and stained with antibodies against GFP and Supernova 2 hours after photobleaching, either in the absence (A) or presence of 1µM wortmannin (W) (B). (C and D) Quantification of normalized eGFP-LC3 intensities within Syp-SN puncta (C) or the normalized number of eGFP-LC3 puncta per unit axon length (D) in bleached and unbleached areas. (C:

unbleached = 1 ± 0.057, n = 174 synapses, 3 independent experiments; bleached = 1.22 ± 0.073, n = 174 synapses, 3 independent experiments) (D: unbleached = 1 ± 0.221, n = 19 axons, 3 independent experiments; bleached = 2.35 ± 0.403, n = 21 axons, 3 independent experiments). (E and F) Quantification of normalized eGFP-LC3 intensities within Syp-SN puncta (E) or number of eGFP-LC3 puncta per unit axon length (F) in culture treated with wortmannin before and after photobleaching. (E: unbleached = 1 ± 0.057, n = 179 synapses, 3 independent experiments; bleached = 0.95 ± 0.055, n = 164 synapses, 3 independent experiments). (F: unbleached = 1 ± 0.228, n = 18 axons, 3 independent experiments; bleached = 2.22 ± 0.348, n = 21 axons, 3 independent experiments). (G and H) Images of hippocampal neurons expressing F-U6-scRNA(SC)-U-Syp-Supernova-P2A-eGFP-LC3 (G) or F-U6-shAtg5-U-Syp-Supernova-P2A-eGFP-LC3 (H) that were fixed and stained with antibodies against GFP and Supernova 2 hours after photobleaching. (I and J) Quantification of normalized eGFP-LC3 intensities within Syp-SN puncta (I) or the normalized number of eGFP-LC3 puncta per unit axon length (J) in cultures expressing F-U6-scRNA(SC)-U-Syp-Supernova-P2A-eGFP-LC3. (I: unbleached = 1 ± 0.058, n = 134 synapses, 3 independent experiments; bleached = 1.35 ± 0.073, n = 178 synapses, 3 independent experiments) (J: unbleached = 1 ± 0.090, n = 27 axons, 3 independent experiments; bleached = 1.67 ± 0.107, n = 27 axons, 3 independent experiments). (K and L) Quantification of normalized eGFP-LC3 intensities within Syp-SN puncta (K) or number of eGFP-LC3 puncta per unit axon length (L) in cultures expressing F-U6-shAtg5-U-Syp-Supernova-P2A-eGFP-LC3. (K: unbleached = 1 ± 0.052, n = 109 synapses, 3 independent experiments; bleached = 0.98 ± 0.055, n = 127 synapses, 3 independent experiments). (L: unbleached = 1 ± 0.103, n = 27 axons, 3 independent experiments; bleached = 1.22 ± 0.122, n = 27 axons, 3 independent experiments). Scale bars: 10µm. Error bars represent SEM. Unpaired T-test was used to evaluate statistical significance. ****p<0.0001, ***p<0.001, **p<0.01, *p<0.05. Adapted from Hoffmann et al. (Hoffmann et al., forthcoming).

6.8 ROS-induced damage to Synaptophysin promotes AV formation

The appearance of eGFP-LC3 positive puncta within the axons and presynaptic boutons of Synaptophysin-Supernova expressing cells following photobleaching suggests that this insult induces the autophagic clearance of damaged SVs and their proteins. To formally test this hypothesis, transmission electron microscopy of FU-Syp-Supernova-P2A-eGFP-LC3 infected hippocampal neurons was performed. Infected neurons grown on sapphire disks were photobleached with 563nm light from a mercury lamp for 60 seconds. Similar to the live imaging experiments, a field diaphragm was used to create bleached and unbleached regions on the same sapphire disk before high pressure freezing and further processing for EM.

The number of double-membraned organelles (autophagic vacuoles = AVs) within presynaptic boutons or SVs containing axonal varicosities was quantified as previously described (Okerlund et al., 2017). Consistent with light level studies (Figure 16F), significantly more AVs per presynaptic terminal were observed 10 minutes after light-induced Synaptophysin damage within the bleached area compared to the unbleached area (Figure 20C and D). Images analyzed ~ 40 minutes after bleaching revealed a slight but non-significant increase in AVs per terminal (Figure 20F and G). These data indicate that most newly formed autophagosomes quickly leave the synapse.

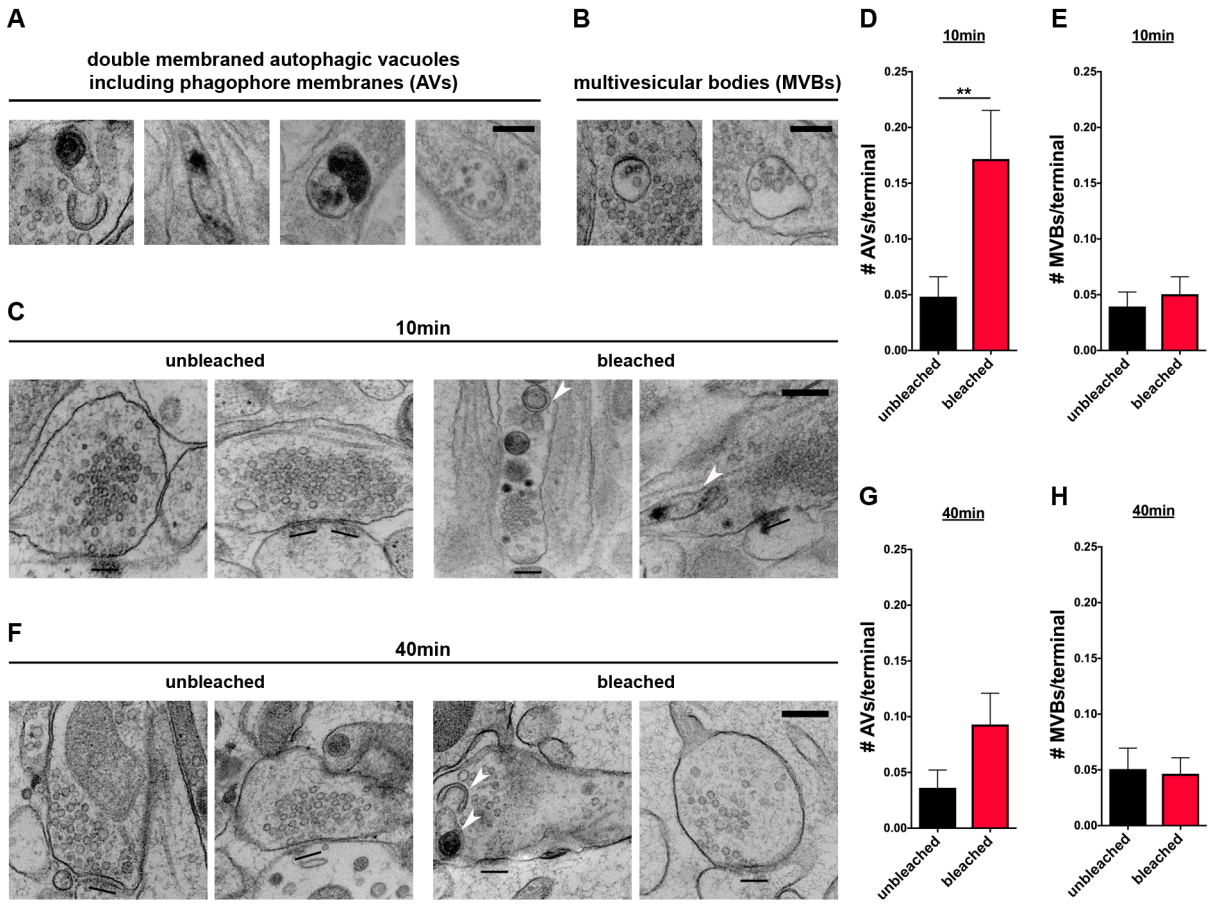

Figure 20: Syp-SN mediated ROS production increases autophagic vacuoles (AVs) in presynaptic terminals. (A and B) Example EM micrographs of organelles quantified as autophagic vacuoles (AVs) (A) or multivesicular bodies (MVBs) (B). (C and F) Representative EM micrographs of bleached or unbleached synapses 10 (C) or 40 (F) minutes after photobleaching. Arrowheads indicate double membraned AVs. Note, # of AVs but not MVBs is significantly increased 10 minutes following Syp-SN mediated ROS production. (D and E) Quantification of the number of AVs (D) or MVBs (E) per terminal 10 minutes after photobleaching (D: unbleached = 0.05 ± 0.018, n = 228 synapses, 1 independent experiments; bleached = 0.17 ± 0.044, n = 198 synapses, 2 independent experiments) (E: unbleached = 0.04 ± 0.013, n = 228 synapses, 2 independent experiments; bleached = 0.05 ± 0.016, n = 198 synapses, 2 independent experiments). (G and H) Quantification of the number of AVs (G) or MVBs (H) per terminal 40 minutes after photobleaching (G: unbleached = 0.04 ± 0.016, n = 138 synapses, 2 independent experiments; bleached = 0.09 ± 0.028, n = 215 synapses, 2 independent experiments) (H: unbleached = 0.05 ± 0.019, n = 138 synapses, 2 independent experiments; bleached = 0.05 ± 0.014, n = 215 synapses, 2 independent experiments). Scale bars: 300nm (C and F), 200nm (A and B). Error bars represent SEM. Unpaired T-test was used to evaluate statistical significance. ****p<0.0001, ***p<0.001, **p<0.01, *p<0.05. Adapted from Hoffmann et al. (Hoffmann et al., forthcoming).

Conceptually, local ROS-induced damage of synaptic proteins could induce not only autophagy but also other degradative pathways such as the endo-lysosomal system. One hallmark of the endo-lysosomal system is the appearance of multivesicular bodies (MVBs) (Ceccarelli et al., 1973; Raiborg and Stenmark, 2009). I thus examined whether the light-induced damage of Synaptophysin also induces the endo-lysosomal pathway by quantifying the presence of

synaptic MVBs within photobleached presynaptic boutons by EM. Intriguingly, no change in their number was observed either 10 or 40 minutes after photobleaching compared to unbleached boutons (Figure 20E and H), indicating that the ROS-mediated damage of Synaptophysin primarily triggers the activation of autophagy.

To confirm this observation, I also monitored whether markers of the endo-lysosomal pathway accumulated in presynaptic boutons following light-activated damage of Synaptophysin. Strikingly, level of the late endosome marker Rab7 (eGFP-Rab7) are increased at presynaptic boutons 5 minutes after bleaching (Figure 21B and E), and stay elevated compared to the unbleached control for at least 2 more hours (Figure 21E, G and I). Since Rab7 is also abundant on autophagosomes (Stenmark, 2009), I stained for another, more specific, MVB marker Chmp2b, which is part of the ESCRT-III complex (Vingtdeux et al., 2012). Interestingly, Chmp2b also accumulates at boutons 1 hour after bleaching (Figure 21C and H).

These observations indicate that ROS-mediated damage to Synaptophysin/SVs may also engage other degradative pathways such as the endo-lysosomal system.

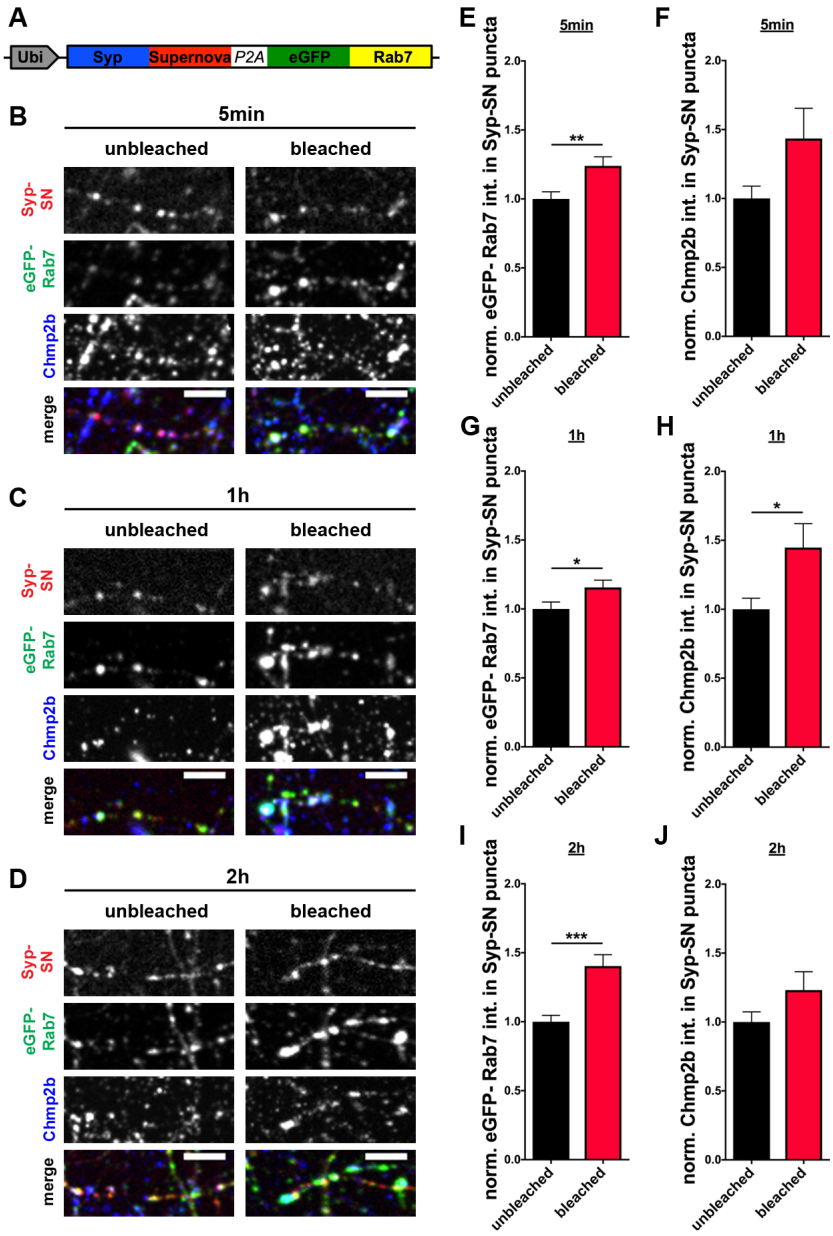

Figure 21: Syp-SN mediated ROS production increases eGFP-Rab7 and Chmp2b levels at presynaptic boutons. (A) Schematic of FU-Syp-Supernova-P2A-eGFP-Rab7 expression vector. (B, C and D) Images of hippocampal neurons expressing FU-Syp-Supernova-P2A-eGFP-Rab7 that were fixed and stained with antibodies against GFP, Supernova and Chmp2b, 5 minutes, 1 hour and 2 hours after Syp-SN mediated ROS production. (E, G and I) Quantification of the normalized eGFP-Rab7 intensity in Syp-SN puncta 5 minutes, 1 hour or 2 hours after photobleaching of Syp-SN (E: unbleached = 1 ± 0.052, n = 249 synapses, 4 independent experiments; bleached = 1.24 ± 0.066, n = 314 synapses, 4 independent experiments) (G: unbleached = 1 ± 0.050, n = 280 synapses, 4 independent experiments; bleached = 1.16 ± 0.053, n = 373 synapses, 4 independent experiments) (I: unbleached = 1 ± 0.046, n = 258 synapses, 4 independent experiments; bleached = 1.40 ± 0.083, n = 352 synapses, 4 independent experiments). Note, Rab7 levels are significantly increased at all three time points. (F, H and J) Quantification of the normalized Chmp2b intensity in Syp-SN puncta 5 minutes, 1 hour or 2 hours after photobleaching of Syp-SN. Levels are significantly increased at 1 hour but not 5 minutes or 2 hours after ROS-mediated damage. (F: unbleached = 1 ± 0.089, n = 67 synapses, 2 independent experiments; bleached = 1.44 ± 0.219, n = 71 synapses, 2 independent experiments) (H: unbleached = 1 ± 0.080, n = 91 synapses, 2 independent experiments; bleached =

1.45 ± 0.174, n = 89 synapses, 2 independent experiments) (J: unbleached = 1 ± 0.074, n = 108 synapses, 2 independent experiments; bleached = 1.23 ± 0.134, n = 118 synapses, 2 independent experiments). Scale bars: 10µm. Error bars represent SEM. Unpaired T-test was used to evaluate statistical significance. ****p<0.0001, ***p<0.001, **p<0.01, *p<0.05. Adapted from Hoffmann et al. (Hoffmann et al., forthcoming).

6.9 ROS-induced damage to several presynaptic proteins induces presynaptic autophagy

As ROS generated by illuminating Supernova are anticipated to damage proteins only within 1-4nm of the sources (Jacobson et al., 2008; Takemoto et al., 2013), it seems reasonable to predict that the induction of presynaptic autophagy is linked to the damage of proteins physically associated with SVs, which are then sorted and gathered into the interior of the newly forming autophagophore membrane. If true, the damage to other presynaptic proteins should then also lead to the induction of autophagy.

To test this hypothesis, I coupled Supernova to two additional SV proteins, Synaptotagmin (Syt), an integral membrane protein with a long cytoplasmic tail (Chapman, 2002; Hilfiker et al., 1999), and Synapsin (Syn), a larger cytosolic protein (Figure 22A) that dynamically associates with the outer surface of SVs in an activity-dependent manner (Chi et al., 2001; Waites and Garner, 2011), potentially allowing for a more attenuated ROS-mediated damage to SVs.

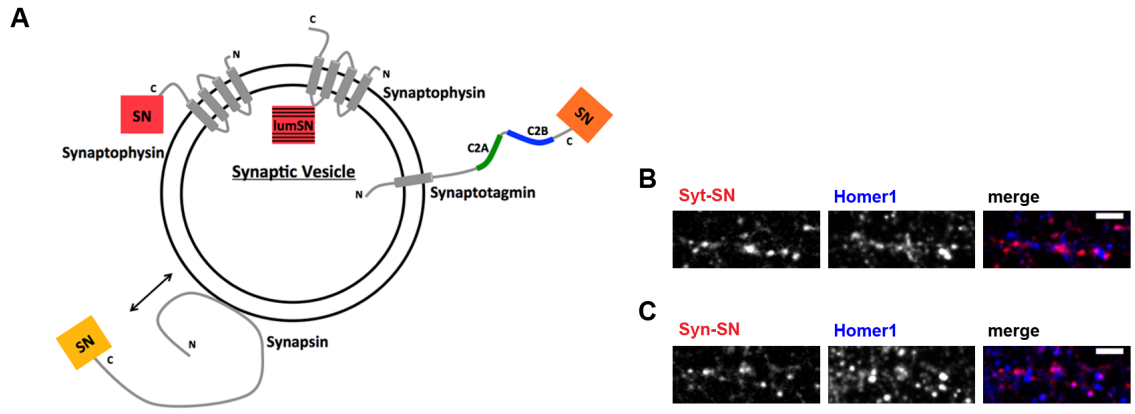

Figure 22: (A) Schematic of a SV containing Synaptophysin, Synaptotagmin and Synapsin tagged with Supernova. Note, the short (95aa) vs. long (346aa, comprised of two C2 domains) cytoplasmic tails of Synaptophysin vs. Synaptotagmin, respectively, which could significantly change the distance of Supernova to the SV membrane and thus its proximity to other SV proteins. Similarly, tagging Supernova to the much larger peripherally associated SV protein Synapsin could also affect its distance to other SV proteins. (B and C) Representative images of hippocampal neurons expressing FU-Syt-Supernova-P2A-eGFP-LC3 (B) or FU-Syn-Supernova-P2A-eGFP-LC3 (C) immunostained with antibodies against the postsynaptic protein Homer1. Colocalization of Syt-SN

(B) or Syn-SN (C) and Homer1 indicate presynaptic targeting of Syt-SN and Syn-SN. Scale bars: 5µm. Adapted from Hoffmann et al. (Hoffmann et al., forthcoming).

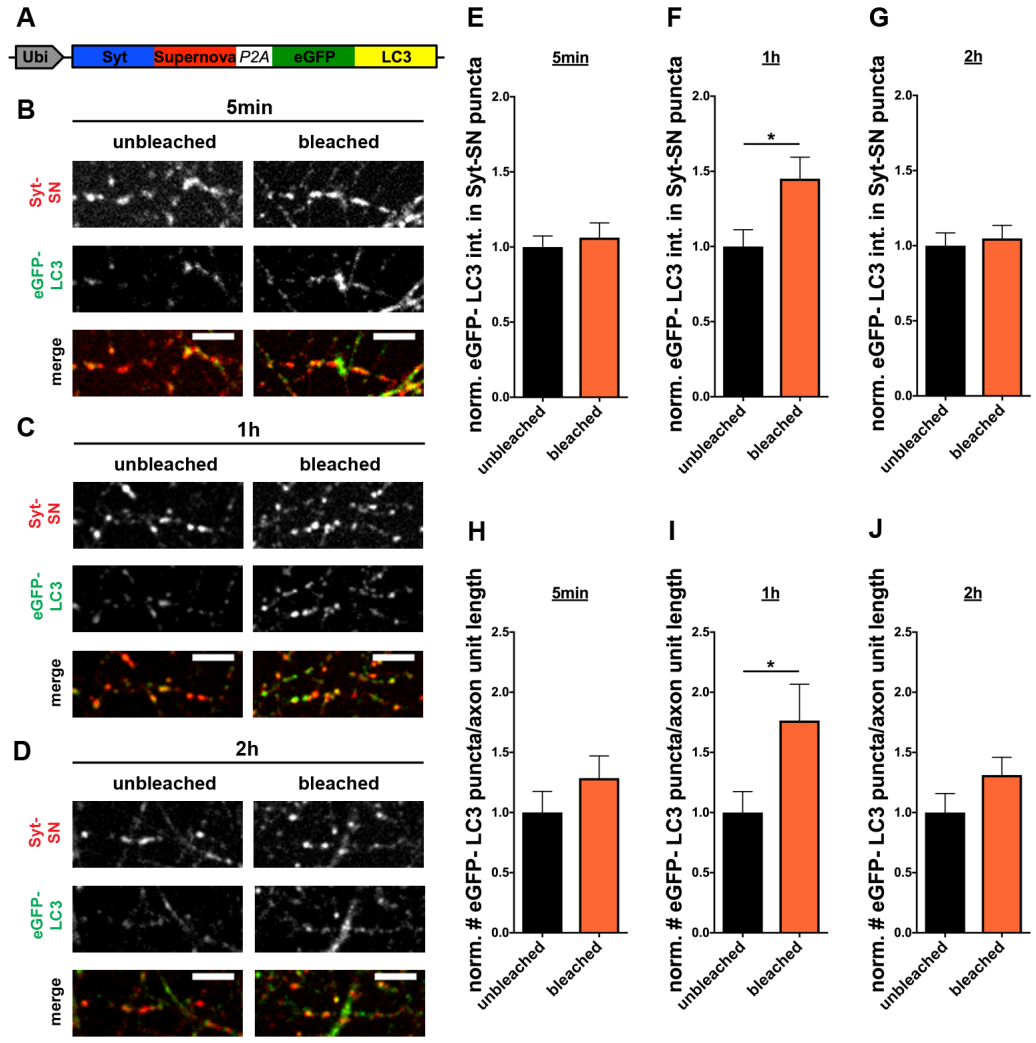

Figure 23: Induction of autophagy by ROS-mediated damage by Synaptotagmin-Supernova is slightly slower than with Synaptophysin-Supernova. (A) Schematic of FU-Syt-Supernova-P2A-eGFP-LC3 expression vector. (B-D) Images of axon segments (5 minutes, 1 hour and 2 hours after bleaching) that were subsequently fixed and stained with antibodies against GFP to detect eGFP-LC3 and Supernova to detect Syt-SN. Data indicate that autophagy at synapses can be induced through Syt-SN photobleaching. (E, F and G) Quantification of normalized eGFP-LC3 intensities within Syt-SN puncta 5 minutes (E), 1 hour (F) and 2 hours (G) after bleaching. (E: unbleached = 1 ± 0.074, n = 62 synapses, 2 independent experiments; bleached = 1.06 ± 0.098, n = 76 synapses, 2 independent experiments) (F: unbleached = 1 ± 0.111, n = 73 synapses, 2 independent experiments; bleached = 1.45 ± 0.143, n = 81 synapses, 2 independent experiments) (G: unbleached = 1 ± 0.085, n = 58 synapses, 2 independent experiments; bleached = 1.05 ± 0.087, n = 68 synapses, 2 independent experiments). (H, I and J) Quantification of the normalized number of eGFP-LC3 puncta per unit axon length in axons 5 minutes (H), 1 hour (I) and 2 hours (J) after photobleaching. (H: unbleached = 1 ± 0.175, n = 19 axons, 2 independent experiments; bleached = 1.29 ± 0.185, n = 19 axons, 2 independent experiments) (I: unbleached = 1 ± 0.174, n = 17 axons, 2 independent experiments; bleached = 1.76 ± 0.302, n = 18 axons, 2 independent experiments) (J: unbleached = 1 ± 0.158, n = 19 axons, 2 independent experiments; bleached = 1.31 ± 0.148, n = 20 axons, 2

independent experiments). Scale bars: 10µm. Error bars represent SEM. Unpaired T-test was used to evaluate statistical significance. ****p<0.0001, ***p<0.001, **p<0.01, *p<0.05. Adapted from Hoffmann et al. (Hoffmann et al., forthcoming).

To permit the simultaneous detection of presynaptic autophagy, I co-expressed Syt-SN or Syn-SN with eGFP-LC3 via my lentiviral vector (FU-Syt-Supernova-P2A-eGFP-LC3; FU-Syn-Supernova-P2A-eGFP-LC3). In control experiments, I confirmed that both Syt-SN and Syn-SN were appropriately processed (data not shown) and that Syt-SN and Syn-SN retained their ability to become selectively localized to presynaptic boutons (Figure 22B and C).

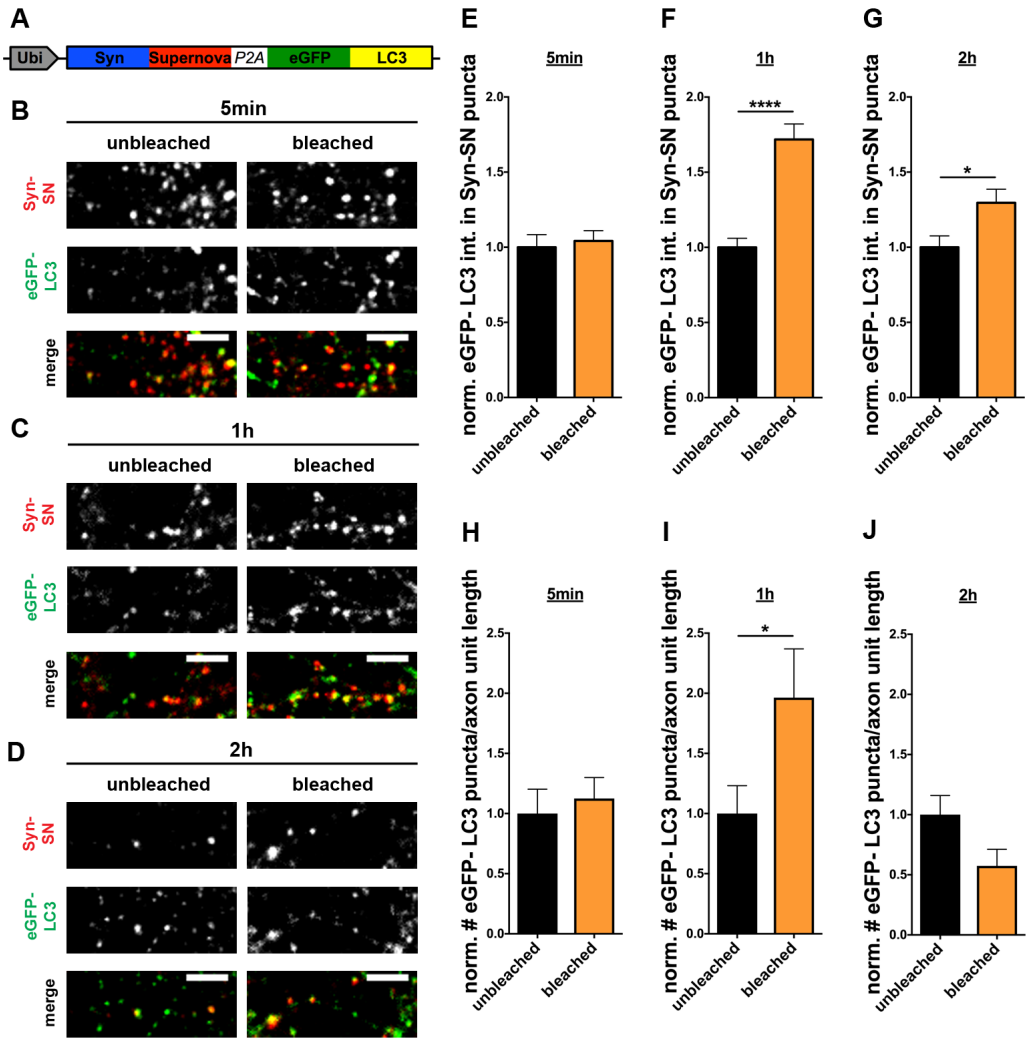

Figure 24: Induction of autophagy by ROS-mediated damage by Synapsin-Supernova is slightly slower than with Synaptophysin-Supernova. (A) Schematic of FU-Syn-Supernova-P2A-eGFP-LC3 expression vector. (B-D) Images of axon segments (5 minutes, 1 hour and 2 hours after bleaching) that were subsequently fixed and stained with antibodies against GFP to detect eGFP-LC3 and Supernova to detect Syn-SN. Data indicate that autophagy at synapses can be induced through Syn-SN photobleaching. (E, F and G) Quantification of normalized eGFP-LC3 intensities within Syn-SN puncta 5 minutes (E), 1 hour (F) and 2 hours (G) after bleaching. (E: unbleached = 1 ± 0.084, n =

58 synapses, 3 independent experiments; bleached = 1.04 ± 0.069, n = 81 synapses, 3 independent experiments) (F: unbleached = 1 ± 0.061, n = 77 synapses, 3 independent experiments; bleached = 1.72 ± 0.103, n = 103 synapses, 3 independent experiments) (G: unbleached = 1 ± 0.075, n = 42 synapses, 3 independent experiments; bleached = 1.30 ± 0.090, n = 71 synapses, 3 independent experiments). (H, I and J) Quantification of the normalized number of eGFP-LC3 puncta per unit axon length in axons 5 minutes (H), 1 hour (I) and 2 hours (J) after photobleaching. (H: unbleached = 1 ± 0.202, n = 18 axons, 3 independent experiments; bleached = 1.13 ± 0.174, n = 18 axons, 3 independent experiments) (I: unbleached = 1 ± 0.231, n = 18 axons, 3 independent experiments; bleached = 1.96 ± 0.405, n = 18 axons, 3 independent experiments) (J: unbleached = 1 ± 0.159, n = 18 axons, 3 independent experiments; bleached = 0.57 ± 0.138, n = 17 axons, 3 independent experiments). Scale bars: 10µm. Error bars represent SEM. Unpaired T-test was used to evaluate statistical significance. ****p<0.0001, ***p<0.001, **p<0.01, *p<0.05. Adapted from Hoffmann et al. (Hoffmann et al., forthcoming).

As described above for Syp-SN, infected neurons were photobleached at 13-15 DIV for 60 seconds and the intensity of eGFP-LC3 and the number of eGFP-LC3 puncta per axon unit length were quantified. Interestingly, eGFP-LC3 intensity in Syt-SN and Syn-SN puncta as well as the number of eGFP-LC3 puncta along axons did not change within 5 minutes of photobleaching (Figure 23E and H) (Figure 24E and H) compared to unbleached boutons. However, 1 hour after light-induced damage to either Synaptotagmin or Synapsin, eGFP-LC3 intensity significantly increased within presynaptic boutons immuno-positive for Syt-SN (Figure 23F) and Syn-SN (Figure 24F).

When fixed 2 hours after ROS production, eGFP-LC3 levels remained slightly elevated at bleached Syn-SN positive synapses (Figure 24G), but returned to unbleached levels in Syt-SN positive synapses (Figure 23G). Similarly, a higher number of eGFP-LC3 puncta along axons was observed 1 hour after photobleaching of both proteins Syt-SN (Figure 23I) and Syn-SN (Figure 24I). Taken together, these data indicate that, as with Synaptophysin, the local ROS-mediated damage to Synaptotagmin and the SV-associated protein Synapsin can induce presynaptic autophagy, albeit at attenuated slower rates.

These data indicate that the induction of presynaptic autophagy is tightly coupled to ROS damage to synaptic proteins, and thus associated with the normal clearance of misfolded or damaged SV proteins.

6.10 Further characterization of ROS-induced damage to Synapsin

After finding that ROS-induced damage to Synaptophysin leads to a PI3K-dependent induction of presynaptic autophagy but a PI3K-independent autophagy induction within the axon (Figure 19), I investigated whether Synapsin-SN bleaching would lead to a PI3K-dependent mode of autophagy. Therefore, 1µM wortmannin was added to neurons before bleaching SN and maintained in the culture for the following hour, after which neurons were fixed and analyzed.

In cells that were not treated with wortmannin, eGFP-LC3 intensity and the number of puncta in axons remained elevated (Figure 25C and D, Figure 24).

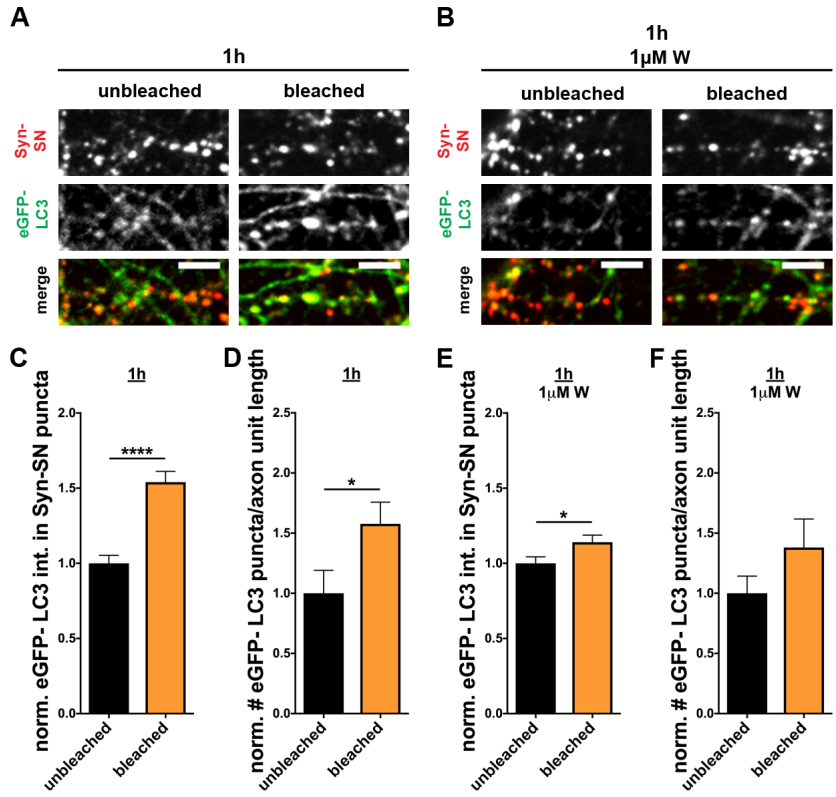

Figure 25: ROS-induced increase in eGFP-LC3 levels at presynaptic boutons is PI3K-dependent. (A and B) Images of hippocampal neurons expressing FU-Syn-Supernova-P2A-eGFP-LC3 that were fixed and stained with antibodies against GFP and Supernova 1 hour after photobleaching, either in the absence (A) or presence of 1µM wortmannin (W) (B). (C and D) Quantification of normalized eGFP-LC3 intensities within Syn-SN puncta (C) or the normalized number of eGFP-LC3 puncta per unit axon length (D) in culture not treated with wortmannin. (C: unbleached = 1 ± 0.053, n = 203 synapses, 2 independent experiments; bleached = 1.54 ± 0.072, n = 259 synapses, 2 independent experiments) (D: unbleached = 1 ± 0.191, n = 19 axons, 2 independent experiments; bleached = 1.58 ± 0.181, n = 20 axons, 2 independent experiments). (E and F) Quantification of normalized eGFP-LC3 intensities within Syn-SN puncta (E) or number of eGFP-LC3 puncta per unit axon length (F) in culture treated with wortmannin before and after photobleaching. (E: unbleached = 1 ± 0.043, n = 206 synapses, 2 independent experiments; bleached = 1.14 ± 0.048, n = 195 synapses, 2 independent experiments). (F: unbleached = 1 ± 0.143, n = 13 axons, 2 independent experiments; bleached = 1.38 ± 0.237, n = 13 axons, 2 independent experiments). Scale bars: 10µm. Error bars represent SEM. Unpaired T-test was used to evaluate statistical significance. ****p<0.0001, ***p<0.001, **p<0.01, *p<0.05.

Similar to Synaptophysin, there is a reduction of eGFP-LC3 accumulation in bleached boutons labeled by Syn-SN compared to unbleached Syn-SN boutons when wortmannin is present (Figure 25C and E). However, the number of eGFP-LC3 puncta was still slightly elevated although not significantly (Figure 25D and F). These results indicate that ROS-induced increase

in eGFP-LC3 levels is partly PI3K-dependent. More precisely, the induction of presynaptic autophagy may be dependent on the canonical autophagy pathway while bleaching of axonal/transported Syn-SN may lead to PI3K-independent forms of autophagy.

As with Synaptophysin, a lentiviral vector expressing Syn-SN and eGFP-Rab7 was created (FU-Syn-Supernova-P2A-eGFP-LC3) and used to evaluate later stages of the autophagy/endo-lysosomal pathway. As nicely reviewed by Stenmark (Stenmark, 2009), the GTPase Rab7 is a widely used late endosome marker. However, it is also present on late phagosomes and late autophagosomes making it a marker for both late autophagy and endo-lysosomal degradation.

Strikingly, I did not observe the same increase in eGFP-Rab7 at bleached boutons immuno-positive for Syn-SN compared to unbleached boutons from the same culture dish, as I observed with Synaptophysin-Supernova (Figure 21), 5 minutes, 1 hour or 2 hours after Syn-SN bleaching (Figure 26). These findings indicate that damage to Synapsin is less potent in inducing the endo-lysosomal pathway, raising the question of whether it is the associated damage to integral SV proteins that is critical for the activation of the endo-lysosomal and autophagy pathways.

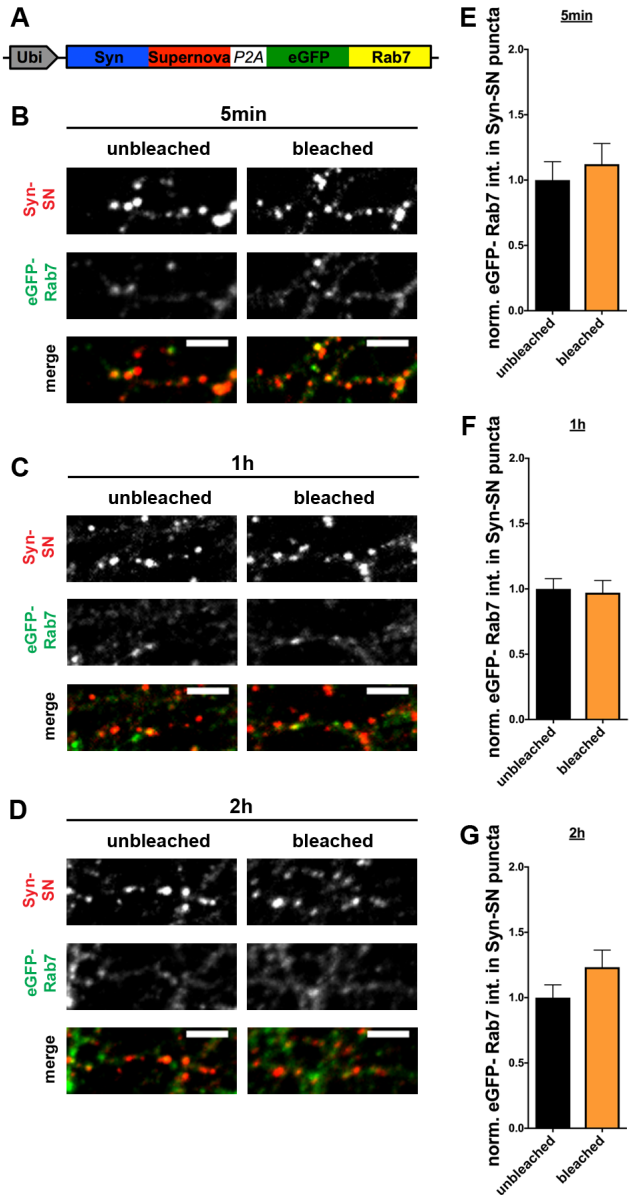

Figure 26: Syn-SN mediated ROS production does not change eGFP-Rab7 levels at presynaptic boutons. (A) Schematic of FU-Syn-Supernova-P2A-eGFP-Rab7 expression vector. (B, C and D) Images of hippocampal neurons expressing FU-Syn-Supernova-P2A-eGFP-Rab7 that were fixed and stained with antibodies against GFP and Supernova 5 minutes, 1 hour and 2 hours after Syn-SN mediated ROS production. (E, F and G) Quantification of the normalized eGFP-Rab7 intensity in Syn-SN puncta 5 minutes, 1 hour or 2 hours after photobleaching of Syn-SN (E: unbleached = 1 ± 0.141, n = 41 synapses, 3 independent experiments; bleached = 1.12 ± 0.158, n = 63 synapses, 3 independent experiments) (F: unbleached = 1 ± 0.079, n = 60 synapses, 3 independent experiments; bleached = 0.97 ± 0.093, n = 61 synapses, 3 independent experiments) (G: unbleached = 1 ± 0.098, n = 48 synapses, 3 independent experiments; bleached = 1.23 ± 0.131, n = 50 synapses, 3 independent experiments). Scale bars: 10µm. Error bars represent SEM. Unpaired T-test was used to evaluate statistical significance.

6.11 Supernova-tagged proteins are more abundant in ROS-induced autophagy organelles than endogenous SV proteins

To date several studies have demonstrated that autophagosomes form in axons upon starvation, rapamycin treatment as well as enhanced synaptic activitiy (Maday and Holzbaur, 2014; Wang et al., 2015) and become retrogradely transported along the axon towards the soma (Cheng et al., 2015; Maday et al., 2012). An unresolved question is which synaptic proteins become associated with autophagic cargo. A related question is whether presynaptic autophagy leads to the en-mass removal of SVs or whether it can selectively scavenge damaged proteins. The ability of my method to damage specific SV proteins with light and induce autophagy provides a unique opportunity to explore these questions.

In an initial experiment, I examined whether Supernova-tagged Synaptophysin (Syp-SN) appears in extrasynaptic eGFP-LC3 positive puncta following light-induced ROS production. To distinguish between synaptic and extrasynaptic eGFP-LC3 organelles, cultures were fixed 1 hour after bleaching and stained with the presynaptic active zone marker Bassoon and quantified for the fraction of extrasynaptic eGFP-LC3 puncta negative for Bassoon but positive for synaptic proteins.

In experiments with Syp-SN, I observed that 70% of extrasynaptic eGFP-LC3 puncta (also referred to as autophagy (cargo) organelles) are positive for Syp-SN (Figure 27A and D). This suggests that ROS damaged Syp-SN is indeed cargo of these organelles. To investigate whether the presence of Syp-SN in autophagy cargo organelles represents the en-mass engulfment of SVs or the selective removal of this damaged protein, I additionally monitored the distribution of endogenous Synaptotagmin1 (Syt1), a second core constituent of SVs, within the same extrasynaptic autophagy organelles following light-induced damage to Syp-SN. As Synaptotagmin1 is not known to directly interact with Synaptophysin, I reasoned that the ROS-mediated damage to Syp-SN would not necessarily damage Synaptotagmin1 on the same SV. Interestingly, the fraction of extrasynaptic autophagy organelles that are positive for Synaptotagmin1 is dramatically smaller than the fraction of Syp-SN positive autophagy cargo organelles (Figure 27A and D), suggesting that damage to Synaptophysin does not necessarily also promote the degradation of Synaptotagmin by synaptic autophagy.

In order to minimize the possibility that Syp-SN and eGFP-LC3 are colocalizing coincidentally, I quantified the fraction of extrasynaptic Syp-SN puncta that were positive for eGFP-LC3 and this fraction was significantly lower than the vice versa (Figure 27D, left panel versus right panel). This indicates that some of the extrasynaptic Syp-SN puncta may be part of the anterograde transport of synaptic proteins in contrast to the retrograde autophagic transport observed for the reciprocal experiment.

To confirm the selectivity of autophagic cargo after Supernova-induced damage, I also quantified the fraction of Syt-SN positive extrasynaptic autophagy cargo organelles 1 hour after bleaching. As with Syp-SN, more than 65% of the extrasynaptic eGFP-LC3 puncta colocalized with Syt-SN, while only 18% of the endogenous Synaptophysin (Syp1) was present at these sites (Figure 27B and E). These data indicate that the autophagic machinery within presynaptic boutons can detect and selectively remove damaged SV proteins. It also shows that damage to other SV proteins can result in their sorting into the autophagy degradative pathway.

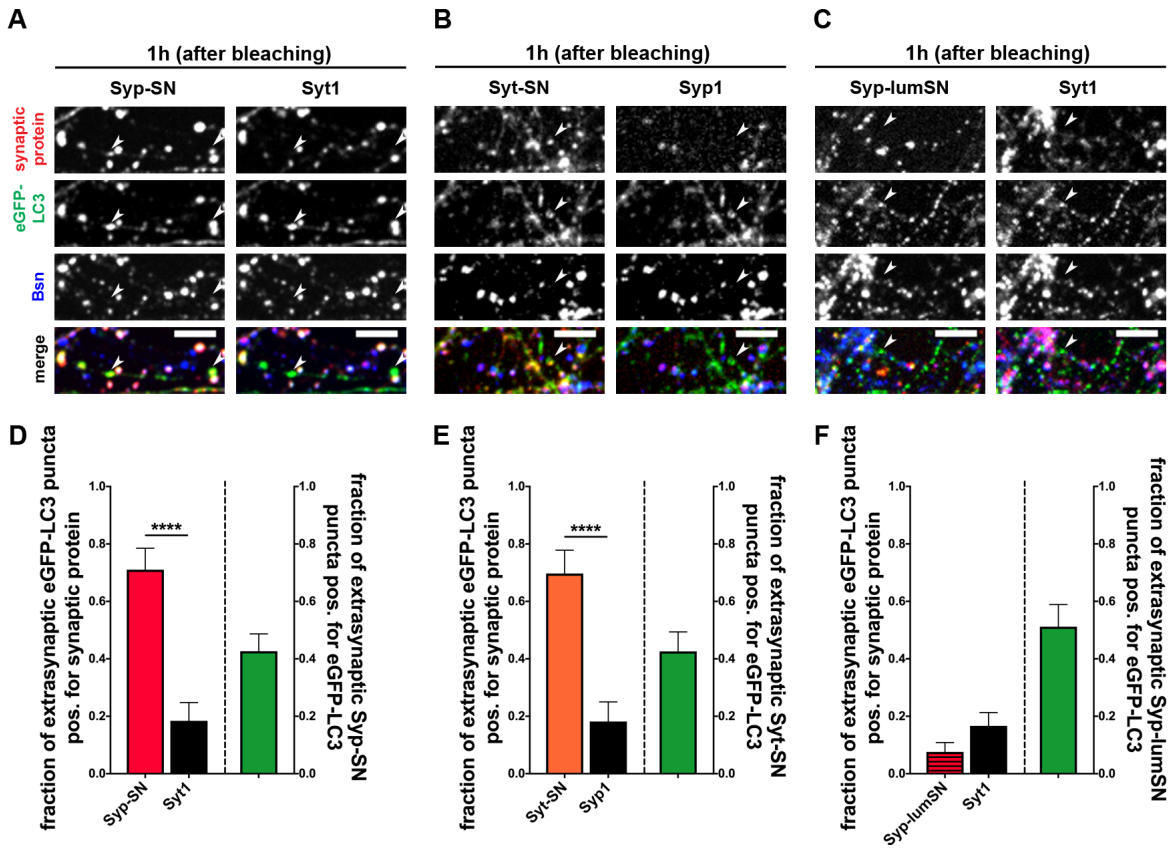

Figure 27: ROS damaged SV proteins selectively accumulate in autophagy organelles. (A, B and C) Images of hippocampal neurons expressing Supernova-tagged synaptic proteins Syp-SN (A), Syt-SN (B) or Syp-lumSN (C) that were fixed 1 hour after bleaching and stained with antibodies against GFP, Supernova, Bassoon and Synaptotagmin1 (Syt1) (A and C) or Synaptophysin1 (Syp1) (B). (D) Quantification of the fraction of extrasynaptic eGFP-LC3 puncta positive for SN-tagged Synaptophysin, indicated by arrowheads in (A), or endogenous Syt1 within the same experiment (Syp-SN = 0.71 ± 0.075, n = 38 puncta, 3 independent experiments; Syt1 = 0.18 ± 0.064, n = 38 puncta, 3 independent experiments). Also quantified is the fraction of extrasynaptic Syp-SN puncta that are positive for eGFP-LC3 (0.43 ± 0.060, n = 68 puncta, 3 independent experiments). (E) Quantification of the fraction of extrasynaptic eGFP-LC3 puncta positive for SN-tagged Synaptotagmin, indicated by arrowheads (B), or endogenous Syp1 within the same experiment (Syt-SN = 0.70 ± 0.081, n = 33 puncta, 2 independent experiments; Syp1 = 0.18 ± 0.068, n = 33 puncta, 2 independent experiments). Also quantified is the fraction of extrasynaptic Syt-SN puncta that are positive for eGFP-LC3 (0.43 ± 0.068, n = 54 puncta, 2 independent experiments). (F)

Quantification of the fraction of extrasynaptic eGFP-LC3 puncta positive for luminal SN-tagged Synaptophysin (Syp-lumSN), indicated by arrowheads in (C), or endogenous Syt1 within the same experiment (Syp-lumSN = 0.08 ± 0.033, n = 66 puncta, 3 independent experiments; Syt1 = 0.17 ± 0.046, n = 66 puncta, 3 independent experiments). Also quantified is the fraction of extrasynaptic Syp-lumSN puncta that are positive for eGFP-LC3 (0.51 ± 0.077, n = 43 puncta, 3 independent experiments). Scale bars: 10µm. Error bars represent SEM. Unpaired T-test was used to evaluate statistical significance. ****p<0.0001, ***p<0.001, **p<0.01, *p<0.05. Adapted from Hoffmann et al. (Hoffmann et al., forthcoming).

The selectivity of the autophagic cargo points towards a selective tagging of the damaged Supernova fusion protein. This tagging likely happens at the cytoplasmic side of the SV as this is where the degradation machinery is located. To test this hypothesis, I fused Supernova to Synaptophysin between the third and fourth transmembrane domain resulting in a luminal Supernova (FU-Syp-lumSN-P2A-eGFP-LC3) (Figure 22A). Here, I did not observe an accumulation of eGFP-LC3 at bleached Syp-lumSN positive boutons (data not shown). Intriguingly, the fraction of Syp-lumSN positive extrasynaptic autophagy cargo organelles is very low (Figure 27C an F) compared to Syp-SN (Figure 27D) indicating that bleached Syp-lumSN does not become cargo of autophagy organelles after ROS-induced damage.

The low but significant presence (~ 20%) of endogenous Synaptophysin1 and Synaptotagmin1 in extrasynaptic eGFP-LC3 puncta could arise either from the peripheral damage of ROS or be part of the basal flux of these proteins through this pathway. I thus examined whether, under basal conditions, endogenous Synaptophysin1 and Synaptotagmin1 versus Synapsin1 associate with autophagy cargo organelles. In order to monitor presynaptic autophagy only, I sparsely infected neurons with the lentiviral vector FU-eGFP-LC3, left them untreated until fixation at 14 DIV, followed by staining with antibodies against the designated SV proteins and Bassoon.

Here, I observed that higher levels of both endogenous Synaptophysin1 and Synaptotagmin1 were found at extrasynaptic eGFP-LC3 puncta compared to Synapsin1 (Figure 28). In line with my previous findings, the fraction of extrasynaptic eGFP-LC3 puncta positive for Syp1 and Syt1 was ~ 30-40%. These data indicate that Syp1 and Syt1 may be cleared through this degradative pathway, whereas Syn1 may be preferentially cleared through a different pathway such as the ubiquitin-proteasome-system (UPS).

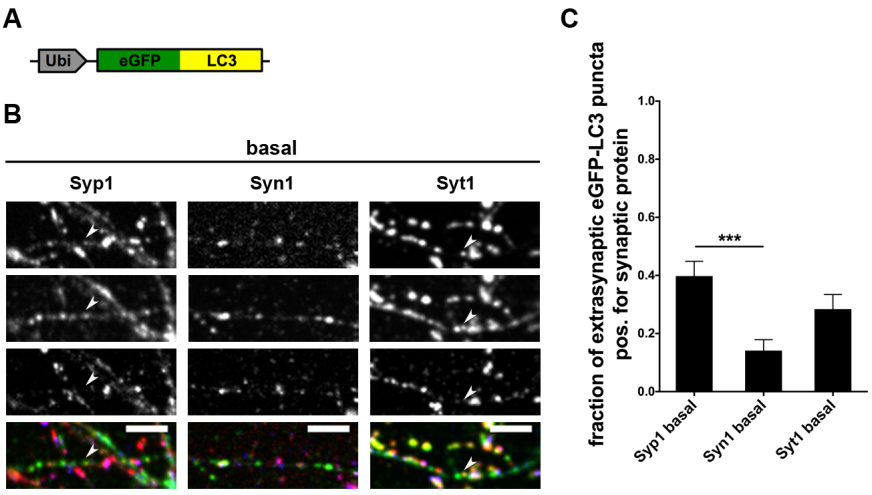

Figure 28: SV proteins are part of the basal autophagy flux. (A) Schematic of FU-eGFP-LC3 expression vector. (B) Images of hippocampal neurons expressing eGFP-LC3 were fixed untreated (basal autophagy) and stained with antibodies against GFP, Bassoon and Synaptophysin1 (Syp1) or Synapsin1 (Syn1) or Synaptotagmin1 (Syt1). (C) Quantification of the fraction of extrasynaptic eGFP-LC3 puncta positive for endogenous Synaptophysin1, Synapsin1 or Synaptotagmin1. Note, the fraction of extrasynaptic eGFP-LC3 puncta positive for Synaptophysin1 is significantly higher than the fraction positive for Synapsin1 (Syp1 basal = 0.40 ± 0.051, n = 93 puncta, 2 independent experiments; Syn1 basal = 0.14 ± 0.038, n = 85 puncta, 2 independent experiments; Syt1 basal = 0.28 ± 0.050, n = 81 puncta, 2 independent experiments). Scale bars: 10µm. Error bars represent SEM. ANOVA Tukey's multiple comparisons test was used to evaluate statistical significance. ****p<0.0001, ***p<0.001, **p<0.01, *p<0.05. Adapted from Hoffmann et al. (Hoffmann et al., forthcoming).

6.12 ROS-induced synaptic autophagy acts as a beneficial surveillance mechanism maintaining synapse function

A fundamental question within the synaptic proteostasis field is what roles different clearance systems play during synaptic transmission. Most studies on autophagy rely either on the analysis of genetic ablation and inactivation of key autophagic proteins (Atg5 and Atg7) (Rubinsztein et al., 2011; Russell et al., 2014) or the activation of autophagy with drugs like rapamycin, none of which are specific for the synapse and generally trigger a homeostatic response from other systems masking a specific role of autophagy.

Having shown that light-activated ROS production can be used to rapidly (5 minutes) trigger the autophagic clearance of selectively damaged SV proteins, I was keen to explore whether presynaptic autophagy contributes to the real-time maintenance of synaptic function. As an initial test of this concept, I examined whether the ROS-induced damage of Synaptophysin-Supernova and subsequent induction of autophagy can affect the functional recycling of SVs based on the activity-dependent uptake of the styryl dye FM 1-43 (Cochilla et al., 1999). This was

accomplished by performing FM 1-43 uptake experiments approximately 5 minutes after photobleaching Syp-SN positive boutons.

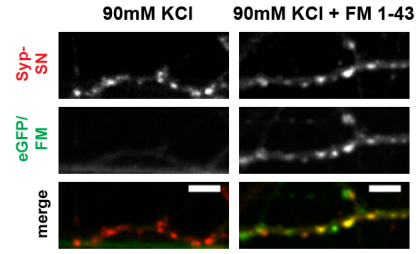

Figure 29: Syp-SN expressing synapses show functional recycling depicted by FM dye uptake. Synapses treated with 90mM KCl only (90mM KCl) exhibit only a weak eGFP(-LC3) signal while synapses loaded with FM 1-43 during a 90mM KCl stimulus (90mM KCl + FM 1-43) depict characteristic FM dye patterns that colocalize with synaptic Syp-SN puncta. Note that both eGFP and FM 1-43 are excited by 491nm light and emit with close peak intensities of 509nm and 579nm, respectively. Scale bars: 5µm.

As an initial experiment, I evaluated whether the levels of eGFP-LC3 after a high potassium (90mM KCl) stimulus do not interfere with the FM 1-43 signal, as both identities have similar fluorescent properties. Indeed, I could show that the eGFP-LC3 signal from live images is insignificantly small compared to the FM 1-43 signal, even after a high potassium stimulus (Figure 29, compare left to right middle panels). This first experiment also showed that Syp-SN expressing synapses are still able to take up FM 1-43 dye indicated by a punctate FM 1-43 pattern that nicely colocalizes with Syp-SN when FM 1-43 is added during the stimulus. Thus, Syp-SN expressing neurons are still able to recycle SVs.

To assess the effect of ROS-mediated damage to SVs, I compared the efficiency of FM dye uptake between bleached and unbleached synapses under basal conditions. More precisely, I plotted the amount of FM 1-43 uptake versus Syp-SN intensity as a measure for the strength of induced damage and quantified the slope of the linear regression. Interestingly, no differences could be detected (Figure 30A and D). These data indicate that either the damage created during ROS production is too gentle to affect synaptic function or that the induced autophagy (Figure 16) is sufficient to remove these damaged SV proteins thus maintaining synaptic function. To test this latter concept, 1µM wortmannin was added 1 minute before photobleaching and maintained in the imaging buffer before and during the loading of synapses with FM 1-43. Note that 1µM wortmannin leads to a total block of presynaptic autophagy as shown in previous experiments (Figure 19). Intriguingly, under these conditions, the ROS-induced damage of Syp-SN decreases the subsequent loading of FM 1-43 within the bleached area compared to those outside (Figure 30B). I quantified the amount of FM dye uptake dependent on the amount of Syp-SN present at

the bouton (before bleaching), assuming that more Syp-SN/bouton causes more damage to the terminal.

ROS-mediated damage of Syp-SN had no effect on the slope of the linear regression when autophagy was allowed to operate normally (Figure 30C and D), but significantly reduced the slope when the induction of synaptic autophagy was inhibited with wortmannin (Figure 30C and E). Importantly, the addition of wortmannin alone did not alter the uptake of FM 1-43 or the slope of the linear regression (Figure 30C, D and E). These data indicate that autophagy may operate in real-time to maintain the integrity and functionality of SVs.

To assess the specificity of this effect, I examined whether the ROS-induced damage of the peripheral SV protein Synapsin also affects the efficiency of FM dye loading. As above, FM 1-43 loading was performed ~ 5 minutes after damaging Syn-SN. Here, I saw no difference in the extent of FM dye uptake between bleached and unbleached synapses under physiological conditions (Figure 30F and I). I also observed no difference in FM dye uptake between bleached and unbleached synapses in the presence of 1µM wortmannin (Figure 30G and J). It should be noted that photodamage to Syn-SN expressing boutons does not induce visible synaptic autophagy during the initial 5 minutes following damage (Figure 24E). This suggests that the superoxides generated by Syn-SN only modestly damage SVs compared to the integral membrane protein Syp-SN. Moreover, these data indicate that autophagy plays a minor role in the clearance of Syn-SN. This is in line with my findings that endogenous Synapsin1 is rarely present in autophagic organelles (Figure 28).

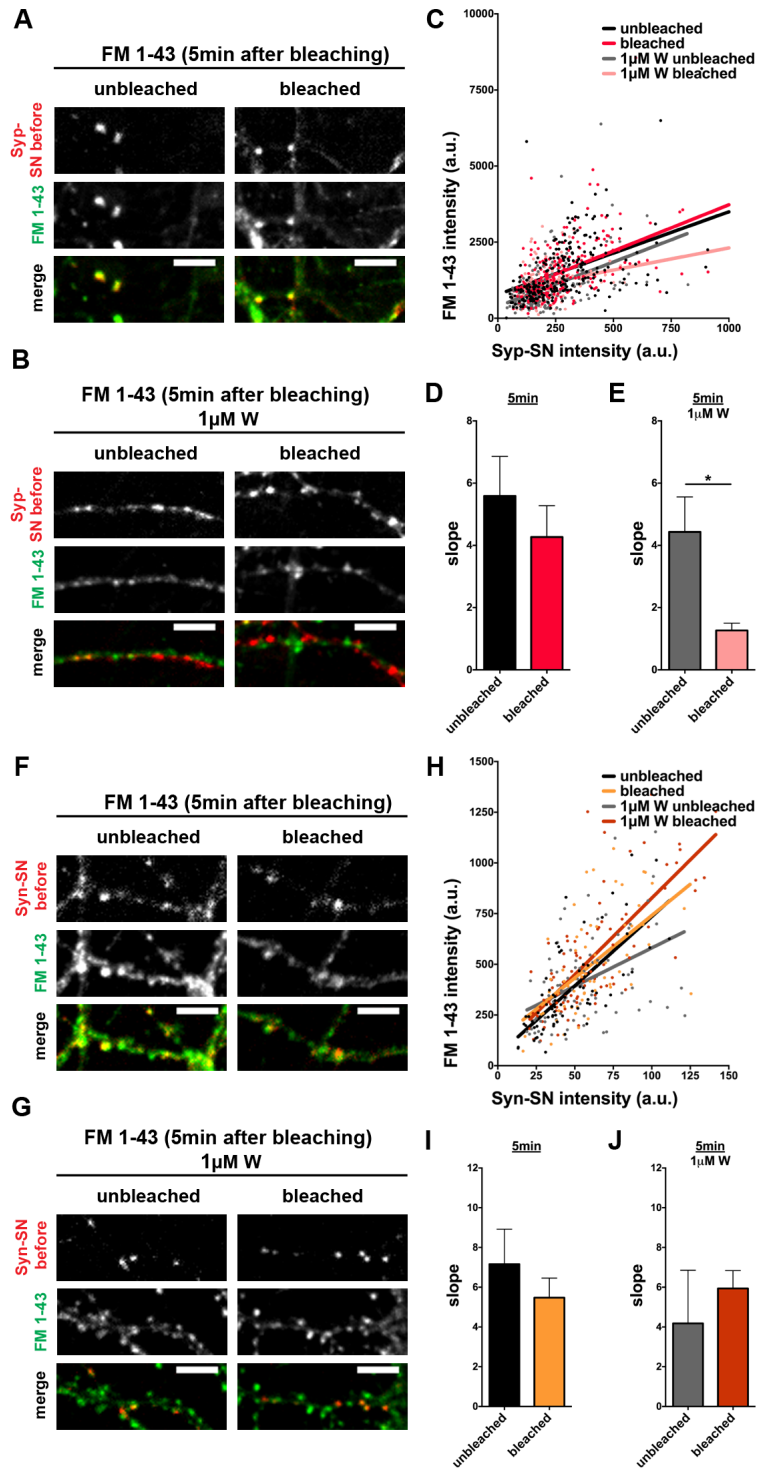

Figure 30: ROS-induced damage to Syp-SN impairs FM 1-43 uptake only when autophagy is inhibited. (A, B, F, G) Images of hippocampal neurons expressing FU-Syp-Supernova-P2A-eGFP-LC3 (A and B) or FU-Syn-Supernova-P2A-eGFP-LC3 (F and G), loaded with FM 1-43 for 90 seconds in 90mM KCl, 5 minutes after photobleaching in the absence (A and F) or presence of 1µM wortmannin (W) (B and G). Note, Syp-SN and Syn-SN images were taken before bleaching. (C) Correlation of FM 1-43 intensity over Syp-SN intensity of (A) and (B) (n = 238 (unbleached), 221 (bleached), 221 (1µM W unbleached), 147 (1µM W bleached) synapses, 4 independent experiments). (D and E) Quantification of the slope of the linear regression between bleached and unbleached synapses either in the absence (D: unbleached = 5.59 ± 1.272, 4 independent experiments; bleached = 4.27 ± 1.007, 4 independent experiments) or presence of (E: unbleached =

4.43 ± 1.126, 4 independent experiments; bleached = 1.26 ± 0.235, 4 independent experiments). Note, in the presence of wortmannin, the slope of the linear regression is significantly reduced in bleached synapses compared to unbleached synapses (E). (H) Correlation of FM 1-43 intensity over Syn-SN intensity of (F) and (G) (n = 69 (unbleached), 64 (bleached), 80 (1µM W unbleached), 88 (1µM W bleached) synapses, 3 independent experiments). (I and J) Quantification of the slope of the linear regression between bleached and unbleached synapses either in the absence (I: unbleached = 7.16 ± 1.762, 3 independent experiments; bleached = 5.47 ± 0.986, 3 independent experiments) or presence of wortmannin (J: unbleached = 4.18 ± 2.674, 3 independent experiments; bleached = 5.94 ± 0.900, 3 independent experiments). Note, wortmannin does not affect the uptake of FM 1-43 dye following ROS-mediated damage to Syn-SN. Scale bars: 10µm. Error bars represent SEM. Unpaired T-test was used to evaluate statistical significance. ****p<0.0001, ***p<0.001, **p<0.01, *p<0.05.

To confirm that autophagy is required to maintain synaptic transmission following ROS-mediated damage to SVs, electrophysiological experiments were performed on neurons expressing Synaptophysin-SN. Here, amplitudes of excitatory postsynaptic currents (EPSCs) were recorded from autaptic neurons at 13-18 DIV, which were infected with FU-Syp-Supernova-P2A-eGFP-LC3 lentivirus at 2-3 DIV. Similar to FM dye uptake experiments, bleaching alone did not robustly change the EPSC amplitude (Figure 31A). The addition of 1µM wortmannin alone (without bleaching) also had no effect on EPSC amplitudes (Figure 31B). However, when autophagy was inhibited with wortmannin during and after light-activated ROS production, the decrease in EPSC amplitudes was significant (Figure 31C and D). A similar effect could be observed when autophagy was inhibited by knocking down Atg5. Intriguingly, neurons expressing shRNA against Atg5 (shAtg5) alone did not show an altered EPSC amplitude (Figure 31F and H) indicating that basal autophagy is not necessary for synapse function. However, challenging the system through the light-activated ROS production leads to a significant decrease of the EPSC amplitude in neurons expressing shAtg5 (Figure 31G and H) but not in neurons expressing scrambled shRNA (Figure 31E and H). Together, these data nicely support the concept that autophagy plays a real-time role in maintaining synaptic function by helping the synaptic terminal to cope with protein damaging insults.

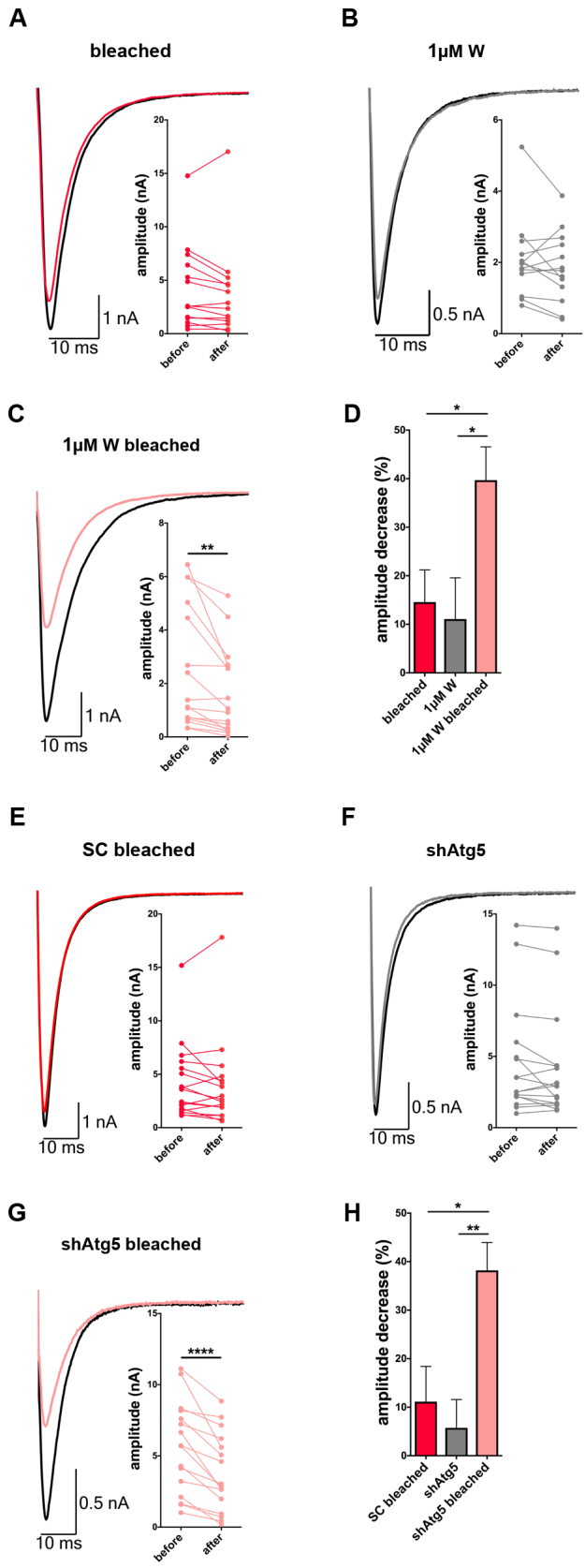

Figure 31: ROS-induced damage to Syp-SN impairs evoked release only when autophagy is inhibited. (A, B and C) Example traces of whole-cell patch recording of evoked EPSCs from autaptic hippocampal neurons expressing FU-Syp-Supernova-P2A-eGFP-LC3 before and 5 minutes after ROS-induced damage to Syp-SN either in the absence (A) or presence of 1µM wortmannin (W) (C).

Neurons treated with wortmannin but were not bleached served as a control (B). (A amplitude: before = 4.25 ± 1.050, after = 3.74 ± 1.134, 14 neurons, 3 independent experiments) (B amplitude: before = 2.07 ± 0.311, after = 1.85 ± 0.277, 13 neurons, 3 independent experiments) (C amplitude: before = 2.50 ± 0.570, after = 1.63 ± 0.409, 16 neurons, 3 independent experiments) (M) Quantification of the percent decrease in EPSC amplitude after photobleaching or wortmannin treament only. Note that the decrease in amplitude is significantly higher when 1µM wortmannin is present during bleaching (bleached = 14.57 ± 6.620, n = 14 neurons, 3 independent experiments; 1µM W = 11.09 ± 8.479, n = 13 neurons, 3 independent experiments; 1µM W bleached = 39.69 ± 6.869, n = 16 neurons, 3 independent experiments). (E, F and G) Example traces of whole-cell patch recording of evoked EPSCs from autaptic hippocampal neurons expressing F-U6-scRNA(SC)-U-Syp-Supernova-P2A-eGFP-LC3 (E) or F-U6-shAtg5-U-Syp-Supernova-P2A-eGFP-LC3 (G) before and 5 min after ROS-induced damage to Syp-SN. Neurons expressing F-U6-shAtg5-U-Syp-Supernova-P2A-eGFP-LC3 that were not bleached served as a control (F). (E amplitude: before = 4.23 ± 0.853, after = 3.87 ± 0.980, 17 neurons, 3 independent experiments) (F amplitude: before = 4.60 ± 0.987, after = 4.22 ± 0.962, 16 neurons, 3 independent experiments) (G amplitude: before = 5.58 ± 0.800, after = 3.79 ± 0.687, 16 neurons, 3 independent experiments). (H) Quantification of the percent decrease in EPSC amplitude after photobleaching. Note that the decrease in amplitude is significantly higher in F-U6-shAtg5-U-Syp-Supernova-P2A-eGFP-LC3 expressing neurons that were bleached (SC bleached = 11.15 ± 7.261, n = 17 neurons, 3 independent experiments; shAtg5 = 5.74 ± 5.836, n = 16 neurons, 3 independent experiments; shAtg5 bleached = 38.19 ± 5.766, n = 16 neurons, 3 independent experiments). Error bars represent SEM. Paired T-test (A-C, E-G) and ANOVA Tukey's multiple comparisons test (D and H) was used to evaluate statistical significance. ****p<0.0001, ***p<0.001, **p<0.01, *p<0.05. Adapted from Hoffmann et al. (Hoffmann et al., forthcoming).

6.13 Bassoon KO leads to elevated presynaptic autophagy in neurons at 21 DIV

An important question raised by these studies is how mechanistically boutons can so quickly respond to ROS-mediated damage to SVs. Recent studies indicate that the presynaptic active zone protein Bassoon may be a negative regulator of presynaptic autophagy via its interaction with the autophagy-related protein Atg5 (Okerlund et al., 2017). To further investigate the role of Bassoon within presynaptic autophagy, I conducted several studies with Bassoon KO (Bsn KO) neurons from the Gundelfinger lab (Davydova et al., 2014). Interestingly, Okerlund and colleagues (Okerlund et al., 2017) found that Bsn KO neurons show an increased number of LC3 puncta along axons and within the soma of these cells (Okerlund et al., 2017) at 14 DIV. At present it is unclear whether this increase in autophagy is associated with the differentiation of neurons, a derepression of autophagy or part of a degenerative process caused by the loss of Bassoon as observed in neurons lacking both Bassoon and Piccolo (Waites et al., 2013). To help distinguish these possibilities, I performed a set of autophagy monitoring experiments on mature neurons that had been in culture for 21 DIV. WT and Bsn KO neurons were infected with a lentivirus expressing LC3 tagged with both eGFP and mRFP (FU-ptf-LC3; tandem fluorescent, eGFP and mRFP) and fixed at 21 DIV. This vector has the advantage that while autophagosomes are double positive (exhibiting both green and red fluorescence), autolysosomes (autophagosomes that have fused with lysosomes) are red only due to the pH sensitive

quenching of eGFP, thus allowing autophagic flux to be monitored. Identification of synaptic autophagosomes was accomplished by staining fixed neurons with antibodies against the SV marker Synaptophysin1 (Syp1).

Intriguingly, Bsn KO neurons have significantly more tf-LC3 puncta along axons than WT neurons (Figure 32C) and additionally they depict a higher colocalization of tf-LC3 and Synaptophysin1 than WT control neurons (Figure 32E). However, the increase is slightly smaller than observed at DIV 14 (Okerlund et al., 2017). As wortmannin diminishes this effect (Figure 32C and E), it can be concluded that high autophagy due to loss of Bassoon is primarily PI3K-dependent. Strikingly, I did not observe a loss of Synaptphysin1 puncta in 21 DIV old neurons (Figure 32A and D) in contrast to 14 DIV old neurons as described previously. Additionally, I could not detect any differences between WT and Bsn KO monitoring RFP-LC3 puncta within the soma (Figure 32F and H) nor the number of tf-LC3 puncta per unit length of dendrite (Figure 32G and I) at 21 DIV. Interestingly, the number of tf-LC3 puncta in dendrites was approximately 10-fold lower than the number of tf-LC3 puncta along axons suggesting that autophagic clearance is more profound in the axonal than in the dendritic arbor.

These data indicate that 21 DIV Bsn KO neurons still have increased autophagy compared to WT neurons but to a lesser extent than neurons at 14 DIV. The continued elevation of autophagy in neurons 21 DIV suggests that these neurons retain an increased autophagic capacity and thus may be more successful in maintaining effective SV pools. Given that SV pool size is maintained in these boutons, I would conclude that the increased autophagy in Bsn KO neurons does not promote synaptic degeneration.

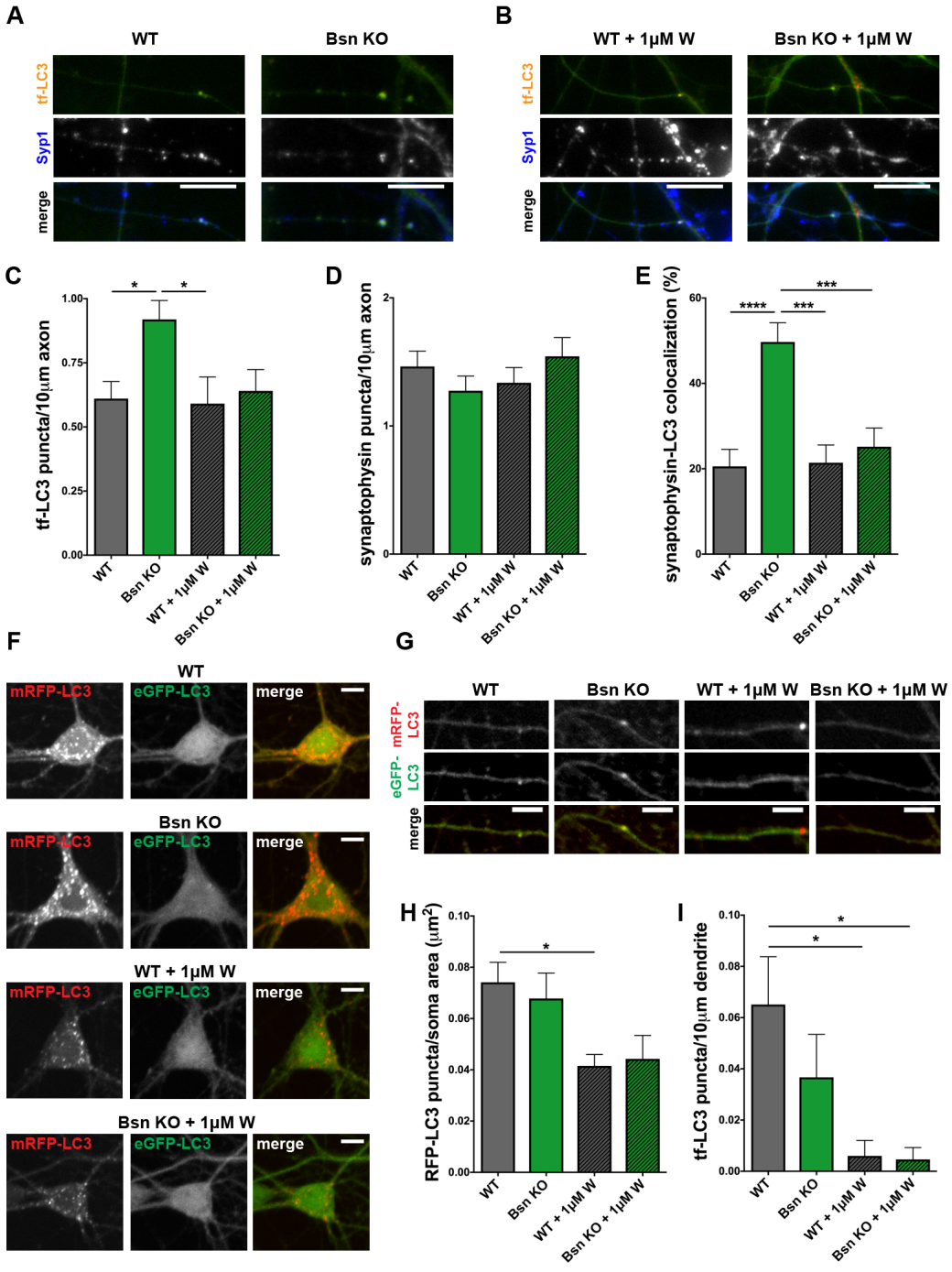

Figure 32: Bsn KO neurons show increased axonal autophagy at 21 DIV. (A and B, F and G) Images of hippocampal neurons expressing FU-ptf-LC3 that were fixed and stained with antibodies against Synaptophysin1 (Syp1). For PI3K inhibition, neurons were incubated with 1µM wortmannin (W) 16 hours prior fixation. (C) Quantification of the number of tf-LC3 puncta per axon unit length (WT = 0.61 ± 0.067, n = 47 axons, 4 independent experiments; Bsn KO = 0.92 ± 0.074, n = 55 axons, 4 independent experiments; WT + 1µM W = 0.59 ± 0.104, n = 22 axons, 3 independent experiments; Bsn KO + 1µM W = 0.64 ± 0.083, n = 32 axons, 3 independent experiments). (D) Quantification of the number of Syp1 puncta per axon unit length (WT = 1.46 ± 0.120, n = 47 axons, 4 independent experiments; Bsn KO = 1.28 ± 0.115, n = 55 axons, 4 independent experiments; WT + 1µM W = 1.34 ± 0.119, n = 22 axons, 3 independent experiments; Bsn KO + 1µM W = 1.54 ± 0.147, n = 32 axons, 3 independent experiments). (E) Quantification of the colocalization of tf-LC3 and Syp1 (WT = 20.56 ± 3.99, n = 47 axons, 4 independent experiments; Bsn KO = 49.71 ± 4.501, n = 55 axons, 4

independent experiments; WT + 1µM W = 21.42 ± 4.155, n = 22 axons, 3 independent experiments; Bsn KO + 1µM W = 25.16 ± 4.383, n = 32 axons, 3 independent experiments). (F and G) Images of somas (F) and dendrites (G) of hippocampal neurons expressing FU-ptf-LC3. (H) Quantification of the number of RFP-LC3 puncta per soma area (WT = 0.074 ± 0.008, n = 38 somas, 4 independent experiments; Bsn KO = 0.068 ± 0.010, n = 39 somas, 4 independent experiments; WT + 1µM W = 0.042 ± 0.004, n = 30 somas, 3 independent experiments; Bsn KO + 1µM W = 0.044 ± 0.009, n = 29 somas, 3 independent experiments). (I) Quantification of the number of tf-LC3 puncta per dendrite unit length (WT = 0.065 ± 0.019, n = 33 dendrites, 4 independent experiments; Bsn KO = 0.037 ± 0.017, n = 30 dendrites, 4 independent experiments; WT + 1µM W = 0.006 ± 0.006, n = 25 dendrites, 3 independent experiments; Bsn KO + 1µM W = 0.005 ± 0.005, n = 24 dendrites, 3 independent experiments). Scale bars: 10µm. Error bars represent SEM. ANOVA Tukey's multiple comparisons test was used to evaluate statistical significance. ****p<0.0001, ***p<0.001, **p<0.01, *p<0.05.

6.14 Bassoon regulates autophagy in an ubiquitin- and Atg5-dependent manner

Autophagy is a complex process requiring dozens of proteins involved in the conjugation of LC3 to nascent phagophore membranes as well as the selection and recruitment of ubiquitin-tagged cargos (Klionsky et al., 2012). However, the precise steps of the autophagy mechanism that Bassoon regulates are not well understood. Therefore, two rescue experiments with Bassoon KO neurons were conducted.

First, a recombinant ubiquitin UbK_0 with no lysine residues, preventing poly-ubiquitination (Okerlund et al., 2017; Waites et al., 2013), was lentivirally overexpressed in hippocampal neurons from Bassoon KO mice and WT littermates. Neurons were co-transduced with FU-RFP-LC3 to monitor synaptic and axonal autophagy. FU-RFP-LC3 only infected neurons served as controls (Figure 33).

Interestingly, both the number of RFP-LC3 puncta per unit length of axon (Figure 33C) as well as the colocalization of Synaptophysin1 and RFP-LC3 (Figure 33E) in Bassoon KO neurons were reduced back to WT levels when poly-ubiquination was impaired. These results suggest that poly-ubiquination is required for increase in autophagy in Bassoon KO neurons. Surprisingly, the expression of FU-eGFP-UbK_0 in WT neurons did not lead to decreased autophagy indicating that basal autophagy is not necessarily dependent on poly-ubiquitination of cargo proteins destined for degradation or that endogenous ubiquitin is sufficient to maintain autophagy levels under basal conditions.

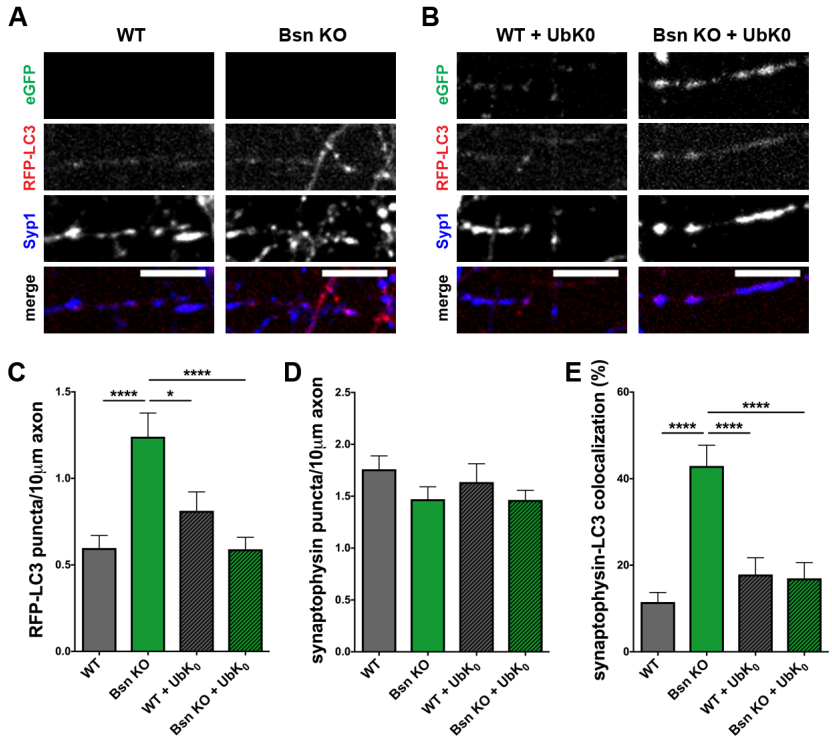

Figure 33: Ubiquitination is required for increased autophagy in Bsn KO neurons. (A and B) Images of hippocampal neurons expressing FU-RFP-LC3 only (A) or FU-RFP-LC3 and FU-eGFP-UbK$_0$ (B) that were fixed and stained with antibodies against Synaptophysin1 (Syp1). (C) Quantification of the number of RFP-LC3 puncta per axon unit length (WT = 0.60 ± 0.073, n = 35 axons, 2 independent experiments; Bsn KO = 1.24 ± 0.137, n = 34 axons, 2 independent experiments; WT + UbK$_0$ = 0.81 ± 0.109, n = 31 axons, 2 independent experiments; Bsn KO + UbK$_0$ = 0.59 ± 0.069, n = 30 axons, 2 independent experiments). (D) Quantification of the number of Syp1 puncta per axon unit length (WT = 1.76 ± 0.128, n = 35 axons, 2 independent experiments; Bsn KO = 1.47 ± 0.119, n = 34 axons, 2 independent experiments; WT + UbK$_0$ = 1.64 ± 0.177, n = 31 axons, 2 independent experiments; Bsn KO + UbK$_0$ = 1.46 ± 0.093, n = 30 axons, 2 independent experiments). (E) Quantification of the colocalization of RFP-LC3 and Syp1 (WT = 11.49 ± 2.211, n = 35 axons, 2 independent experiments; Bsn KO = 42.96 ± 4.779, n = 34 axons, 2 independent experiments; WT + UbK$_0$ = 17.86 ± 3.86, n = 31 axons, 2 independent experiments; Bsn KO + UbK$_0$ = 16.97 ± 3.626, n = 30 axons, 2 independent experiments). Scale bars: 10µm. Error bars represent SEM. ANOVA Tukey's multiple comparisons test was used to evaluate statistical significance. ****p<0.0001, ***p<0.001, **p<0.01, *p<0.05.

Studies of neurons lacking both Bassoon and Piccolo revealed that Atg5, a key protein in the formation of phagophore membranes, was required for the elevated levels of autophagy in these boutons (Okerlund et al., 2017). Atg5 was also found to interact with the CC2v1 domain of Bassoon (Okerlund et al., 2017), though a direct role in the elevated autophagy seen in neurons lacking Bassoon was not explored. I thus designed experiments to assess whether Atg5 was required for the elevated autophagy in Bassoon lacking boutons. This was accomplished by infecting Bsn KO neurons and neurons from WT littermates with a lentiviral vector expressing an shRNA to knock down (KD) Atg5 (FU-eGFP-shAtg5) (Okerlund et al., 2017).

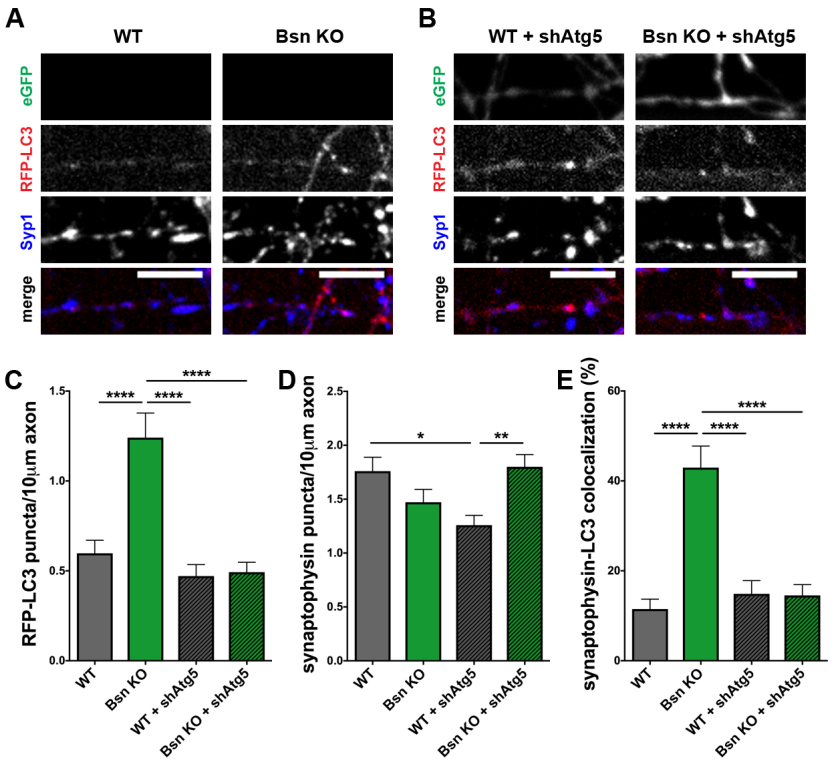

Figure 34: Increased autophagy in Bsn KO neurons is Atg5-dependent. (A and B) Images of hippocampal neurons expressing FU-RFP-LC3 only (A) or FU-RFP-LC3 and FU-eGFP-shAtg5 (B) that were fixed and stained with antibodies against Synaptophysin1 (Syp1). (C) Quantification of the number of RFP-LC3 puncta per axon unit length (WT = 0.60 ± 0.073, n = 35 axons, 2 independent experiments; Bsn KO = 1.24 ± 0.137, n = 34 axons, 2 independent experiments; WT + shAtg5 = 0.47 ± 0.064, n = 33 axons, 2 independent experiments; Bsn KO + shAtg5 = 0.49 ± 0.055, n = 40 axons, 2 independent experiments). (D) Quantification of the number of Syp1 puncta per axon unit length (WT = 1.76 ± 0.128, n = 35 axons, 2 independent experiments; Bsn KO = 1.47 ± 0.119, n = 34 axons, 2 independent experiments; WT + shAtg5 = 1.26 ± 0.091, n = 33 axons, 2 independent experiments; Bsn KO + shAtg5 = 1.8 ± 0.114, n = 40 axons, 2 independent experiments). (E) Quantification of the colocalization of RFP-LC3 and Syp1 (WT = 11.49 ± 2.211, n = 35 axons, 2 independent experiments; Bsn KO = 42.96 ± 4.779, n = 34 axons, 2 independent experiments; WT + shAtg5 = 14.87 ± 2.952, n = 33 axons, 2 independent experiments; Bsn KO + shAtg5 = 14.53 ± 2.39, n = 40 axons, 2 independent experiments). Scale bars: 10µm. Error bars represent SEM. ANOVA Tukey's multiple comparisons test was used to evaluate statistical significance. ****p<0.0001, ***p<0.001, **p<0.01, *p<0.05.

Hippocampal neurons from Bassoon KO mice and WT littermates were infected with either FU-RFP-LC3 alone or with FU-RFP-LC3 and FU-eGFP-shAtg5 and fixed at 14 DIV. The axons of neurons expressing FU-eGFP-shAtg5 were identified in these cultures by the appearance of eGFP in their cytoplasm. Cells expressing both FU-RFP-LC3/FU-eGFP-shAtg5 were detected by the colocalization of eGFP and RFP-LC3 in the same axons. As anticipated, the KD of Atg5 dramatically reduces the number of RFP-LC3 puncta per axon unit length in Bassoon KO neurons to WT levels (Figure 34C) as well as the percentage of RFP-LC3 puncta colocalizing with Synaptophysin1 (Figure 34E). However, infection with shRNA against Atg5 did not change RFP-

LC3 levels in WT neurons, perhaps because basal autophagy is so low. FU-eGFP-shAtg5 also rescues the slight decrease in the number of Synaptophysin1 puncta in Bassoon KO neurons back to WT levels (Figure 34D). Strikingly, I observed that Atg5 KD in WT neurons reduces the number of Synaptophysin1 immuno-positive puncta per unit length of axon. This decrease was not seen in Bsn KO neurons (Figure 34D). These findings suggest that one or more other degradative pathways may become activated trying to substitute for altered basal autophagy in WT neurons leading to an over-activation of degradation and subsequently to a loss of Synaptophysin1 positive synapses.

Together, these data indicate that increased synaptic autophagy levels in Bsn KO neurons are indeed dependent on the autophagy-related protein Atg5 and that suppressing autophagy in WT neurons may lead to a degenerative phenotype.

7. Discussion

Mechanisms regulating quality control and turnover of SV proteins are fundamental to synapse integrity, however, they are not well understood. In this study, I provide evidence that autophagy can be rapidly induced within presynaptic boutons either by the mTOR inhibitor rapamycin or by the selective damage of SV proteins through superoxides. The time range of autophagy induction is consistent with the concept that the machinery is maintained and regulated within presynaptic boutons. My data also suggest a real-time role for autophagy in maintaining synapse function, as without it the accumulation of damaged SV proteins can compromise synaptic transmission.

A prerequisite for a real-time functionality for autophagy within presynaptic boutons is its activation on short time scales (seconds/minutes) after insults that damage presynaptic proteins. Studies show that autophagic organelles appear within axons and presynaptic boutons 3-7 hours following the addition of rapamycin (Hernandez et al., 2012), 48 hours after treatment with Sonic Hedgehog (Petralia et al., 2013) and after neuronal activity (Soukup et al., 2016; Wang et al., 2015). Moreover, Bassoon, as well as presynaptic proteins like Rab26 and Endophilin A have been functionally linked to the autophagy machinery (Binotti et al., 2015; Okerlund et al., 2017; Vanhauwaert et al., 2017) of which Atg5, Atg16, LC3 and p62 have been localized to presynaptic boutons (Okerlund et al., 2017). However, as autophagosomes are highly mobile (Cheng et al., 2015; Maday et al., 2012), it remains unclear whether they arise within boutons or simply accumulate there.

7.1 Rapamycin-induced autophagy leads to impaired FM dye uptake and a loss of synapse number

A major challenge in the field of neuronal autophagy is the general lack of potent inducers that reliably trigger autophagy, for example in synapses. In fact, it is often debated whether neurons induce autophagy during nutrient deprivation. For example, maintaining neurons in amino acid free salt solution for 24 hours leads to increases in neuronal autophagy as shown in Boland et al. (Boland et al., 2008). Serum- and supplement-deprivation was also shown to induce neuronal autophagy (Cheng et al., 2015; Kononenko et al., 2017; Young et al., 2009) as well as 24 hour fasting of eGFP-LC3 expressing mice (Chen et al., 2015).

On the contrary, Mizushima et al. (2004) were not able to find higher autophagy levels after nutrient starvation in GFP-LC3 transgenic mice. In line with that, a 2 hour incubation of hippocampal neurons in an amino acid free salt solution was not sufficient to induce neuronal autophagy (Maday and Holzbaur, 2016) leading Maday et al. to postulate that the primary

purpose of constitutive autophagy in neurons is the turnover of aging proteins rather than a response to starvation. However, although mTOR inhibition is involved in nutrient-dependent autophagy (Chan, 2009; Cota et al., 2006; Hosokawa et al., 2009), whose existence is highly discussed in neurons as mentioned earlier, there are strong lines of evidence that mTOR inhibition by rapamycin leads to increased autophagy in neurons (Boland et al., 2008; Hernandez et al., 2012; Spilman et al., 2010).

In my studies, I also explored whether the mTOR inhibitor rapamycin, among others, can induce autophagy in primary hippocampal neurons. Similar to studies reported by Hernandez and colleagues (Hernandez et al., 2012), I observed that treating hippocampal neurons with rapamycin leads to an accumulation of endogenous LC3, an autophagy marker, at synapses (Figure 7B and D). This increase was partially blocked by the PI3K inhibitor wortmannin, known to inhibit rapamycin-dependent autophagy induction (Klionsky et al., 2012). Thus, activation of the canonical autophagy pathway that requires mTOR inhibition and PI3K Vps34 activation participates in synaptic autophagy.

Consistently, I found that a 2-hour mTOR inhibition leads to an increased LC3-II/LC3-I ratio in Western Blot analyses (Figure 7A and C) as previously reported by at least two studies (Boland et al., 2008; Hernandez et al., 2012), however not observed by others (Maday and Holzbaur, 2016). In addition, I examined endogenous LC3 levels in both axons and somas of hippocampal neurons. Here, I could not detect any significant differences after rapamycin treatment (Figure 7E, F, G and H). These data indicate that either rapamycin predominantly induces synaptic autophagy or that the somatodendritic arbor poses a bigger challenge for detecting minor changes in a highly abundant protein such as LC3.

Importantly, the antibody staining for endogenous LC3 did not allow me to discriminate between pre- and postsynaptic LC3, which are not resolvable without super-resolution microscopy. Moreover, given that axons fasciculate around dendrites in mass cultures, it was not possible to distinguish between autophagic vacuoles labeled with LC3 in these two compartments. It is thus likely that these confounds greatly contribute to the ongoing debate in the literature on where and when autophagy is induced. To meet this challenge, I created a cell-autonomous expression vector that allows the accumulation of LC3 puncta in axons and boutons to be distinguished from dendritic accumulations (see chapter 7.2).

An important unresolved question in the field is whether changing autophagic flux is beneficial or detrimentral to neuronal health and synaptic transmission. In my own studies, I observed that a 2-hour treatment with rapamycin, that induced autophagy, causes a reduction of FM dye uptake (Figure 8) implying a negative effect on synaptic transmission. Similar results were observed by Hernandez and colleagues, who observed that a several hour treatment with rapamycin decreased the evoked release of dopamine in dopaminergic neurons (Hernandez et

al., 2012), implying that prolonged activation of autophagy has a negative impact on synaptic function. Importantly, autophagy also appears to contribute to the function of the postsynapse, specifically the degradation of AMPA receptors following chemical LTP (Shehata et al., 2012). Perhaps not surprisingly, the genetic suppression of autophagy by knockout of Atg5 or Atg7 also adversely affects synapse integrity (Hara et al., 2006; Komatsu et al., 2006). Together these data indicate that an altered balance (increased or decreased) in autophagy can be detrimental for synapse integrity and compromise synapse health.

7.2 Monitoring synaptic and axonal autophagy with FU-Syp-mCherry-eGFP-LC3

With the goal of enhancing the detection of autophagic events in axon and synapse, I developed a lentiviral vector that expressed not only eGFP-tagged LC3 but also mCherry-tagged Synaptophysin (Figure 9 and 10). This arrangement allows the simultaneous, cell-autonomous, detection of presynaptic boutons via the synaptic vesicle protein Synaptophysin (Fykse et al., 1993) and autophagic vacuoles labeled with eGFP-LC3. Importantly, with a low infection rate ($\sim 30\%$), this vector enables to visualize axonal and synaptic eGFP-LC3 signal of infected neurons growing on top of uninfected neurons (Figure 9), excluding any dendritic contribution of the LC3 signal from the analyses.

As an initial test of this new vector system, I explored whether autophagy could be detected in sparsely infected hippocampal neurons treated with rapamycin to induce autophagy. Similar to earlier studies (Hernandez et al., 2012), I observed low basal autophagy levels within axons (Figure 11A). However, eGFP-LC3 levels increase within 10 minutes at presynaptic boutons following rapamycin treatment (Figure 11B and F), which is dramatically shorter than previous reports (Boland et al., 2008; Hernandez et al., 2012). Furthermore, Western Blot analyses using synaptosome suspensions support the rapid autophagy induction. Here, increased LC3-II levels were detected already after 10 minutes of rapamycin treatment nicely confirming the induction of autophagy at the synapse (Figure 12E).

Interestingly, eGFP-LC3 intensity at synapses treated for 2 hours with rapamycin was less compared to the 10-minute time point (Figure 11A and D). These data indicate that there is a fast presynaptic autophagy response that slowly levels out. Changes in LC3 levels in axons following rapamycin treatment could reflect either an enhanced “induction of autophagy, reduction in autophagosome turnover or the inability of turnover to keep pace with increased autophagosome formation” (Klionsky et al., 2012). With this in mind, my data indicate that the rapid increase in synaptic autophagy within 10 minutes after rapamycin addition represents autophagy induction, while the levels observed at 2 hours appear to reflect steady-state turnover rates of autophagy due to the ongoing presence of rapamycin.

Analysis of the number of autophagosomes per unit length of axon revealed an increased level of eGFP-LC3 puncta after both 10 minutes and 2 hours of rapamycin treatment (Figure 11E and G). This suggests that inducing autophagy at the synapse also leads to higher numbers of autophagosomes along axons that are most likely transported to the soma (Maday and Holzbaur, 2016). The increase of eGFP-LC3 intensity at synapses as well as the number of autophagosomes per unit axon length is returned to control levels in the presence of wortmannin (Figure 11I, J and K). These data indicate that rapamycin-induced autophagy is indeed PI3K-dependent and presumably part of the canonical autophagy pathway (Codogno et al., 2011; Mizushima et al., 2011). These results are in agreement with Hernandez et al.'s (Hernandez et al., 2012) findings showing that the induction of autophagy by rapamycin requires Atg7 expression. Atg7 is a vital autophagy-related protein that is essential for the initiation of canonical autophagy (Codogno et al., 2011).

7.3 Bleaching Supernova-expressing synapses leads to increased autophagy

Although the induction of axonal and presynaptic autophagy is faster than previously recognized, the addition of rapamycin is neither specific for any one neuronal compartment, nor a natural inducer of autophagy (Deng et al., 2017). I was therefore interested in developing a local insult that would induce autophagy at the synapse in a spatiotemporally controlled manner.

Intriguingly, Ashrafi et al. (2014) were able to induce and study mitophagy in neuronal axons by utilizing a genetically encoded photosensitizer, named Killerred, which they targeted to mitochondria. Light-mediated Killerred activation was found to locally generate reactive oxygen species (ROS) in the context of mitochondria (Ashrafi et al., 2014; Bulina et al., 2006; Jarvela and Linstedt, 2014). This not only damaged mitochondria but induced mitophagy, the degradation of mitochondria through autophagy (Ashrafi et al., 2014; Wang et al., 2012; Yang and Yang, 2011). As the dimerization properties of Killerred can affect the localization and function of tagged proteins, I took advantage of a monomeric version of Killerred, called Supernova (Takemoto et al., 2013) for my studies. I tethered Supernova to the cytosolic tail of the SV protein Synaptophysin, and established a new vector that expressed both Synaptophysin-Supernova and eGFP-LC3 (Figure 14A). My expectation is that excitation of Supernova with an external light source specifically at synapses would generate ROS (Jarvela and Linstedt, 2014) on the surface of SVs and in turn damage at least a subset of SV proteins in proximity to the Supernova tag.

Similar to the reports for Killerred tethered to mitochondria (Ashrafi et al., 2014), I observed that photobleaching Synaptophysin-Supernova causes a dramatic increase in synaptic autophagy on a minute time scale (Figure 16C, F and G) and a rise in axonal autophagosomes

within 1-2 hours (Figure 16E, J and K). Ever since autophagy was discovered, the gold standard for the detection of autophagosomes is transmission electron microscopy because it enables the visualization of double-membraned organelles (Eskelinen et al., 2011). Electron micrographs taken from bleached and unbleached synapses also show a selective increase in the number of double-membraned autophagic vacuoles (AVs) within bleached presynaptic boutons within minutes after bleaching (Figure 20C and D). These data support the conclusion that the observed increase in synaptic eGFP-LC3 puncta is associated with the formation of synaptic autophagosomes. Additionally, newly forming phagophores have been observed within the presynaptic terminal (Figure 20) further indicating that autophagosomes are indeed formed locally at boutons.

A fundamental question raised by my study is whether ROS damage to SV proteins exclusively turns on autophagy or multiple protein degradation systems. The endo-lysosomal system has been reported to also clear SV proteins in response to ongoing synaptic activity (Sheehan et al., 2016; Uytterhoeven et al., 2011). One hallmark of this pathway is the appearance of multivesicular bodies (MVB) (Raiborg and Stenmark, 2009). I did not observe a significant increase in the number of synaptic MVBs on electron microscopy level (Figure 20E and H), indicating that in contrast to autophagy, the endo-lysosomal system is not robustly engaged by ROS-mediated protein damage to Synaptophysin.

However, monitoring Rab7 and Chmp2b levels (Sheehan et al., 2016; Stenmark, 2009) by light microscopy, I did observe a modest increase in their colocalization with Synaptophysin-SN, following ROS production (Figure 21). Thus I cannot rule out that ROS-mediated damage to SV proteins can trigger the activation of several degradative systems. Interestingly, the study from Sheehan et al. (Sheehan et al., 2016) shows that only a subset of SV proteins is preferentially degraded by the endo-lysosomal system (e.g. VAMP2 and SV2), highlighting the importance to address in the future if distinct SV proteins are degraded via specific and therefore separate degradative pathways.

Intriguingly, my study also reveals that, while ROS-induced autophagy at synapses, where Synaptophysin-Supernova positive vesicles are mainly clustered, is PI3K-dependent (Figure 19C and E), ROS-induced axonal autophagy is not (Figure 19D and F). One possibility for the difference in PI3K-dependence is that a fraction of the Synaptophysin-Supernova-tagged SVs are not confined to presynaptic boutons but are in constant motion, moving along axons between synapses (Cohen et al., 2013; Maas et al., 2012; Tsuriel et al., 2006). As both protein pools (synaptic and axonal) are damaged during photobleaching, and thus candidates for autophagy mediated degradation, it is interesting to consider if they both use the same autophagic machinery. Intriguingly, these findings indicate that these two pools of autophagosomes are indeed generated by different autophagy pathways, of which one is PI3K-independent. Several

other groups described PI3K-independent autophagy pathways such as type 2 mitophagy, which is induced by photodamage (Chu et al., 2007; Lemasters, 2014; Zhu et al., 2007). Thus, presynaptic autophagy appears to be regulated via the canonical autophagy pathway, while axonal autophagy of ROS damaged proteins utilizes a different, PI3K-independent, pathway. A caveat to using wortmannin as an inhibitor of autophagy is its broad effect on numerous kinases (Bain et al., 2007). Therefore, I performed similar experiments with a knock down approach using an shRNA against Atg5. Here, both synaptic and axonal autophagy were dependent on Atg5 (Figure 19K and L). These data indicate that ROS-induced eGFP-LC3 accumulation requires Atg5 and thus is likely caused by the increased formation of autophagosomes.

My data also indicate that autophagy induction is not solely dependent on the damage of Synaptophysin, as the ROS-mediated damage to Synaptotagmin and Synapsin can also elevate autophagy within presynaptic boutons (Figure 23 and 24). A notable difference is that eGFP-LC3 levels increased with a slower time course for Synaptotagmin and Synapsin versus Synaptophysin (~ 1 hour vs. 5 minutes, respectively) (Figure 23 and 24). The discrepancy could be indicative of less ROS-mediated damage to juxtaposed SV proteins, possibly due to an increased distance of Supernova from the surface of SVs. Here it is interesting to note that Synaptotagmin has a large cytoplasmic domain (346aa; comprised of two C2 domains) (Ybe et al., 2000), compared to the shorter 95aa C-terminal tail in Synaptophysin (Gordon and Cousin, 2014). Synapsin is a much larger protein and only peripherally associated with SV membranes (Chi et al., 2001), thus potentially placing Supernova at a greater distance from the SV surface and other SV proteins.

Additionally, the abundance of all three proteins on SVs differs. For example, Synaptophysin has the highest copy number per SV (31.5 copies/SV) whereas Synaptotagmin (15.2 copies/SV) and Synapsin (8.3 copies/SV) have lower copy numbers (Takamori et al., 2006). This alone could generate more damage to the SV and thus lead to a faster onset of ROS-mediated autophagy. Considering all these caveats, I would still conclude that ROS damage to SVs is a potent trigger for presynaptic autophagy.

The unique properties of Synapsin provided an opportunity to address other fundamental questions, including whether a soluble synaptic protein induced not only autophagy but endo-lysosomal degradative systems.

In another set of experiments, I characterized Synapsin-Supernova bleaching in greater detail. Addition of the autophagy inhibitor wortmannin is able to diminish eGFP-LC3 levels within synapses but not necessarily within axons (Figure 25), indicating that Synapsin-Supernova induced autophagy shows a very similar PI3K-dependency as Synaptophysin-Supernova induced autophagy. This further suggests that damaging either one of these proteins leads to the activation of a similar or even of the same autophagy pathway. Intriguingly, Synapsin-Supernova

bleaching does not have any effect on Rab7-eGFP levels at synapses (Figure 26) indicating that the endo-lysosomal pathway is not turned on within the time frame investigated (5 minutes to 2 hours). This is not surprising since the endo-lysosomal pathway is described to preferentially degrade bigger aggregates and integral membrane proteins such as Synaptophysin (Sheehan et al., 2016) rather than mainly soluble proteins such as Synapsin (Lamark and Johansen, 2010; Lilienbaum, 2013).

Soluble proteins get predominantly degraded via the UPS and not via autophagy or the endo-lysosomal pathway. This concept is further supported by my finding that under basal conditions endogenous Synapsin is rarely present in extrasynaptic autophagy organelles compared to endogenous Synaptophysin (Figure 28).

Taken together, these data support the hypothesis that it is the ROS-mediated damage to SVs (either to the lipid bilayer or more likely to neighboring SV proteins in close proximity) that triggers the activation of presynaptic autophagy. Additionally, the damage to an integral SV protein may activate – besides autophagy – the endo-lysosomal pathway whereas the damage to mainly soluble Synapsin may not activate the endo-lysosomal pathway. Future studies would be interesting to determine if Synapsin-Supernova bleaching also leads to the induction of UPS-dependent degradation.

7.4 Autophagy is activated for the clearance of damaged synaptic proteins

Studies by Lin et al. (Lin et al., 2013) showed that targeting the photosensitizer miniSOG via Synaptophysin or VAMP2 to SVs leads to a real-time disruption of neurotransmitter release following light activation. Although the precise mechanism was not investigated, loss of function is most likely due to the inactivation of the tagged and/or neighboring SV proteins (Bulina et al., 2006; Jacobson et al., 2008; Qi, 2012; Surrey et al., 1998). A fundamental question not answered in the Lin et al. study is what synapses do with these damaged proteins? In the present study, I used a less potent free radical oxygen generator Supernova (Takemoto et al., 2013) to similarly damage Synaptophysin and explore the cellular and molecular consequences.

Initially, I focussed on whether for example autophagy was involved in the clearance of Synaptophysin-Supernova, and/or whether the ROS-mediated damage led to the selective removal of only the damaged SV protein or SVs en-mass. Intriguingly, approximately 70% of extrasynaptic eGFP-LC3 puncta were also positive for Synaptophysin-Supernova following ROS-mediated damage (Figure 27D), suggesting that autophagy contributes to the degradation of synaptic pools of Synaptophysin. Interesting mechanistic studies by Wheeler and collaegues identified the E3 ubiquitin ligase Siah not only as a binding partner for Synaptophysin but its ubiquitination together with the E2 ligase UbcH8 in non-neuronal cells and degradation by the

ubiquitin-protesome-system (UPS) (Wheeler et al., 2002). How the UPS functions to degrade an integral membrane protein is unclear and or whether Siah and the UPS operate at synapses to degrade this and other SV proteins. Given this caveat, one cannot exclude a role of the UPS in the clearance of Synaptophysin following light mediated production of ROS. Thus, I posit that ROS-mediated damage of Synaptophysin could conceptually activate several degradation pathways within boutons, of which at least one is autophagy. This interplay of several degradational systems in order to keep the synapse healthy is in accordance with the literature as nicely reviewed by Wang et al. (Wang et al., 2017).

Intriguingly, a much smaller fraction (18%) of the extrasynaptic eGFP-LC3 puncta generated following the ROS-induced damage of Synaptophysin were also positive for the endogenous SV protein Synaptotagmin. These data suggest that presynaptic autophagy can selectively remove damaged SV proteins from SVs without degrading SVs en-mass. This concept is supported by the reciprocal experiments with Synaptotagmin-Supernova. Here, I also observed a dramatic recruitment of Synaptotagmin-Supernova into extrasynaptic eGFP-LC3 puncta, but only modest levels of endogenous Synaptophysin (Figure 27E). Thus, while both SV proteins are abundant on the same SVs (Rizzoli, 2014; Takamori et al., 2006; Wilhelm et al., 2014), the ROS-mediated damage to each by Supernova does not necessarily trigger the simultaneous degradation of all other SV proteins.

At present the mechanism underlying this specificity is unclear. Of note, the very short half-radius of ROS dramatically restricts the area of damage (half radius of photodamage of 3-4 nm; (Takemoto et al., 2013)) and thus the fraction of additional SV proteins that become damaged. The degree of damage may also be related to the potency of Supernova as a ROS generator, the presence of these molecules in distinct complexes and/or the relative proximity of Supernova to these proteins. At present, there is limited data on the proximity of Synaptophysin and Synaptotagmin. Functional studies have shown that Synaptotagmin1 functions as a calcium sensor and is involved in both exo- and endocytosis (Rizzoli, 2014; Shupliakov and Brodin, 2010). In contrast, Synaptophysin function remains enigmatic though it can interact with the SNARE protein VAMP2 and may act as a cholesterol stabilizing system, facilitating the recruitment of proteins into SVs (Bonanomi et al., 2007; Rizzoli, 2014). This issue of proximity affecting the extent of damage is also consistent with differences in the potency of Supernova to induce autophagy when tethered close to the SV membrane (Synaptophysin) or more distally (Synaptotagmin and Synapsin) (see above).

In summary, the observed specificity implies that ROS-mediated damage caused by Supernova (Shu et al., 2011; Trewin et al., 2018) is rather limited and primarily affects co-tethered proteins, a concept consistent with its low quantum yield and the limited damage half-radius of 3-4nm (Takemoto et al., 2013). Presumably, using the more potent photosensitizer miniSOG (Lin et al.,

2013; Qi, 2012; Shu et al., 2011), more SV proteins could be damaged, causing a much bigger insult perhaps leading to the wholesale removal of SVs.

These results suggest that autophagy is a key surveillance mechanism that is able to specifically target damaged SV proteins for clearance, in a manner similarly to that reported for damaged mitochondria (Ashrafi et al., 2014; Chu et al., 2007; Zhu et al., 2007). In addition, these findings reveal that SVs are not necessarily degraded en-mass and that presynaptic boutons possess a sophisticated sorting system that supports the rapid removal of damaged proteins. This concept is supported by data indicating that not only SV proteins have different half-lives (Cohen et al., 2013), but they can be differentially degraded by the endo-lysosomal pathway in an activity-dependent manner (Sheehan et al., 2016). Importantly, photodamaging Synaptophysin that is luminally tagged with Supernova did not lead to a recruitment of Synaptophysin-lumSupernova into autophagy organelles (Figure 27F) indicating that ROS damage has to occur on the cytoplasmic face of SV proteins to be recognized by the autophagy machinery. Conceptually, a selective removal model also makes metabolic sense, as it would allow for the differential removal of specific mis-folded or damaged proteins, consistent with different half-lives of SV proteins (Cohen et al., 2013). Although the mechanism of selective removal remains unclear, I hypothesize either that SV proteins are directly removed from SVs or that their removal is dependent on an intermediary endosomal sorting step. Further studies will be necessary to discriminate between these two options.

Clearly unraveling the molecular mechanisms of this specificity will be a major focus of future studies. In addition to Rab35 (Sheehan et al., 2016), other important molecules regulating the clearance of SV proteins include Bassoon (Okerlund et al., 2017) and the GTPase Rab26 (Binotti et al., 2015). Synaptojanin, a lipid phosphatase that is essential for SV trafficking, also appears important for presynaptic autophagy (Vanhauwaert et al., 2017). Importantly, this role for Synaptojanin was diminished by the Parkinson's disease mutation R258Q, confirming once more the fundamental role of autophagy for the integrity of synapses. However, which form of autophagy is the most important is unclear. This is exemplified by studies showing that chaperone-mediated autophagy, also known as endosomal microautophagy, is also important for the clearance of synaptic proteins (McPherson, 2015; Uytterhoeven et al., 2015).

Taken together, my data provide new mechanistic insights into the specific degradation of ROS damaged SV proteins via the autophagy pathway. The exact mechanism which marks damaged SV proteins for degradation needs further investigation, but I propose that one likely candidate could be ubiquitination at the cytoplasmic side of defective proteins (Deng et al., 2017; Lilienbaum, 2013; Nelson et al., 2013; Okerlund et al., 2017; Waites et al., 2013).

7.5 Autophagy can be beneficial for synapse function and acts in real-time

The rapid induction of presynaptic autophagy within minutes suggests that autophagy possibly has real-time functions at synapses, e.g. helping to maintain synaptic health, function and integrity. Previous studies, using the ROS generator miniSOG, observed that damage to the SV protein Synaptophysin can lead to a rapid disruption of neurotransmitter release (Lin et al., 2013). Although the mechanism was not explored, I posit that it was not only due to the acute damage to Synaptophysin and other SV proteins but also to the inability of the clearance systems, such as autophagy to adequately and efficiently remove these damaged proteins, as recovery of function took hours (Lin et al., 2013). My observations showing that ROS-mediated damage to Synaptophysin via Supernova triggers presynaptic autophagy, suggests that autophagy plays a role in the clearance of ROS damaged proteins and maintaining functionality. To test this hypothesis, several functional studies, e.g. FM dye uptake and electrophysiology experiments were performed to examine how ROS damage and autophagy contribute to synaptic health and function.

As an initial measure of synaptic function, I utilized the styryl dye FM 1-43 to monitor the ability of SVs to recycle following stimulation-evoked exocytosis (Gaffield and Betz, 2006), allowing a direct comparison of whether bleached synapses are as active as unbleached synapses. In contrast to the recent study from Lin et al., in my experiments with Supernova-tagged Synaptophysin, I did not observe an overt change in synaptic function, assessed by the uptake of FM 1-43 dye (Figure 30D) following light-activated ROS production. Furthermore, no change in the evoked release of neurotransmitter using whole cell patch-clamp recording of autaptic neurons (Figure 31A) could be observed. These data suggest that protein damage caused by Supernova radiation is less potent than that induced with miniSOG-Synaptophysin (Lin et al., 2013). Intriguingly, when the induction of autophagy was blocked with wortmannin (Figure 19) during ROS-mediated damage of Synaptophysin-SN, the extent of FM 1-43 uptake, as well as the evoked EPSC amplitude, were reduced (Figure 30E and 31C), indicating that the ROS production does cause damage to SVs that affects presynaptic function, yet clearance mechanisms such as autophagy are able to handle this more limited damage. Additionally, a knock down approach using shRNA against Atg5 also led to a bleaching-induced decrease in EPSC amplitues (Figure 31G), further confirming that upon autophagy inhibition, damaged synaptic proteins accumulate within presynaptic terminals and have a direct impact on neurotransmitter release. This in turn could decrease the number of functional presynaptic boutons and thus EPSC amplitude. Conceptually, the decrease in EPSC amplitude could also be explained by a postsynaptic effect, e.g. a down-regulation of postsynaptic receptors and thus increased fraction of silent synapses. Given that Supernova is directly tethered to a SV protein, the most likely effect of ROS is on the neurotransmitter release machinery, a concept requiring further study. Either way, these data

suggest that autophagy is required to maintain synaptic transmission while the synapse is challenged by protein damaging insults.

As a control, I also examined the effects of ROS-mediated damage to Synapsin, a peripherally associated SV protein. Interestingly, Synapsin-SN bleaching did not show any bleaching induced changes in FM 1-43 within 5 minutes, either under basal conditions or while inhibiting autophagy (Figure 25) (Figure 30I and J). This could be due to the minor role of Synapsin during synaptic transmission and/or less damage to integral SV proteins key for synaptic transmission due to the displacement of Supernova from the SV surface. This latter concept is consistent with the delayed onset of autophagy (1 hour) when Supernova is tethered to Synapsin. Finally, it cannot be excluded that autophagy plays only a minor role in the clearance of ROS damaged Synapsin, a consideration supported by my finding that endogenous Synapsin is only infrequently present in extrasynaptic autophagy organelles (Figure 28).

Very interestingly, another recent study showed that H_2O_2 treatment of boutons expressing recombinant Synaptotagmin with Horse Radish Peroxidase (an enzyme that produces ROS upon addition of peroxide) impaired synaptic transmission in a manner that recapitulates a Synaptotagmin1 loss-of-function phenotype (Afuwape et al., 2017). These data show that ROS damage within the lumen of a SV can adversely affect SV function, by affecting proteins such as Synaptotagmin that are critical for calcium-dependent neurotransmitter relesase. Interestingly these deficits occurred even in the absence of autophagy inhibitors. This raises many questions of whether such damage also triggers the clearance of SV proteins through the autophagy and/or endolysosomal system. It would also be interesting to explore whether these SVs are cleared en-mass or whether subsets of SV proteins such as HRP-Synaptotagmin are selectively cleared. Importantly, these studies with HRP and miniSOG as compared to my studies with Supernova indicate that though locally operating within presynaptic boutons, clearance mechanisms such as autophagy have a maximum capacity, wherein they are not able to maintain synaptic function, following extensive damage. Exploring these limitations would be fundamental for understanding neurodegenerative disorders, whether excessive damage leads to synaptic and neuronal loss. With regard to my studies, I find that using Supernova as a photosensitizer is a gentler insult from which synapses can recover, which allows to examine more subtle responses to ROS-mediated damage. For example, it could be a potent system for identifying key SV proteins critical for the induction of autophagy and or their acute real-time roles in synaptic transmission and integrity. This is exemplified by my studies revealing that function is lost, following damage to Synaptophysin-Supernova, if the surveillance mechanism dependent on autophagy is blocked. Thus, Supernova is a powerful tool to spatiotemporally induce damage to synapses and thus increase our understanding of how different clearance systems function during both health and disease. This information is particularly relevant to

neurodegenerative disease (Hara et al., 2006; Komatsu et al., 2006; Nixon, 2013; Rubinsztein et al., 2012), where imbalanced protein degradation, including too much or not enough autophagy, can contribute to synaptic and neuronal loss (Nixon, 2013; Waites et al., 2013).

7.6 Bassoon regulates presynaptic autophagy in an ubiquitin- and Atg5-dependent manner

In earlier studies, increased autophagy alongside with a loss of Synaptophysin1 in neurons from Bassoon KO mice compared to WT neurons at 14 DIV were detected (Okerlund et al., 2017). As synapse loss is one of the early hallmarks of neurodegenerative diseases (Bae and Kim, 2017; Jackson et al., 2017; Scheff et al., 2014), I asked whether this is a developmental or degenerative phenotype. Interestingly, at 21 DIV the increase in autophagy is diminished and there is no detectable loss of Synaptophysin1 anymore (Figure 32) suggesting that older Bassoon KO neurons are able to compensate for the increased activity of autophagy and subsequent synapse loss. This is in line with other findings showing an increase, rather than a decrease, of the hippocampus and the cortex of 3-month-old mice lacking Bassoon (Heyden et al., 2011).

Additionally, Waites et al. (Waites et al., 2013) could rescue the loss of SV2 protein levels in Piccolo and Bassoon DKD neurons with overexpression of FU-eGFP-UbK_0 demonstrating the role of poly-ubiquitination in Piccolo/Bassoon regulated protein degradation. Thus, I introduced lysine-deprived ubiquitin into the Bassoon KO neurons leading to a full rescue of axonal and synaptic autophagy back to WT levels (Figure 33C and E) indicating that poly-ubiquitination is essential for the increased rates of autophagy in Bassoon KO neurons compared to WT neurons. One possible mechanism of action is that, in the absence of Bassoon, more proteins are being ubiquitinated thus leading to an increased amount of synaptic autophagy cargo and subsequently to increased numbers of formed autophagosomes. Another interesting finding was that inhibition of poly-ubiquitination did not decrease autophagy levels in WT neurons suggesting that autophagy under basal conditions is either poly-ubiquitination-independent or that endogenous ubiquitin is sufficient to generate cargo for basal autophagy.

Being a large scaffold protein at the presynapse, Bassoon has been shown to regulate presynaptic autophagy potentially by binding and inhibiting Atg5. In this regard, Okerlund et al. (Okerlund et al., 2017) were able to show that not only the CC2v1 domain of Bassoon binds Atg5 in Co-IP assays but also that the overexpression of CC2v1 reduces the appearance of mRFP-LC3 at synaptic sites. These findings and sequence alignments indicate that CC2v1 disrupts the Atg12-Atg5 interaction with Atg16L, thereby impairing autophagy initiation (Okerlund et al., 2017).

As a follow up question, I asked whether the knock down (KD) of Atg5 via shRNA would block the increased autophagy levels that were observed in Bassoon KO neurons at 14 DIV. Indeed, RFP-LC3 levels were rescued back to WT levels when shAtg5 was expressed (Figure 34C) further indicating that Atg5 plays an essential role in Bassoon regulated autophagy. Surprisingly, I did not detect any shAtg5-dependent changes in the number of RFP-LC3 puncta in the WT neurons suggesting either that basal autophagy in WT neurons is not necessarily Atg5-dependent or that the KD of Atg5 to approx. 50% protein level (data not shown) is not sufficient to inhibit very low basal autophagy levels in the WT control. Considering the fact that suppression of basal autophagy leads to neurodegeneration (Hara et al., 2006), WT neurons may have surveillance mechanisms that ensure functional basal autophagy, even in the absence of 50% of the endogenous Atg5 protein.

Another interesting finding was that FU-eGFP-shAtg5 expressing WT neurons showed a decreased number of Synaptophysin1 puncta (Figure 34D), a hallmark not investigated in the Okerlund study. I postulate that the loss of Synaptophysin1 levels is caused by one or more other degradative pathways, such as the endo-lysosomal pathway or the UPS, being turned on as a response to inhibited autophagy. There is increasing evidence showing that different degradational pathways function in parallel and that blocking for example the UPS can lead to increased autophagic activity (Ding et al., 2007; Wang et al., 2017) and probably vice versa. This may then lead to an over-degradation of synaptic proteins such as Synaptophysin1 and to a loss of synapse integrity as shown for example for high Siah1 activity after a Piccolo/Bassoon DKD (Waites et al., 2013). Consequently, further studies are important to unravel the whole interplay of degradational pathways that are present in the synapse.

Together, these data indicate that Bassoon regulates autophagy indeed in an ubiquitin- and in an Atg5-dependent manner and that increased autophagy in Bassoon KO mice is not showing a neurodegenerative progression. Future questions to be investigated could be 1) are Bassoon KO neurons more vulnerable or more resistant to stress because of their increased autophagy and 2) what is the molecular mechanism of Bassoon-regulated presynaptic autophagy. Thus, Bassoon KO mice can also be a useful model to better understand synaptic autophagy.

7.7 Balanced presynaptic autophagy is required to maintain synaptic function and integrity

Altogether, my data indicate that monitoring presynaptic autophagy can be facilitated by a bicistronic vector expressing a mCherry-tagged SV protein and the eGFP-tagged autophagy marker LC3. Additionally, by tagging SV proteins with a photosensitizer such as Supernova (Takemoto et al., 2013), it is possible to spatiotemporally damage SV proteins, and thus to

manipulate and study ROS-mediated synaptic clearance mechanisms. Using this technique, I was able to show that photodamaged SV proteins selectively become cargo of autophagy organelles that appear within minutes after photobleaching.

Interestingly, my data using rapamycin to strongly induce autophagy recapitulate the findings of other studies showing that excessive autophagy may have destructive consequences for neurons (Boland et al., 2008; Hernandez et al., 2012). In contrast, my results also suggest that functional autophagy is required to diminish negative effects of ROS-mediated damage to SV proteins, thus acting as a beneficial surveillance mechanism to keep the synapse functional.

One of the most fundamental questions in the neuronal autophagy field is whether changing autophagic flux is beneficial or detrimental to neuronal health and synaptic transmission. I propose that artificially increased autophagy in a healthy cell is as harmful as the inhibition of basal autophagy, especially after an insult. As a consequence, neuronal autophagy has to be precisely balanced. It is essential to fully understand the autophagic phenotype (reduced/elevated autophagy initiation vs. block/increase of autophagic flux), which would enable its targeted manipulation to provide the opportunity to successfully decelerate disease progression, of for example neurodegenerative disorders.

8. References

Ackermann, F., Waites, C.L., and Garner, C.C. (2015). Presynaptic active zones in invertebrates and vertebrates. EMBO Rep *16*, 923-938.

Afuwape, O.A., Wasser, C.R., Schikorski, T., and Kavalali, E.T. (2017). Synaptic vesicle pool-specific modification of neurotransmitter release by intravesicular free radical generation. J Physiol *595*, 1223-1238.

Alvarez-Castelao, B., and Schuman, E.M. (2015). The Regulation of Synaptic Protein Turnover. J Biol Chem *290*, 28623-28630.

Ashrafi, G., Schlehe, J.S., LaVoie, M.J., and Schwarz, T.L. (2014). Mitophagy of damaged mitochondria occurs locally in distal neuronal axons and requires PINK1 and Parkin. J Cell Biol *206*, 655-670.

Baba, M., Takeshige, K., Baba, N., and Ohsumi, Y. (1994). Ultrastructural analysis of the autophagic process in yeast: detection of autophagosomes and their characterization. J Cell Biol *124*, 903-913.

Bae, J.R., and Kim, S.H. (2017). Synapses in neurodegenerative diseases. BMB Reports *50*, 237-246.

Bain, J., Plater, L., Elliott, M., Shpiro, N., Hastie, C.J., McLauchlan, H., Klevernic, I., Arthur, J.S., Alessi, D.R., and Cohen, P. (2007). The selectivity of protein kinase inhibitors: a further update. Biochem J *408*, 297-315.

Banker, G., and Goslin, K. (1988). Developments in neuronal cell culture. Nature *336*, 185-186.

Bento, C.F., Renna, M., Ghislat, G., Puri, C., Ashkenazi, A., Vicinanza, M., Menzies, F.M., and Rubinsztein, D.C. (2016). Mammalian Autophagy: How Does It Work? Annu Rev Biochem *85*, 685-713.

Binotti, B., Pavlos, N.J., Riedel, D., Wenzel, D., Vorbruggen, G., Schalk, A.M., Kuhnel, K., Boyken, J., Erck, C., Martens, H.*, et al.* (2015). The GTPase Rab26 links synaptic vesicles to the autophagy pathway. Elife *4*, e05597.

Bishop, N.A., Lu, T., and Yankner, B.A. (2010). Neural mechanisms of ageing and cognitive decline. Nature *464*, 529-535.

Blommaart, E.F.C.K., Ulrike; Schellens, Jacques P. M.; Vreeling-Sindelarova, Heleen and Meijer, Alfred J (1997). The phosphatidylinositol 3-kinase inhibitors wortmannin and LY294002 inhibit autophagy in isolated rat hepatocytes. European Journal of Biochemistry *243*.

Boland, B., Kumar, A., Lee, S., Platt, F.M., Wegiel, J., Yu, W.H., and Nixon, R.A. (2008). Autophagy induction and autophagosome clearance in neurons: relationship to autophagic pathology in Alzheimer's disease. J Neurosci *28*, 6926-6937.

Bonanomi, D., Rusconi, L., Colombo, C.A., Benfenati, F., and Valtorta, F. (2007). Synaptophysin I selectively specifies the exocytic pathway of synaptobrevin 2/VAMP2. Biochem J *404*, 525-534.

Bulina, M.E., Chudakov, D.M., Britanova, O.V., Yanushevich, Y.G., Staroverov, D.B., Chepurnykh, T.V., Merzlyak, E.M., Shkrob, M.A., Lukyanov, S., and Lukyanov, K.A. (2006). A genetically encoded photosensitizer. Nat Biotechnol *24*, 95-99.

Cai, Q., Lu, L., Tian, J.H., Zhu, Y.B., Qiao, H., and Sheng, Z.H. (2010). Snapin-regulated late endosomal transport is critical for efficient autophagy-lysosomal function in neurons. Neuron *68*, 73-86.

Ceccarelli, B., Hurlbut, W.P., and Mauro, A. (1973). Turnover of transmitter and synaptic vesicles at the frog neuromuscular junction. J Cell Biol *57*, 499-524.

Chan, E.Y. (2009). mTORC1 phosphorylates the ULK1-mAtg13-FIP200 autophagy regulatory complex. Sci Signal *2*, pe51.

Chang, S., Trimbuch, T., and Rosenmund, C. (2018). Synaptotagmin-1 drives synchronous Ca(2+)-triggered fusion by C2B-domain-mediated synaptic-vesicle-membrane attachment. Nat Neurosci *21*, 33-40.

Chapman, E.R. (2002). Synaptotagmin: a Ca(2+) sensor that triggers exocytosis? Nat Rev Mol Cell Biol *3*, 498-508.

Chen, X., Kondo, K., Motoki, K., Homma, H., and Okazawa, H. (2015). Fasting activates macroautophagy in neurons of Alzheimer's disease mouse model but is insufficient to degrade amyloid-beta. Sci Rep *5*, 12115.

Cheng, X.T., Zhou, B., Lin, M.Y., Cai, Q., and Sheng, Z.H. (2015). Axonal autophagosomes recruit dynein for retrograde transport through fusion with late endosomes. J Cell Biol *209*, 377-386.

Chi, P., Greengard, P., and Ryan, T.A. (2001). Synapsin dispersion and reclustering during synaptic activity. Nat Neurosci *4*, 1187-1193.

Chin, L.S., Vavalle, J.P., and Li, L. (2002). Staring, a novel E3 ubiquitin-protein ligase that targets syntaxin 1 for degradation. J Biol Chem *277*, 35071-35079.

Chu, C.T. (2006). Autophagic stress in neuronal injury and disease. J Neuropathol Exp Neurol *65*, 423-432.

Chu, C.T., Zhu, J., and Dagda, R. (2007). Beclin 1-independent pathway of damage-induced mitophagy and autophagic stress: implications for neurodegeneration and cell death. Autophagy *3*, 663-666.

Ciechanover, A. (2005). Intracellular protein degradation: from a vague idea thru the lysosome and the ubiquitin-proteasome system and onto human diseases and drug targeting. Cell Death Differ *12*, 1178-1190.

Cochilla, A.J., Angleson, J.K., and Betz, W.J. (1999). Monitoring secretory membrane with FM1-43 fluorescence. Annu Rev Neurosci *22*, 1-10.

Codogno, P., Mehrpour, M., and Proikas-Cezanne, T. (2011). Canonical and non-canonical autophagy: variations on a common theme of self-eating? Nat Rev Mol Cell Biol *13*, 7-12.

Cohen, L.D., Zuchman, R., Sorokina, O., Muller, A., Dieterich, D.C., Armstrong, J.D., Ziv, T., and Ziv, N.E. (2013). Metabolic turnover of synaptic proteins: kinetics, interdependencies and implications for synaptic maintenance. PLoS One *8*, e63191.

Corti, O., Lesage, S., and Brice, A. (2011). What genetics tells us about the causes and mechanisms of Parkinson's disease. Physiol Rev *91*, 1161-1218.

Cota, D., Proulx, K., Smith, K.A., Kozma, S.C., Thomas, G., Woods, S.C., and Seeley, R.J. (2006). Hypothalamic mTOR signaling regulates food intake. Science *312*, 927-930.

Davydova, D., Marini, C., King, C., Klueva, J., Bischof, F., Romorini, S., Montenegro-Venegas, C., Heine, M., Schneider, R., Schroder, M.S., *et al.* (2014). Bassoon specifically controls presynaptic P/Q-type Ca(2+) channels via RIM-binding protein. Neuron *82*, 181-194.

Deng, Z., Purtell, K., Lachance, V., Wold, M.S., Chen, S., and Yue, Z. (2017). Autophagy Receptors and Neurodegenerative Diseases. Trends Cell Biol *27*, 491-504.

Ding, W.X., Ni, H.M., Gao, W., Yoshimori, T., Stolz, D.B., Ron, D., and Yin, X.M. (2007). Linking of autophagy to ubiquitin-proteasome system is important for the regulation of endoplasmic reticulum stress and cell viability. Am J Pathol *171*, 513-524.

Duran, A., Amanchy, R., Linares, J.F., Joshi, J., Abu-Baker, S., Porollo, A., Hansen, M., Moscat, J., and Diaz-Meco, M.T. (2011). p62 is a key regulator of nutrient sensing in the mTORC1 pathway. Mol Cell *44*, 134-146.

Ebrahimi-Fakhari, D., Saidi, L.J., and Wahlster, L. (2013). Molecular chaperones and protein folding as therapeutic targets in Parkinson's disease and other synucleinopathies. Acta Neuropathol Commun *1*, 79.

Eisenberg, T., Knauer, H., Schauer, A., Buttner, S., Ruckenstuhl, C., Carmona-Gutierrez, D., Ring, J., Schroeder, S., Magnes, C., Antonacci, L., *et al.* (2009). Induction of autophagy by spermidine promotes longevity. Nat Cell Biol *11*, 1305-1314.

Ericsson, J.L. (1969). Studies on induced cellular autophagy. I. Electron microscopy of cells with in vivo labelled lysosomes. Exp Cell Res *55*, 95-106.

Eskelinen, E.L., Reggiori, F., Baba, M., Kovacs, A.L., and Seglen, P.O. (2011). Seeing is believing: the impact of electron microscopy on autophagy research. Autophagy *7*, 935-956.

Fejtova, A., and Gundelfinger, E.D. (2006). Molecular organization and assembly of the presynaptic active zone of neurotransmitter release. Results Probl Cell Differ *43*, 49-68.

Fernandes, A.C., Uytterhoeven, V., Kuenen, S., Wang, Y.C., Slabbaert, J.R., Swerts, J., Kasprowicz, J., Aerts, S., and Verstreken, P. (2014). Reduced synaptic vesicle protein degradation at lysosomes curbs TBC1D24/sky-induced neurodegeneration. J Cell Biol *207*, 453-462.

Fleming, A., Noda, T., Yoshimori, T., and Rubinsztein, D.C. (2011). Chemical modulators of autophagy as biological probes and potential therapeutics. Nat Chem Biol *7*, 9-17.

Fykse, E.M., Takei, K., Walch-Solimena, C., Geppert, M., Jahn, R., De Camilli, P., and Sudhof, T.C. (1993). Relative properties and localizations of synaptic vesicle protein isoforms: the case of the synaptophysins. J Neurosci *13*, 4997-5007.

Gaffield, M.A., and Betz, W.J. (2006). Imaging synaptic vesicle exocytosis and endocytosis with FM dyes. Nat Protoc *1*, 2916-2921.

Galluzzi, L., Bravo-San Pedro, J.M., Blomgren, K., and Kroemer, G. (2016). Autophagy in acute brain injury. Nat Rev Neurosci *17*, 467-484.

Ganley, I.G., Wong, P.M., Gammoh, N., and Jiang, X. (2011). Distinct autophagosomal-lysosomal fusion mechanism revealed by thapsigargin-induced autophagy arrest. Mol Cell *42*, 731-743.

Gibson, D.G., Young, L., Chuang, R.-Y., Venter, J.C., Hutchison, C.A., and Smith, H.O. (2009). Enzymatic assembly of DNA molecules up to several hundred kilobases. Nature Methods *6*, 343-345.

Gordon, S.L., and Cousin, M.A. (2014). The Sybtraps: control of synaptobrevin traffic by synaptophysin, alpha-synuclein and AP-180. Traffic *15*, 245-254.

Gupta, V.K., Pech, U., Bhukel, A., Fulterer, A., Ender, A., Mauermann, S.F., Andlauer, T.F., Antwi-Adjei, E., Beuschel, C., Thriene, K.*, et al.* (2016). Spermidine Suppresses Age-Associated Memory Impairment by Preventing Adverse Increase of Presynaptic Active Zone Size and Release. PLoS Biol *14*, e1002563.

Hanna, J., and Finley, D. (2007). A proteasome for all occasions. FEBS Lett *581*, 2854-2861.

Hara, T., Nakamura, K., Matsui, M., Yamamoto, A., Nakahara, Y., Suzuki-Migishima, R., Yokoyama, M., Mishima, K., Saito, I., Okano, H.*, et al.* (2006). Suppression of basal autophagy in neural cells causes neurodegenerative disease in mice. Nature *441*, 885-889.

Haucke, V., Neher, E., and Sigrist, S.J. (2011). Protein scaffolds in the coupling of synaptic exocytosis and endocytosis. Nat Rev Neurosci *12*, 127-138.

Heras-Sandoval, D., Perez-Rojas, J.M., Hernandez-Damian, J., and Pedraza-Chaverri, J. (2014). The role of PI3K/AKT/mTOR pathway in the modulation of autophagy and the clearance of protein aggregates in neurodegeneration. Cell Signal *26*, 2694-2701.

Hernandez, D., Torres, C.A., Setlik, W., Cebrian, C., Mosharov, E.V., Tang, G., Cheng, H.C., Kholodilov, N., Yarygina, O., Burke, R.E.*, et al.* (2012). Regulation of presynaptic neurotransmission by macroautophagy. Neuron *74*, 277-284.

Heuser, J.E., and Reese, T.S. (1973). Evidence for recycling of synaptic vesicle membrane during transmitter release at the frog neuromuscular junction. J Cell Biol *57*, 315-344.

Heyden, A., Ionescu, M.C., Romorini, S., Kracht, B., Ghiglieri, V., Calabresi, P., Seidenbecher, C., Angenstein, F., and Gundelfinger, E.D. (2011). Hippocampal enlargement in Bassoon-mutant mice is associated with enhanced neurogenesis, reduced apoptosis, and abnormal BDNF levels. Cell Tissue Res *346*, 11-26.

Hilfiker, S., Pieribone, V.A., Nordstedt, C., Greengard, P., and Czernik, A.J. (1999). Regulation of synaptotagmin I phosphorylation by multiple protein kinases. J Neurochem *73*, 921-932.

Hirokawa, N., Niwa, S., and Tanaka, Y. (2010). Molecular motors in neurons: transport mechanisms and roles in brain function, development, and disease. Neuron *68*, 610-638.

Hosokawa, N., Hara, T., Kaizuka, T., Kishi, C., Takamura, A., Miura, Y., Iemura, S., Natsume, T., Takehana, K., Yamada, N.*, et al.* (2009). Nutrient-dependent mTORC1 association with the ULK1-Atg13-FIP200 complex required for autophagy. Mol Biol Cell *20*, 1981-1991.

Ichimura, Y., Kirisako, T., Takao, T., Satomi, Y., Shimonishi, Y., Ishihara, N., Mizushima, N., Tanida, I., Kominami, E., Ohsumi, M.*, et al.* (2000). A ubiquitin-like system mediates protein lipidation. Nature *408*, 488-492.

Jackson, J.S., Witton, J., Johnson, J.D., Ahmed, Z., Ward, M., Randall, A.D., Hutton, M.L., Isaac, J.T., O'Neill, M.J., and Ashby, M.C. (2017). Altered Synapse Stability in the Early Stages of Tauopathy. Cell Rep *18*, 3063-3068.

Jacobson, K., Rajfur, Z., Vitriol, E., and Hahn, K. (2008). Chromophore-assisted laser inactivation in cell biology. Trends Cell Biol *18*, 443-450.

Jarvela, T.S., and Linstedt, A.D. (2014). The application of KillerRed for acute protein inactivation in living cells. Curr Protoc Cytom *69*, 12 35 11-12 35 10.

Jay, D.G. (1988). Selective destruction of protein function by chromophore-assisted laser inactivation. Proc Natl Acad Sci U S A *85*, 5454-5458.

Jin, Y., and Garner, C.C. (2008). Molecular mechanisms of presynaptic differentiation. Annu Rev Cell Dev Biol *24*, 237-262.

Kamada, Y., Funakoshi, T., Shintani, T., Nagano, K., Ohsumi, M., and Ohsumi, Y. (2000). Tor-mediated induction of autophagy via an Apg1 protein kinase complex. J Cell Biol *150*, 1507-1513.

Kegel, K.B., Kim, M., Sapp, E., McIntyre, C., Castano, J.G., Aronin, N., and DiFiglia, M. (2000). Huntingtin expression stimulates endosomal-lysosomal activity, endosome tubulation, and autophagy. J Neurosci *20*, 7268-7278.

Kim, J.H., Lee, S.R., Li, L.H., Park, H.J., Park, J.H., Lee, K.Y., Kim, M.K., Shin, B.A., and Choi, S.Y. (2011). High cleavage efficiency of a 2A peptide derived from porcine teschovirus-1 in human cell lines, zebrafish and mice. PLoS One *6*, e18556.

Klionsky, D.J., Abdalla, F.C., Abeliovich, H., Abraham, R.T., Acevedo-Arozena, A., Adeli, K., Agholme, L., Agnello, M., Agostinis, P., Aguirre-Ghiso, J.A.*, et al.* (2012). Guidelines for the use and interpretation of assays for monitoring autophagy. Autophagy *8*, 445-544.

Klionsky, D.J., and Codogno, P. (2013). The mechanism and physiological function of macroautophagy. J Innate Immun *5*, 427-433.

Klionsky, D.J., Eskelinen, E.L., and Deretic, V. (2014). Autophagosomes, phagosomes, autolysosomes, phagolysosomes, autophagolysosomes... wait, I'm confused. Autophagy *10*, 549-551.

Knecht, E., Aguado, C., Carcel, J., Esteban, I., Esteve, J.M., Ghislat, G., Moruno, J.F., Vidal, J.M., and Saez, R. (2009). Intracellular protein degradation in mammalian cells: recent developments. Cell Mol Life Sci *66*, 2427-2443.

Komatsu, M., Waguri, S., Chiba, T., Murata, S., Iwata, J., Tanida, I., Ueno, T., Koike, M., Uchiyama, Y., Kominami, E.*, et al.* (2006). Loss of autophagy in the central nervous system causes neurodegeneration in mice. Nature *441*, 880-884.

Kononenko, N.L., Classen, G.A., Kuijpers, M., Puchkov, D., Maritzen, T., Tempes, A., Malik, A.R., Skalecka, A., Bera, S., Jaworski, J.*, et al.* (2017). Retrograde transport of TrkB-containing autophagosomes via the adaptor AP-2 mediates neuronal complexity and prevents neurodegeneration. Nat Commun *8*, 14819.

Kopitz, J., Kisen, G.O., Gordon, P.B., Bohley, P., and Seglen, P.O. (1990). Nonselective autophagy of cytosolic enzymes by isolated rat hepatocytes. J Cell Biol *111*, 941-953.

Labbadia, J., and Morimoto, R.I. (2015). The biology of proteostasis in aging and disease. Annu Rev Biochem *84*, 435-464.

Lamark, T., and Johansen, T. (2010). Autophagy: links with the proteasome. Curr Opin Cell Biol *22*, 192-198.

Lamb, C.A., Yoshimori, T., and Tooze, S.A. (2013). The autophagosome: origins unknown, biogenesis complex. Nat Rev Mol Cell Biol *14*, 759-774.

Leal-Ortiz, S., Waites, C.L., Terry-Lorenzo, R., Zamorano, P., Gundelfinger, E.D., and Garner, C.C. (2008). Piccolo modulation of Synapsin1a dynamics regulates synaptic vesicle exocytosis. J Cell Biol *181*, 831-846.

Lee, J.H., Yu, W.H., Kumar, A., Lee, S., Mohan, P.S., Peterhoff, C.M., Wolfe, D.M., Martinez-Vicente, M., Massey, A.C., Sovak, G.*, et al.* (2010). Lysosomal proteolysis and autophagy require presenilin 1 and are disrupted by Alzheimer-related PS1 mutations. Cell *141*, 1146-1158.

Lee, S., Sato, Y., and Nixon, R.A. (2011). Lysosomal proteolysis inhibition selectively disrupts axonal transport of degradative organelles and causes an Alzheimer's-like axonal dystrophy. J Neurosci *31*, 7817-7830.

Lemasters, J.J. (2014). Variants of mitochondrial autophagy: Types 1 and 2 mitophagy and micromitophagy (Type 3). Redox Biol *2*, 749-754.

Liang, Y., and Sigrist, S. (2018). Autophagy and proteostasis in the control of synapse aging and disease. Curr Opin Neurobiol *48*, 113-121.

Liao, J.C., Roider, J., and Jay, D.G. (1994). Chromophore-assisted laser inactivation of proteins is mediated by the photogeneration of free radicals. Proc Natl Acad Sci U S A *91*, 2659-2663.

Lilienbaum, A. (2013). Relationship between the proteasomal system and autophagy. Int J Biochem Mol Biol *4*, 1-26.

Lin, J.Y., Sann, S.B., Zhou, K., Nabavi, S., Proulx, C.D., Malinow, R., Jin, Y., and Tsien, R.Y. (2013). Optogenetic inhibition of synaptic release with chromophore-assisted light inactivation (CALI). Neuron *79*, 241-253.

Linares, J.F., Duran, A., Yajima, T., Pasparakis, M., Moscat, J., and Diaz-Meco, M.T. (2013). K63 polyubiquitination and activation of mTOR by the p62-TRAF6 complex in nutrient-activated cells. Mol Cell *51*, 283-296.

Linden, K.G., Liao, J.C., and Jay, D.G. (1992). Spatial specificity of chromophore assisted laser inactivation of protein function. Biophys J *61*, 956-962.

Lois, C., Hong, E.J., Pease, S., Brown, E.J., and Baltimore, D. (2002). Germline transmission and tissue-specific expression of transgenes delivered by lentiviral vectors. Science *295*, 868-872.

Maas, C., Torres, V.I., Altrock, W.D., Leal-Ortiz, S., Wagh, D., Terry-Lorenzo, R.T., Fejtova, A., Gundelfinger, E.D., Ziv, N.E., and Garner, C.C. (2012). Formation of Golgi-derived active zone precursor vesicles. J Neurosci *32*, 11095-11108.

Maday, S. (2016). Mechanisms of neuronal homeostasis: Autophagy in the axon. Brain Res *1649*, 143-150.

Maday, S., and Holzbaur, E.L. (2014). Autophagosome biogenesis in primary neurons follows an ordered and spatially regulated pathway. Dev Cell *30*, 71-85.

Maday, S., and Holzbaur, E.L. (2016). Compartment-Specific Regulation of Autophagy in Primary Neurons. J Neurosci *36*, 5933-5945.

Maday, S., Wallace, K.E., and Holzbaur, E.L. (2012). Autophagosomes initiate distally and mature during transport toward the cell soma in primary neurons. J Cell Biol *196*, 407-417.

Martinez-Vicente, M., Talloczy, Z., Wong, E., Tang, G., Koga, H., Kaushik, S., de Vries, R., Arias, E., Harris, S., Sulzer, D.*, et al.* (2010). Cargo recognition failure is responsible for inefficient autophagy in Huntington's disease. Nat Neurosci *13*, 567-576.

McNamara, C.R., and Degterev, A. (2011). Small-molecule inhibitors of the PI3K signaling network. Future Med Chem *3*, 549-565.

McPherson, P.S. (2015). Eating Locally: Microautophagy and Protein Turnover at the Synapse. Neuron *88*, 619-621.

Meberg, P.J., and Miller, M.W. (2003). Culturing hippocampal and cortical neurons. Methods Cell Biol *71*, 111-127.

Mizushima, N., Levine, B., Cuervo, A.M., and Klionsky, D.J. (2008). Autophagy fights disease through cellular self-digestion. Nature *451*, 1069-1075.

Mizushima, N., Yamamoto, A., Matsui, M., Yoshimori, T., and Ohsumi, Y. (2004). In vivo analysis of autophagy in response to nutrient starvation using transgenic mice expressing a fluorescent autophagosome marker. Mol Biol Cell *15*, 1101-1111.

Mizushima, N., Yoshimori, T., and Levine, B. (2010). Methods in mammalian autophagy research. Cell *140*, 313-326.

Mizushima, N., Yoshimori, T., and Ohsumi, Y. (2011). The role of Atg proteins in autophagosome formation. Annu Rev Cell Dev Biol *27*, 107-132.

Musiwaro, P., Smith, M., Manifava, M., Walker, S.A., and Ktistakis, N.T. (2013). Characteristics and requirements of basal autophagy in HEK 293 cells. Autophagy *9*, 1407-1417.

Nelson, D.E., Randle, S.J., and Laman, H. (2013). Beyond ubiquitination: the atypical functions of Fbxo7 and other F-box proteins. Open Biol *3*, 130131.

Nixon, R.A. (2013). The role of autophagy in neurodegenerative disease. Nat Med *19*, 983-997.

Nixon, R.A., Wegiel, J., Kumar, A., Yu, W.H., Peterhoff, C., Cataldo, A., and Cuervo, A.M. (2005). Extensive involvement of autophagy in Alzheimer disease: an immuno-electron microscopy study. J Neuropathol Exp Neurol *64*, 113-122.

Okerlund, N.D., Schneider, K., Leal-Ortiz, S., Montenegro-Venegas, C., Kim, S.A., Garner, L.C., Waites, C.L., Gundelfinger, E.D., Reimer, R.J., and Garner, C.C. (2017). Bassoon Controls Presynaptic Autophagy through Atg5. Neuron *93*, 897-913 e897.

Pankiv, S., Clausen, T.H., Lamark, T., Brech, A., Bruun, J.A., Outzen, H., Overvatn, A., Bjorkoy, G., and Johansen, T. (2007). p62/SQSTM1 binds directly to Atg8/LC3 to facilitate degradation of ubiquitinated protein aggregates by autophagy. J Biol Chem *282*, 24131-24145.

Petralia, R.S., Schwartz, C.M., Wang, Y.X., Kawamoto, E.M., Mattson, M.P., and Yao, P.J. (2013). Sonic hedgehog promotes autophagy in hippocampal neurons. Biol Open *2*, 499-504.

Pickrell, A.M., and Youle, R.J. (2015). The roles of PINK1, parkin, and mitochondrial fidelity in Parkinson's disease. Neuron *85*, 257-273.

Qi, Y.B.G., Emma J.; Shu, Xiaokun; Tsien, Roger Y., and Jin, Yishi (2012). Photo-inducible cell ablation in Caenorhabditis elegans using the genetically encoded singlet

oxygen generating protein miniSOG. PNAS *109*.

Raiborg, C., and Stenmark, H. (2009). The ESCRT machinery in endosomal sorting of ubiquitylated membrane proteins. Nature *458*, 445-452.

Ravikumar, B., Sarkar, S., Davies, J.E., Futter, M., Garcia-Arencibia, M., Green-Thompson, Z.W., Jimenez-Sanchez, M., Korolchuk, V.I., Lichtenberg, M., Luo, S., *et al.* (2010). Regulation of mammalian autophagy in physiology and pathophysiology. Physiol Rev *90*, 1383-1435.

Ravikumar, B., Vacher, C., Berger, Z., Davies, J.E., Luo, S., Oroz, L.G., Scaravilli, F., Easton, D.F., Duden, R., O'Kane, C.J.*, et al.* (2004). Inhibition of mTOR induces autophagy and reduces toxicity of polyglutamine expansions in fly and mouse models of Huntington disease. Nat Genet *36*, 585-595.

Rizzoli, S.O. (2014). Synaptic vesicle recycling: steps and principles. EMBO J *33*, 788-822.

Rizzoli, S.O., and Betz, W.J. (2005). Synaptic vesicle pools. Nat Rev Neurosci *6*, 57-69.

Rosenmund, C., and Stevens, C.F. (1996). Definition of the readily releasable pool of vesicles at hippocampal synapses. Neuron *16*, 1197-1207.

Roy, S., Winton, M.J., Black, M.M., Trojanowski, J.Q., and Lee, V.M. (2007). Rapid and intermittent cotransport of slow component-b proteins. J Neurosci *27*, 3131-3138.

Rubinsztein, D.C., Codogno, P., and Levine, B. (2012). Autophagy modulation as a potential therapeutic target for diverse diseases. Nat Rev Drug Discov *11*, 709-730.

Rubinsztein, D.C., Marino, G., and Kroemer, G. (2011). Autophagy and aging. Cell *146*, 682-695.

Russell, R.C., Yuan, H.X., and Guan, K.L. (2014). Autophagy regulation by nutrient signaling. Cell Res *24*, 42-57.

Sanchez-Wandelmer, J., and Reggiori, F. (2013). Amphisomes: out of the autophagosome shadow? EMBO J *32*, 3116-3118.

Satoo, K., Noda, N.N., Kumeta, H., Fujioka, Y., Mizushima, N., Ohsumi, Y., and Inagaki, F. (2009). The structure of Atg4B-LC3 complex reveals the mechanism of LC3 processing and delipidation during autophagy. EMBO J *28*, 1341-1350.

Scheff, S.W., Neltner, J.H., and Nelson, P.T. (2014). Is synaptic loss a unique hallmark of Alzheimer's disease? Biochem Pharmacol *88*, 517-528.

Schikorski, T., and Stevens, C.F. (2001). Morphological correlates of functionally defined synaptic vesicle populations. Nat Neurosci *4*, 391-395.

Sheehan, P., Zhu, M., Beskow, A., Vollmer, C., and Waites, C.L. (2016). Activity-Dependent Degradation of Synaptic Vesicle Proteins Requires Rab35 and the ESCRT Pathway. J Neurosci *36*, 8668-8686.

Shehata, M., Matsumura, H., Okubo-Suzuki, R., Ohkawa, N., and Inokuchi, K. (2012). Neuronal stimulation induces autophagy in hippocampal neurons that is involved in AMPA receptor degradation after chemical long-term depression. J Neurosci *32*, 10413-10422.

Shu, X., Lev-Ram, V., Deerinck, T.J., Qi, Y., Ramko, E.B., Davidson, M.W., Jin, Y., Ellisman, M.H., and Tsien, R.Y. (2011). A genetically encoded tag for correlated light and electron microscopy of intact cells, tissues, and organisms. PLoS Biol *9*, e1001041.

Shupliakov, O., and Brodin, L. (2010). Recent insights into the building and cycling of synaptic vesicles. Exp Cell Res *316*, 1344-1350.

Shvets, E., Fass, E., Scherz-Shouval, R., and Elazar, Z. (2008). The N-terminus and Phe52 residue of LC3 recruit p62/SQSTM1 into autophagosomes. J Cell Sci *121*, 2685-2695.

Soukup, S.F., Kuenen, S., Vanhauwaert, R., Manetsberger, J., Hernandez-Diaz, S., Swerts, J., Schoovaerts, N., Vilain, S., Gounko, N.V., Vints, K.*, et al.* (2016). A LRRK2-Dependent EndophilinA Phosphoswitch Is Critical for Macroautophagy at Presynaptic Terminals. Neuron *92*, 829-844.

Speese, S.D., Trotta, N., Rodesch, C.K., Aravamudan, B., and Broadie, K. (2003). The Ubiquitin Proteasome System Acutely Regulates Presynaptic Protein Turnover and Synaptic Efficacy. Current Biology *13*, 899-910.

Spencer, B., Potkar, R., Trejo, M., Rockenstein, E., Patrick, C., Gindi, R., Adame, A., Wyss-Coray, T., and Masliah, E. (2009). Beclin 1 gene transfer activates autophagy and ameliorates the neurodegenerative pathology in alpha-synuclein models of Parkinson's and Lewy body diseases. J Neurosci *29*, 13578-13588.

Spilman, P., Podlutskaya, N., Hart, M.J., Debnath, J., Gorostiza, O., Bredesen, D., Richardson, A., Strong, R., and Galvan, V. (2010). Inhibition of mTOR by rapamycin abolishes cognitive deficits and reduces amyloid-beta levels in a mouse model of Alzheimer's disease. PLoS One *5*, e9979.

Stenmark, H. (2009). Rab GTPases as coordinators of vesicle traffic. Nat Rev Mol Cell Biol *10*, 513-525.

Sudhof, T.C. (2004). The synaptic vesicle cycle. Annu Rev Neurosci *27*, 509-547.

Sudhof, T.C. (2012). The presynaptic active zone. Neuron *75*, 11-25.

Surrey, T., Elowitz, M.B., Wolf, P.E., Yang, F., Nedelec, F., Shokat, K., and Leibler, S. (1998). Chromophore-assisted light inactivation and self-organization of microtubules and motors. Proc Natl Acad Sci U S A *95*, 4293-4298.

Takamori, S., Holt, M., Stenius, K., Lemke, E.A., Gronborg, M., Riedel, D., Urlaub, H., Schenck, S., Brugger, B., Ringler, P.*, et al.* (2006). Molecular anatomy of a trafficking organelle. Cell *127*, 831-846.

Takemoto, K., Matsuda, T., Sakai, N., Fu, D., Noda, M., Uchiyama, S., Kotera, I., Arai, Y., Horiuchi, M., Fukui, K.*, et al.* (2013). SuperNova, a monomeric photosensitizing fluorescent protein for chromophore-assisted light inactivation. Sci Rep *3*, 2629.

Takeshige, K., Baba, M., Tsuboi, S., Noda, T., and Ohsumi, Y. (1992). Autophagy in yeast demonstrated with proteinase-deficient mutants and conditions for its induction. J Cell Biol *119*, 301-311.

Tammineni, P., Ye, X., Feng, T., Aikal, D., and Cai, Q. (2017). Impaired retrograde transport of axonal autophagosomes contributes to autophagic stress in Alzheimer's disease neurons. Elife *6*.

Trewin, A.J., Berry, B.J., Wei, A.Y., Bahr, L.L., Foster, T.H., and Wojtovich, A.P. (2018). Light-induced oxidant production by fluorescent proteins. Free Radic Biol Med.

Tsukada, M., and Ohsumi, Y. (1993). Isolation and characterization of autophagy-defective mutants of Saccharomyces cerevisiae. FEBS Lett *333*, 169-174.

Tsuriel, S., Geva, R., Zamorano, P., Dresbach, T., Boeckers, T., Gundelfinger, E.D., Garner, C.C., and Ziv, N.E. (2006). Local sharing as a predominant determinant of synaptic matrix molecular dynamics. PLoS Biol *4*, e271.

Uytterhoeven, V., Kuenen, S., Kasprowicz, J., Miskiewicz, K., and Verstreken, P. (2011). Loss of skywalker reveals synaptic endosomes as sorting stations for synaptic vesicle proteins. Cell *145*, 117-132.

Uytterhoeven, V., Lauwers, E., Maes, I., Miskiewicz, K., Melo, M.N., Swerts, J., Kuenen, S., Wittocx, R., Corthout, N., Marrink, S.J., *et al.* (2015). Hsc70-4 Deforms Membranes to Promote Synaptic Protein Turnover by Endosomal Microautophagy. Neuron *88*, 735-748.

Vanhauwaert, R., Kuenen, S., Masius, R., Bademosi, A., Manetsberger, J., Schoovaerts, N., Bounti, L., Gontcharenko, S., Swerts, J., Vilain, S., *et al.* (2017). The SAC1 domain in synaptojanin is required for autophagosome maturation at presynaptic terminals. EMBO J *36*, 1392-1411.

Vijayan, V., and Verstreken, P. (2017). Autophagy in the presynaptic compartment in health and disease. J Cell Biol *216*, 1895-1906.

Vingtdeux, V., Sergeant, N., and Buee, L. (2012). Potential contribution of exosomes to the prion-like propagation of lesions in Alzheimer's disease. Front Physiol *3*, 229.

Waites, C.L., and Garner, C.C. (2011). Presynaptic function in health and disease. Trends Neurosci *34*, 326-337.

Waites, C.L., Leal-Ortiz, S.A., Okerlund, N., Dalke, H., Fejtova, A., Altrock, W.D., Gundelfinger, E.D., and Garner, C.C. (2013). Bassoon and Piccolo maintain synapse integrity by regulating protein ubiquitination and degradation. EMBO J *32*, 954-969.

Wang, T., Martin, S., Papadopulos, A., Harper, C.B., Mavlyutov, T.A., Niranjan, D., Glass, N.R., Cooper-White, J.J., Sibarita, J.B., Choquet, D., *et al.* (2015). Control of autophagosome axonal retrograde flux by presynaptic activity unveiled using botulinum neurotoxin type a. J Neurosci *35*, 6179-6194.

Wang, Y., Nartiss, Y., Steipe, B., McQuibban, G.A., and Kim, P.K. (2012). ROS-induced mitochondrial depolarization initiates PARK2/PARKIN-dependent mitochondrial degradation by autophagy. Autophagy *8*, 1462-1476.

Wang, Y.C., Lauwers, E., and Verstreken, P. (2017). Presynaptic protein homeostasis and neuronal function. Curr Opin Genet Dev *44*, 38-46.

Wheeler, T.C., Chin, L.S., Li, Y., Roudabush, F.L., and Li, L. (2002). Regulation of synaptophysin degradation by mammalian homologues of seven in absentia. J Biol Chem *277*, 10273-10282.

Wilhelm, B.G., Mandad, S., Truckenbrodt, S., Krohnert, K., Schafer, C., Rammner, B., Koo, S.J., Classen, G.A., Krauss, M., Haucke, V., *et al.* (2014). Composition of isolated synaptic boutons reveals the amounts of vesicle trafficking proteins. Science *344*, 1023-1028.

Yang, J.Y., and Yang, W.Y. (2011). Spatiotemporally controlled initiation of Parkin-mediated mitophagy within single cells. Autophagy *7*, 1230-1238.

Ybe, J.A., Wakeham, D.E., Brodsky, F.M., and Hwang, P.K. (2000). Molecular structures of proteins involved in vesicle fusion. Traffic *1*, 474-479.

Young, J.E., Martinez, R.A., and La Spada, A.R. (2009). Nutrient deprivation induces neuronal autophagy and implicates reduced insulin signaling in neuroprotective autophagy activation. J Biol Chem *284*, 2363-2373.

Yue, Z., Friedman, L., Komatsu, M., and Tanaka, K. (2009). The cellular pathways of neuronal autophagy and their implication in neurodegenerative diseases. Biochim Biophys Acta *1793*, 1496-1507.

Zhu, J.H., Horbinski, C., Guo, F., Watkins, S., Uchiyama, Y., and Chu, C.T. (2007). Regulation of autophagy by extracellular signal-regulated protein kinases during 1-methyl-4-phenylpyridinium-induced cell death. Am J Pathol *170*, 75-86.

Ziv, N.E., and Garner, C.C. (2004). Cellular and molecular mechanisms of presynaptic assembly. Nat Rev Neurosci *5*, 385-399.

9. Abbreviations

#	number
AD	Alzheimer's disease
approx.	approximately
Atg	autophagy-related protein
a. u.	arbitrary units
AV	autophagic vacuole
AZ	active zone
BafA1	bafilomycin A1
bp	base pair(s)
BSA	bovine serum albumin
Bsn	Bassoon
CALI	chromophore-assisted light inactivation
CC	coiled-coil domain
CMA	chaperone-mediated autophagy
CNS	central nervous system
Co-IP	Co-Immunoprecipitation
CQ	chloroquine
DHE	dihydroethidium
DIV	days in vitro
DKD	double knock down
DMSO	dimethyl sulfoxide
EDTA	ethylenediaminetetraacetic acid
e.g.	exempli gratia, for example
eGFP	enhanced green fluorescent protein
EM	electron microscopy
EPSC	excitatory postsynaptic current
ER	endoplasmatic reticulum
ESCRT	endosomal sorting complex required for transport
FCS	fetal calf serum

GFP	green fluorescent protein
HD	Huntington's disease
ICC	immunocytochemistry
int.	intensity
KD	knock down
KO	knockout
KR	Killerred
LC3	microtubule-associated protein light chain 3
LTP	long-term depression
lumSN	luminal Supernova
mCh	mCherry
mRFP	monomeric red fluorescent protein
mTOR	mammalian target of rapamycin
MVB	multivesicular bodies
NMJ	neuromuscular junction
norm.	normalized
ON	overnight
P2A	2A peptide derived from porcine
PBS	phosphate buffered saline
PBST	0.2 % Tween 20 in phosphate buffered saline
PD	Parkinson's disease
PE	phosphatidylethanolamine
PI3K	phosphoinositide 3 kinase
PFA	paraformaldehyde
PS	penicillin/streptomycin
PSD	postsynaptic density
R	rapamycin
RFP	red fluorescent protein
ROS	reactive oxygen species
RT	room temperature
scRNA/SC	scrambled shRNA

shAtg5	Atg5 shRNA
SN	Supernova
SV	synaptiv vesicle
Syn	Synapsin
Syp	Synaptophysin
Syt	Synaptotagmin
tf	tandem fluorescence
TD	transduced/infected
U6	U6 promoter
U/Ubi	ubiquitin promoter
UbK_0	recombinant ubiquitin, all lysine residues have been substituted with arginine
UPS	ubiquitin-proteasome-system
UT	untransduced/uninfected/untransfected
W	wortmannin
WT	wildtype
XY	Supernova or mCherry
ZnF	zinc finger domain

10. Units

°C	degrees Celsius
µg	microgram
µl	microlitre
µm	micrometer
µM	micromolar
cm^2	square centimetre
eV	electronvolt
g	gram/gravity
Hz	Hertz
k	10^3
M	mole
MΩ	megaohm
mg	milligram
min	minute
ml	millilitre
mOsm	milliosmole
mm	millimetre
mM	millimolar
ms	milliseconds
mV	millivolt
ng	nanogram
nm	nanometer
pmol	picomole
s/sec	seconds
U/ml	units per millilitre

11. Contributions

- **Figure 5:** The majority of lentiviral vectors were created by Dr. Thorsten Trimbuch and viruses were produced by the Viral Core Facility of the Charité – Universitätsmedizin Berlin.
- **Figure 12**: Western Blots were performed by Christine Bruns, Deutsches Zentrum für Neurodegenerative Erkrankungen.
- **Figure 20:** Electron microscopy was performed by Dr. Marta Orlando, Charité – Universitätsmedizin Berlin.
- **Figure 31:** Electrophysiology was performed by Ewa Andrzejak, Deutsches Zentrum für Neurodegenerative Erkrankungen.
- **Figure 32, 33 and 34:** Bassoon KO neurons were plated and infected by Dr. Carolina Montenegro-Venegas, Leibniz-Institut für Neurobiologie.

12. Publications

Hoffmann, S., Orlando, M., Andrzejak, E., Bruns, C., Trimbuch, T., Rosenmund, C., Garner, C.C. and Ackermann, F. (forthcoming). Light-activated ROS production induces synaptic autophagy. The Journal of Neuroscience; bioRxiv/440719.

Trepte, P., Kruse, S., Kostova, S., **Hoffmann, S.**, Buntru, A., Tempelmeier, A., Secker, C., Diez, L., Schulz, A., Klockmeier, K., Zenkner, M., Golusik, S., Rau, K., Schnoegl, S., Garner, C.C. and Wanker, E.E. (2018), LuThy: a double-readout bioluminescence-based two-hybrid technology for quantitative mapping of protein-protein interactions in mammalian cells. Molecular Systems Biology.

13. Acknowledgments

First of all, I would like to thank Craig for letting me persue my work in his lab. He provided strong guidance throughout my time in the lab while also giving me a lot of responsibility and freedom to conduct my research. He became a role model for me in life because he is not just an extraordinary scientist but also one of the best human beings that I fortunately have come to know in my life.

I owe sincere gratitute to Prof. Dr. Stephan Sigrist for reviewing this thesis.

Of course, I would also like to thank all the people in the lab for their advice and help, and a very comfortable working atmosphere.

I address special thanks to Frauke who helped me with her exceptional scientific input, her ability to see things from a different perspective and her numerous motivating words. I would also like to thank Kathi not only for letting me be part of the Bassoon team but also for providing good discussions.

I am grateful to Christine and Anny for technical support and a lot of fun in the lab. My friend Philipp has been a great partner in scientific discussions and he gave me the opportunity to contribute to his LuTHy project resulting in a publication in a prestigious journal. I would like to thank him sincerely.

Thanks also go to Ewa, Marta, Thorsten, Bettina, Katja, Carolina, Eckart and Christian, because without them some of this work would have been impossible.

Last but not least, I want to thank Jonathan, my family and all of my friends for their tireless support and love.